

617342
3181356

**TR diss
2502**

TR diss 2502

Dynamic Analysis of Three-Phase AC Converters

Dynamic Analysis of Three-Phase AC Converters

A method for the dynamic analysis
and synthesis of pulse-modulated
three-phase AC converters

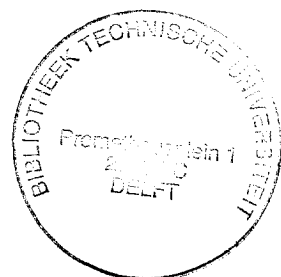
PROEFSCHRIFT

ter verkrijging van de graad van doctor
aan de Technische Universiteit Delft,
op gezag van de Rector Magnificus, prof. ir. K.F. Wakker,
in het openbaar te verdedigen ten overstaan van een commissie,
door het College van Dekanen aangewezen,
op maandag 16 januari 1995 te 13.30 uur

door

Pavol BAUER

inžinier
geboren te Košice, Slowakije



Dit proefschrift is goedgekeurd door de promotor:

Prof. Dr.-Ing. W. Deleroi

en de toegevoegd promotor:

Dr. ir. J.B. Klaassens

Printed by:

Copy Print 2000

De Reulver 106

7500 AH Enschede

The Netherlands

Telephone

053-776262

Fax

053-776200

CIP-DATA KONINKLIJKE BIBLIOTHEEK, DEN HAAG

Bauer, Pavol

Dynamic Analysis of Three-Phase AC Converters: A method for the dynamic analysis and synthesis of pulse-modulated three-phase AC converters / Pavol Bauer - Delft : Copy Print 2000.

Thesis Technische Universiteit Delft. - With ref.

ISBN 90-9007789

NUGI 841

Subject headings: dynamic analysis / switching space phasor / power electronics/ resonant link converters.

Copyright © 1994 by P. Bauer

All rights reserved.

No part of the material protected by this copyright notice may be reproduced or utilized in any form or by any means, electronic or mechanical, including photocopying, recording or by any information storage and retrieval system, without permission from the publisher: P. Bauer, Sweelinckstraat 52, 2625 VL Delft, The Netherlands.

to Kate, Petra and Erik

to my parents

PREFACE

The dynamic analysis of DC-to-DC power converters is a well established design tool which led to the improved modulation and control design of this class of power converters. Having the disposal of its counterpart for AC power converters would be of great value and therefore, in autumn 1990 the objective of this research project was to find and analyze a method for dynamic analysis of AC power converters.

In fact, this work started with recognizing the problems concerning the modulation process of a three-phase-to-three-phase series-resonant converter and its input power factor control. These problems led to a search for a suitable modelling technique. Although the research started as a search for a solution for a specific converter topology of a series resonant converter, the obtained solution proved to be generally valid. Because of the lack of any modelling techniques in the area of three-phase AC power converters, the research interest did not cover only the resonant link converters but was extended for the entire class of three-phase AC power conversion.

Two modelling techniques of the switching operation of switches in a bridge configuration are suggested: a switching function and a switching space phasor. Dynamic models of pulse-width modulated and discrete-pulse modulated converters based on these modelling techniques are established. Especially the switching space phasor modelling technique is proved to be suitable for the design of the modulation and the control of three-phase power converters. Idea of a switching space phasor brings also a new understanding of a power conversion and its switching behaviour. Between others, the desired modulation process of a three-phase-to-three-phase series-resonant converter is solved with a switching space phasor. The original research path with many detours was straightened to a logical line in this thesis.

During four years of research many people were of great help to me. I would like to thank in particular:

- Prof. W.Deleroi and Dr J.B. Klaassens who gave me freedom in exploring my topic,
- Members of the promotion committee: prof. P.P.J. van den Bosch, prof. W.I. Kling, prof. J.A.A. Melkebeek, prof. J.A. Schot, prof. A.J.A. Vandenput for their purposful suggestions and comments,
- R Schoevaars for his help, friendship and mental encouragement,
- F. de Beer, D. Antic, P.J. van Duijsen and E. van Dijk for friendship and collegiality,
- The staff of the Laboratory for Power Electronics and Electrical Machines who surrounded me with a friendly working atmosphere,
- My wife and my family for their support and help.

CONTENTS

1 INTRODUCTION	1
1.1 General	2
1.2 Survey of modelling techniques for DC-to-DC conversion	5
1.3 Classification of AC power converters	10
1.4 Conclusions	16
2 MATHEMATICAL MODEL OF A CONVERTER	19
2.1 Introduction	20
2.2 Configuration	21
2.3 Switching function	23
2.4 Space phasor definition	26
2.5 Space switching phasor	29
2.5.1 Current configuration	30
2.5.2 Voltage configuration	35
2.6 Instantaneous power in three-phase switching circuits	40
2.7 Relation between switching leg function and switching space phasor	44
2.8 Conclusions	45
3 PWM AC CONVERTERS	47
3.1 Introduction	48
3.2 AC-to-DC and DC-to-AC PWM converters	49
3.2.1 Suboscillation carrier PWM	51
3.2.2 Space phasor PWM	53
3.2.3 Summary of control principles	55
3.3 Space phasor PWM in rotating reference frame	56
3.4 AC-to-DC buck converter	58
3.4.1 Transfer function of AC-to-DC buck converter	63
3.5 Carrier suboscillation PWM in rotating reference frame	71
3.6 Conclusions	74
4 MODULATION OF SOFT-SWITCHING AC POWER CONVERTERS	75
4.1 Introduction	76
4.2 Hard switching and soft switching	76
4.2.1 Soft switching	77
4.2.2 Hard switching	78
4.3 Topologies of the soft-switching power converters	80
4.4 Methods of modulation	84
4.5 Conclusions	88
5 PULSE-MODULATION TECHNIQUES AND VARIABLE STRUCTURE CONTROL	91
5.1 Introduction	92

5.2	Variable structure control - survey	92
5.2.1	Multiple-input variable structure system	94
5.3	Resonant pulse-modulation techniques and sliding mode	95
5.4	Quasi-sliding mode modulators and models of a three-phase switching bridge	97
5.5	Conclusions	99
6	SERIES-RESONANT CONVERTER	101
6.1	Introduction	102
6.2	A three-phase-to-three-phase series-resonant converter	103
6.3	Dynamic equations of a three-phase-to-three-phase series-resonant converter	104
6.4	Resonant link current and quantum transformation	105
6.5	Phasor transformation	111
6.6	Switching space phasor selection	117
6.7	Simulation results	120
6.8	Conclusions	123
7	PARALLEL-RESONANT CONVERTER	125
7.1	Introduction	126
7.2	AC-to-DC parallel-resonant DC link step-up power converter ..	127
7.2.1	Forward operation	128
7.2.2	Reverse operation	132
7.3	Modulation of source currents based on a switching function ...	132
7.4	Simulation of an AC-to-DC converter	134
7.5	A three-phase-to-three-phase parallel-resonant converter	138
7.6	Conclusions	140
8	CONCLUSIONS	141
8.1	Open-loop modulated converters	143
8.2	Closed-loop modulated converters	144
	BIBLIOGRAPHY	147
	LIST OF NOTATIONS AND SYMBOLS	155
	SUMMARY	159
	SAMENVATTING	163
	CURRICULUM VITAE	167

1

INTRODUCTION

1.1 General

Electric power is processed by electronic power converters to make it acceptable for various applications such as regulated DC and AC power supplies, electrochemical processes, heating, lighting, electrical machine drives, electronic welding, active power line filtering, static var compensation and many other applications. Power processing includes the conversion of waveforms (DC-to-AC, AC-to-DC, DC-to-DC and AC-to-AC) employing power semiconductor switches. Besides the semiconductor switches, the essential elements of switching converters are energy storage components like inductors and capacitors. The dynamic behaviour of the converter itself is dominated by the elements storing energy and by the semiconductor switches that control the flow of energy between the input and the output terminals.

In recent years, significant advances in AC conversion have been reported. The wide acceptance of gate turnoff devices has encouraged the development of power converters for many areas of application. A significant application is formed by variable speed drives. The ruggedness and cheapness of AC machines have also contributed to the evolution of AC converters using pulse-width modulation and vector control.

The development of static power converters has reached the stage where further improvement of switching devices and their control networks will yield only a marginal gain. Consequently, the research in the area of AC conversion has been shifted towards improving the process of power conversion by improving also the quality of the input and output waveforms and the control strategies.

Increased attention is being paid to the dynamic behaviour and the control algorithm of the converters to achieve a high performance level. A central issue involved in the study of the dynamics of a converter is the model of the system. Models are simplified, abstracted concepts used to predict a system's behaviour [Karnopp, et.al. 1990]. The development of new resonant converter topologies applying soft-switching and pulse modulation techniques, increased the need for accurate models and analysis. The design of a control without understanding the operation principles of a model is difficult. Another problem is the power factor correction of polyphase converters.

The most accurate and simple dynamic model is developed from a set of differential equations prescribing the propagation of the power in the converter. Due to the switching behaviour, these differential equations are discontinuous and difficult to solve. Therefore, new ways of model development based on simplifications are looked for.

In Fig. 1.1 a generalized model of a dynamical conversion system is shown. The dynamic system (*DS*) is characterized by a set of state variables x , which are influenced by a set of input variables s representing the action of the system's environment. This type of dynamic system model is useful in three ways:

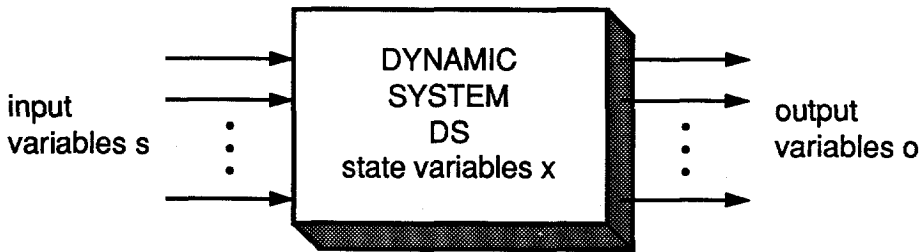


Fig. 1.1 General model of dynamic system

1. *Analysis*

For a given s , while x describes the present state of a model DS , the future of o is predicted. Under the assumption that the system model is an accurate representation of the actual system, the analysis predicts the system behaviour.

2. *Identification*

For given time histories of s and o usually obtained by experimental work on an actual system, a model DS and state variables x are found for the system, which is consistent with s and o . This is the essence of scientific experiments. Clearly, a reliable model is a model that is consistent for a great variety of s 's and o 's.

3. *Synthesis*

For a given s and some desired o , a model DS has to be found in such a way that s acting on DS will produce o . Primarily, engineering deals with synthesis but only in limited contexts where direct synthesis methods are available. Often we must be content to accomplish the synthesis of systems through a trial-and-error process of repetitive analysis of a series of candidate systems. In this regard, a dynamic model plays a vital role since progress would be slow if one had to construct each candidate system in the laboratory to discover its properties.

In this thesis we concentrate on establishing converter models and predicting the behaviour of the converter by analytical and/or computational techniques. It is important to remember that the techniques are useful to employ for solving identification problems. The major challenge for an engineer is to synthesize the described system which is also the subject of our interest. The dynamic system in our case is embodied by an AC power converter.

In the past, a converter has often been presented as an amplifier with a specific gain and if possible with a time delay. To fully use the potential of the converter and to account the uncertainties in the system, it is important to understand and qualify the dynamic performances of the converter especially in the presence of parameter variations and disturbances. The arguments leading to the requirement

for a dynamic model and a dynamic analysis of power converters is summarized in the following:

1. The designed control system must be able to deal with the consequences of the inevitable disturbances or errors that cause circuit operation to deviate from its rated operation. These disturbances include variations and uncertainties in the source, load and circuit parameters, perturbation in the switching time and events such as start-up and shut-down. Therefore an analysis based on a dynamic model has to be established.
2. The analysis and modelling of the converter control and operation lead to an improved control design. This is understood as the synthesis of the dynamic model.
3. Power converters are a part of a complex system, e.g. an electrical drive or a power supply. For the design of the converter control and regulation, a mathematical representation of the converter is required. An accurate mathematical solution even for the cyclic-stable mode of operation can involve an unmanageable set of equations. A designer of the controller needs a model that represents the dynamic effects. The steady-state mathematical solution of converter quantities (voltages and current) does not help in the proper design of the converter control and regulation if the dynamic behaviour describing the variations is unknown.

The analysis and synthesis is focused on the dynamic processes. The operation of the semiconductor devices must be considered ideal to avoid complexity. Thus the analysis and synthesis of the converter operation and the dynamic behaviour becomes much easier. This approach has the advantage that the details of device operation will not obscure the primary operation of the converter, and therefore, the important converter characteristics are more clearly understood. With the advance in power semiconductor devices in industrially manufactured drives and the improvements in protection networks (like snubbers) for these devices, the switching operation is approaching close to the ideal. The switching operation has therefore a little influence on the dynamic behaviour of the converter and is considered as ideal.

A lot of valuable work has been done in the field of the dynamic modelling of DC-to-DC converters. However, this work is not readily transferred to the analysis of AC converters because the system has a fundamental time-varying frequency component. Thus, alternative methods have to be looked for, or existing methods have to be extended. The complexity of AC power converters is much greater than the complexity of DC converters and so is the analysis of their operation and dynamics.

The purpose of this thesis is to establish a systematic approach to the methods of dynamic modelling and analysis for three-phase AC power converters. Recent developments in AC power conversion (converters with soft-switching of the

semiconductor switches) and the application of different pulse modulation techniques only increased the need for dynamic modelling.

The proposed method of approach to the problem is to:

1. Examine the existing DC-to-DC modelling techniques and investigate the possibility of extending the techniques to AC converter analysis,
2. Classify systematically AC converter topologies and related control techniques to study the control system configuration.

1.2 Survey of modelling techniques for DC-to-DC conversion

The dynamic analysis of DC-to-DC converters has already been accepted as a design tool [Kassakian et.al., 1991]. All methods are based on the step of averaging and/or linearization. Once accomplished, a process of averaging eliminates the influence of the exact waveshapes on the mathematical relationship between averaged quantities. This fact can lead to a dramatic simplification of the mathematical expressions. Although a relationship between the averaged models and the original systems is unclear, the comparison of predicted and measured parameters proves the accuracy and reliability of these methods.

Averaging steps often yield a nonlinear network model. The assessment of the stability and the design of the controllers for nonlinear models is usually difficult. The linearization yields a linear model that approximately describes small perturbations and deviations from the nominal operation of the system. The stability of the linearized models, often called small-signal models, shows that the rated operating condition is stable for small perturbations at least.

Modelling techniques are equation-oriented (the result is an averaged and linearized set of equations) and circuit-oriented, where the circuit components are replaced by their averaged and linearized equivalents. Circuit-oriented techniques are occasionally more illustrative but in a broader context they are equivalent to the equation-oriented techniques. Therefore, in the following survey the equation-oriented model is subject of our interest.

The *extended injected-absorbed-current analysis method* [Kislovski, 1983, 1985] is one of the simplest linear methods. The validity of this method is limited to the investigation of low-frequency, small-amplitude phenomena. The method of analysis implicitly admits the existence of a linear relationship between the small increments of the involved quantities. This idea is mathematically expressed, and applied to the functions of the averaged input "injected" current and output "absorbed" current, resulting in total differentials (See Fig. 1.2).

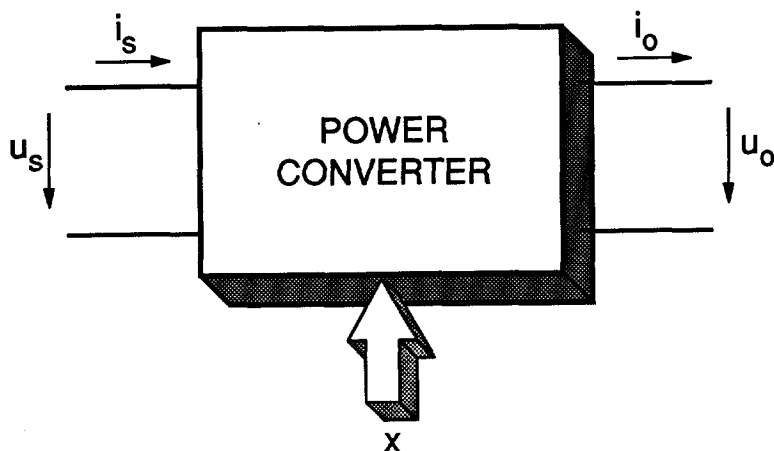


Fig. 1.2 Power converter

$$i_s = i_s(x, u_s, u_o) \quad (1.1)$$

$$i_o = i_o(x, u_s, u_o) \quad (1.2)$$

$$di_s = \frac{\partial i_s}{\partial x} dx + \frac{\partial i_s}{\partial u_s} du_s + \frac{\partial i_s}{\partial u_o} du_o \quad (1.3)$$

$$di_o = \frac{\partial i_o}{\partial x} dx + \frac{\partial i_o}{\partial u_s} du_s + \frac{\partial i_o}{\partial u_o} du_o \quad (1.4)$$

where:

- i_s - input "injected" current,
- i_o - output "absorbed" current,
- u_s - input (source) voltage,
- u_o - output voltage,
- x - control quantities.

Partial derivations are constants for a given operating point, so that the equations (1.3) and (1.4) are linear relations. From the obtained linear equations, the model of the switching cell and the transfer functions can be developed.

In case that the input and the output current depend also on an additional quantity, e.g. inductor current, an additional equation is necessary. This is characteristic for the continuous mode of operation for which the stored energy is transferred from one switching cycle to the other. The additional equation represents the derivation of this quantity.

The application of the *injected-absorbed-current analysis* method to AC power converters is difficult. The relation between injected (input) and absorbed (output) current is established by simplified linearized waveforms. A similar procedure cannot be realized for AC converters. The *injected-absorbed-current method* fails to predict the stability of the phase-controlled resonant converters where a linear approximation does not hold.

The *state-space averaging modelling* method [Cuk, Middlebrook, 1976, 1977] has the virtue of starting from a standardized and general system representation, namely a state-space description of the circuit for each of its equivalent switch configurations. The basic principle is to replace the state-space description of the linear equivalent circuits (two or more) by a single state-space description that represents the average effect of the system through one cycle of operation. In matrix notation, set of state-space equations, e.g. two configurations, is as follows:

$$\dot{x} = A_1x + B_1u \quad (1.5)$$

$$\dot{x} = A_2x + B_2u \quad (1.6)$$

where:

- x - vector of state variables,
- u - vector of independent sources,
- A_1, B_1, A_2, B_2 - system matrices for two different configurations of a switching network.

The basic idea in state-space averaging is the replacement of two sets of state-space equations by a single equivalent set:

$$\dot{x} = Ax + Bu \quad (1.7)$$

The equivalent matrices A and B are the weighted averages of the actual matrices that alternately describe the switched system:

$$A = dA_1 + (1-d)A_2 \quad (1.8)$$

$$B = dB_1 + (1-d)B_2 \quad (1.9)$$

where:

- d - duty ratio.

The steady-state solution for which DC values are shown in capital letters is obtained by setting $\dot{x} = 0$ in (1.7):

$$X = -A^{-1}BU \quad (1.10)$$

The AC small-signal solution is found by linearization using the perturbation of variables and substitution in the usual way:

$$\begin{aligned} \mathbf{u} &= \mathbf{U} + \tilde{\mathbf{u}} \\ \mathbf{x} &= \mathbf{X} + \tilde{\mathbf{x}} \\ \mathbf{d} &= \mathbf{D} + \tilde{\mathbf{d}} \end{aligned} \quad (1.11)$$

where the capital letters denote DC steady-state values and the lower case letters with a tilde denote the perturbations around the steady-state operation.

After subtracting the DC terms and omitting the second-order terms (small-signal restriction), the resulting equation is:

$$\begin{aligned} \dot{\tilde{\mathbf{x}}} &= \mathbf{A}\tilde{\mathbf{x}} + \mathbf{B}\tilde{\mathbf{u}} + \mathbf{B}_d\tilde{\mathbf{d}} \\ \mathbf{B}_d &= [(\mathbf{A}_1 - \mathbf{A}_2)\mathbf{X} + (\mathbf{B}_1 - \mathbf{B}_2)\mathbf{U}] \end{aligned} \quad (1.12)$$

By Laplace transformation the solution can be written:

$$\tilde{\mathbf{x}}(s) = (s\mathbf{I} - \mathbf{A})^{-1}[\mathbf{B}\tilde{\mathbf{u}}(s) + \mathbf{B}_d\tilde{\mathbf{d}}(s)] \quad (1.13)$$

where:

\mathbf{I} - identity matrix.

A required transfer function can be developed in the frequency domain based on equation (1.13).

For the discontinuous current mode, the state-space equation is supplemented by equations for the additional constraints. These equations contain averaged discontinuous state variables. State-space averaging was originally proposed to model a pulse-width modulated converter. The natural frequency of each linear circuit of a PWM converter is much lower than the switching frequency. This provides the justification of the linear ripple assumption. This method does not work on resonant converters where the energy of the state variables is carried mainly by the switching frequency and not by the DC components. State-space averaging fails to predict the high-frequency response of current-programmed converter systems [Lau, Middlebrook, 1986].

Sampled-data modelling [Verghese, et al, 1986] was developed to overcome the problem encountered when using the state-space averaging method to calculate the frequency response of current-programmed converter systems. A sampled-data model describes the evolution of state variables for one cycle of operation from the beginning to the beginning of the next one. For every model the state vector is calculated from the previous state:

$$\mathbf{x}(t_i) = e^{\mathbf{A}_i d_i T} \mathbf{x}(t_{i-1}) + \int_{t_{i-1}}^{t_i} e^{\mathbf{A}_i(t_i - \tau)} \mathbf{B}_i \mathbf{u}_i(\tau) d\tau \quad (1.14)$$

where:

- A_i, B_i - system matrixes in time interval i ,
- $x(t_{i-1})$ - vector of the state variable in instant t_{i-1} ,
- $x(t_i)$ - vector of the state variable in instant t_i ,
- u_i - vector of the sources in time interval i ,
- d_i - duty cycle in interval i ,
- T - period of the switching cycle.

A small-signal model is developed by applying a Taylor-series expansion and retaining only the linear forms. For an exact solution of the state equations in the time-domain, the steady-state trajectory is found under given operating conditions. Perturbation of the periodic trajectory provides the small-signal evolution of the dynamic behaviour represented by a linear time-invariant difference equation with the sample interval equal to the switching period. A similar approach to sampled-data modelling is studied in [Visser, van den Bosch, 1991].

Sampled-data modelling is a general method which is valid for all converters with periodic operating trajectories. Because there is no linear ripple assumption made, the method is valid also for resonant converters [Elbuluk, et al, 1988]. The effectivity of sampled-data modelling for AC converters is limited because of the large number of switching states.

The use of sampled-data modelling for resonant converters [Verghese, 1982] yields a small-signal model for the underlying resonant converter with the perturbation in the switching frequency as the input. The complication in this approach is the requirement to obtain a nominal periodic solution as a first step in the analysis.

The phase-plane method [Oruganti, Lee, 1985] is a basic approach to obtain a steady-state solution for resonant converters. The control scheme based on this method is evidently effective [Oruganti, Lee, 1987]. A limitation of this approach is its restriction to second-order systems. It is not obvious how to include additional state variables that are associated with the load or source filters. Therefore, the application of the method in polyphase resonant converters is not effective. An extension of the method has been reported in recent literature [Cheron, Foch, 1993]. The inclusion of the snubbers in the analysis results in a discontinuous phase plane.

Small-signal analysis of resonant converters [Cuk, Vorperian, 1977] has been developed primarily for application in resonant converter systems. This method employs state-space analysis without the linear ripple approximation, since such an approximation is clearly not valid for resonant converters. The crux of the analysis requires the retention of terms of the form e^{AT_s} , and linearization under small-signal assumption requires retention of terms of the form e^{At_s} which arise from small-signal perturbations \tilde{t}_s of the steady-state switching time T_s . This is summarized by the following equation:

$$e^{At_s} = e^{A(T_s + \tilde{t}_s)} = e^{AT_s} e^{A\tilde{t}_s} \approx e^{AT_s} [I + A\tilde{t}_s] \quad (1.15)$$

The justification of the linearization in the last step simply requires \bar{f} 's to be small compared to the time constants of the circuit and the switching time T_s . Since for resonant converters T_s cannot be considered small compared to the natural time constants of the circuit as in PWM converters, the approximation of e^{AT_s} is not valid in this case. Another reason why resonant topologies present more difficulties for small-signal analysis than the minimum element topologies (buck, buck-boost and boost converters) resides in the fact that resonant topologies have one state variable more. The small-signal model for the resonant converter became a challenging task and was realized by several authors [King, Stuart, 1985], [Nakahara, et al, 1989], [Witulski, Hernandez, 1987, 1991], [Vorperian, 1989].

Because of the switching behaviour, power converters are nonlinear, time-varying systems. Dynamic modelling and analysis for these classes of systems is not studied extensively in comparison to linear time-invariant systems. The step of averaging and linearization when applied to the analysis of the DC-to-DC power conversion simplifies the nonlinear time-varying model of a converter. The obtained model is a linear, time-invariant (LTI) or a piecewise-linear time-invariant system (PLTI).

The small-signal analysis method, based on an averaged model, establishes efficiency and accuracy. The justification of the method of averaging was defined by a small-ripple condition and linear ripple approximation. With the small-ripple approximation, it is assumed that a Fourier series expansion for a finite segment of a circuit waveform is dominated by its DC term. Therefore, the averaging methods are not directly applicable for AC power converters.

Since the steady-state solutions for AC power converters are time-varying functions, a small-signal model cannot be obtained by straightforward linearization. There is an analogy between averaging and linearization. In the broader context, averaging and linearization can be classified as a perturbation method that yields a simple approximated model. Linearization provides a linear approximation of a nonlinear system, while averaging provides a time-invariant approximation to a time-varying system. In both cases, the simpler approximate model is exact at some rated operating points. Linearization considers a neighbourhood in the state-space and averaging considers a neighbourhood in the parameter space.

1.3 Classification of AC power converters

There are many procedures used to classify converters. They include the classification according to the type of semiconductor device used, to the function of the converter and to the method used to switch devices in the converters. The classification of AC converters according to the modelling and analysis differs from the conventional classification because the modelling problems are different.

A generalized classification of AC converters on a functional basis leads to a

division into AC-to-DC converters (rectifiers), DC-to-AC converters (inverters) and AC-to-AC converters. A practical power system may comprise more than one conversion system. An AC-to-AC converter with a voltage or current DC link combines an AC-to-DC and a DC-to-AC converter.

Some insight can be gained by classifying converters according to the way in which the semiconductor devices in the converter are switched [Mohan, et.al., 1989]. There are two possible categories.

1. *Line frequency converters*, where the source voltages present at one side of the converter facilitates the turnoff of the power semiconductor devices. Similarly, the devices are turned on, locked in phase to the source voltage waveform. Therefore the devices switch on and off at the *line frequency* of 50 or 60 Hz.
2. *Switching converters*, where the controllable switches in the converter are turned on and off at frequencies that are usually high compared to the line frequency. In spite of the internal switching frequency of the converter, the converter output may be either DC or at a frequency comparable to the line frequency.

These two categories can be further divided into subcategories according to the type of conversion. *Switching converters* with high switching frequency are subject of our interest in this thesis. For the purpose of analysis, the important aspect to study is the control system configuration.

Control system configuration

Proposed analysis methods in the literature differ with respect to the control system configuration. Power converters are usually a part of a complex system, e.g. an electrical drive or a power supply. The control and regulation of the entire system is a separate problem. The term control is assigned only to the control of a power converter [Kassakian, 1991]. A typical control system configuration is depicted in Fig. 1.3. It should be noted that this figure depicts only a power converter with the inverter loop controller. The required operation is related to the reference voltage or current which results from the *outer loop* controller (not shown in Fig. 1.3). The purpose of the *inner loop* controller is the translation of the required operation into a switching action of semiconductor switches. The outer loop controller is a matter of interest in control engineering and results in a PID controller or other, more sophisticated regulation schemes. However, the inner loop controller is a vital part of a power converter. Therefore, in this thesis the inner loop controller is a matter of further study.

The terms *modulation* and *modulator* are often used to establish the method for creation of the converter waveforms. The term "controller" is more general and its use emphasize the inclusion of both open-loop and closed-loop operation.

For a simple open-loop control, the controller does not provide information about the system during operation, although the construction of the open-loop controller

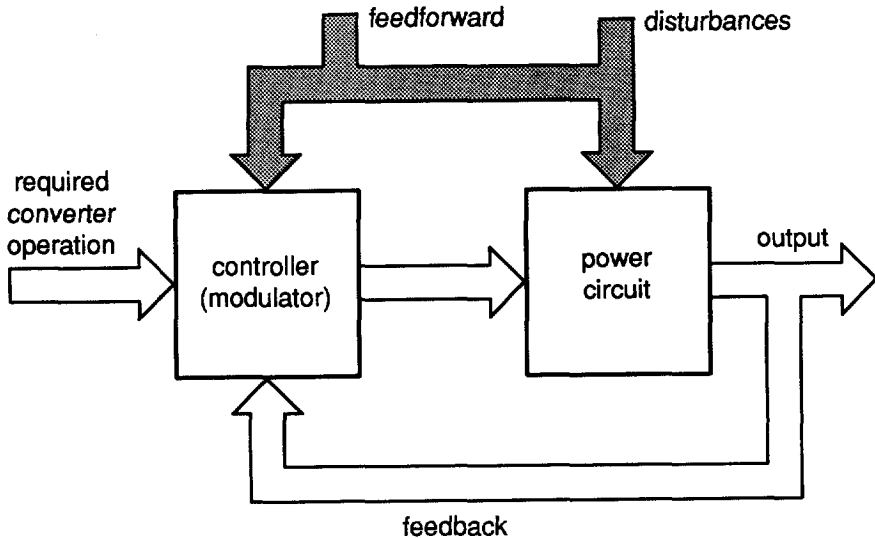


Fig. 1.3 Typical control system configuration

may be based on a prior information or models. In an open-loop control with feedforward, the control employs measured information about disturbances affecting the system. Feedforward alone is usually insufficient to obtain a satisfactory performance of the power converter. For the closed-loop control or feedback control, the controller manipulates the measurements that reveal the behaviour of a circuit. The controller can assess the extent of the departure from the required behaviour by employing the measurements and choosing the control actions aimed at a fast and safe restoration of the system to its required operation.

AC topologies

AC topologies are usually classified into categories depending on the type of the intermediate power transfer link (DC link, AC link or direct link).

Another widely used method of classification is the classification into DC link, resonant link and direct link or, more recently, into hard-switched and soft-switched power converters.

These classifications are based on the traditional converter topologies. A review of topologies is shown in Fig. 1.4. There is some overlap between the different groups of converters. An example of this phenomenon is the soft-switched, resonant direct link converter as presented by [Cho, Cho, 1992].

For the dynamic analysis and modelling, the AC converter topology and the related control techniques are divided into three basic groups.

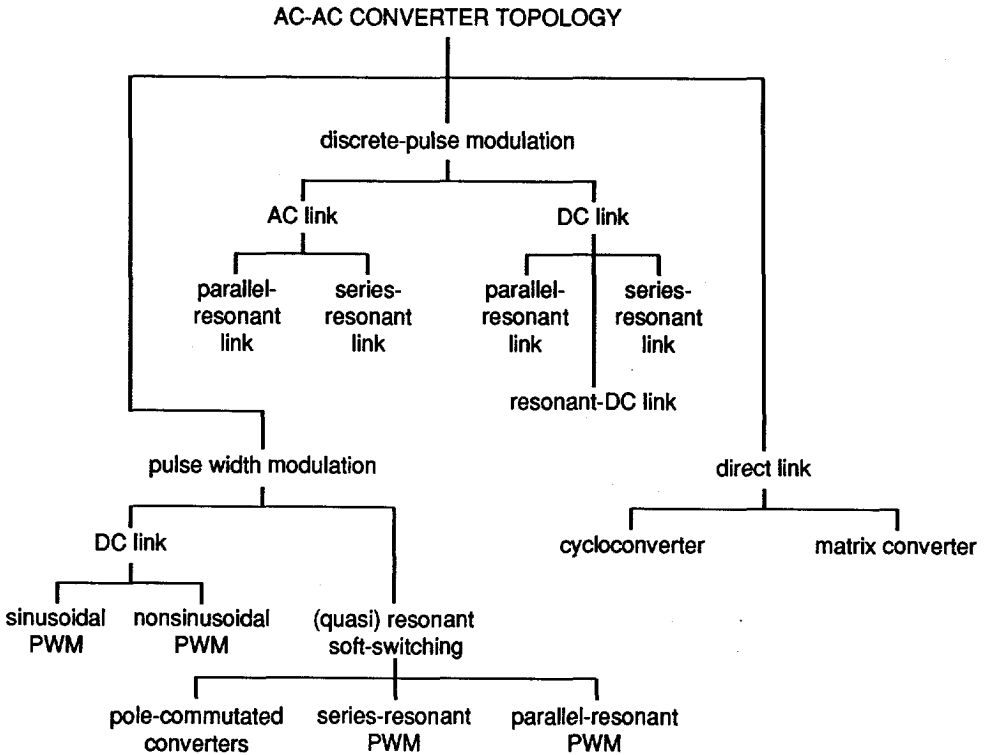


Fig. 1.4 Review AC-to-AC power converter topology

1. *Pulse-width modulated (PWM) AC-to-DC or DC-to-AC converters*
 The common feature of this group is the DC current or DC voltage link. This group includes also soft-switching PWM converters. The PWM method is presented as an open-loop method with the possibility of applying a feedforward control.
2. *Discrete-pulse modulated converters*
 The common topological feature is the high-frequency resonant-link based on a series-resonant or parallel-resonant circuit. Various pulse modulation techniques are applied. The hysteresis PWM or sliding PWM is a element of this group.
3. *Direct link converters*
 The dynamics of this last group of converters (matrix converter, cycloconverter) are provided by their switching function since no dynamic elements (energy storage elements) are involved in the conversion process. The analysis of the matrix converter is studied in detail in [Gyugy, Pelly, 1976]. Therefore, in this work we do not deal with this class of power converters.

In the following, the group of pulse-width modulated converters and discrete-pulse modulated converters is evaluated more in details.

Pulse-width modulated converters

For PWM converters, the procedure of feedback is usually used for regulation and not for synthesis of the low-frequency waveforms. It is thus an open-loop control with the possible use of feedforward.

PWM converters with soft-switching features are also part of the group referred to. Soft-switching is achieved by introducing additional components and it does not influence the energy transfer or the dynamic behaviour of a converter. As stated at the beginning of this section, the switching power converter transfers the energy and achieves the required shape of an electrical quantity (current, voltage) via pulses with a high repetition frequency. An example of a pulse-width modulated electrical quantity is shown in Fig. 1.5. Pulse-width modulation can change the width $T_{on,k}$ of the k th pulse in a required way while the period $T_{sw,k}$ is kept constant:

$$\begin{aligned} T_{on,k} &\neq T_{on,k+1} \\ T_{sw,k} &= T_{sw,k+1} \end{aligned} \quad (1.16)$$

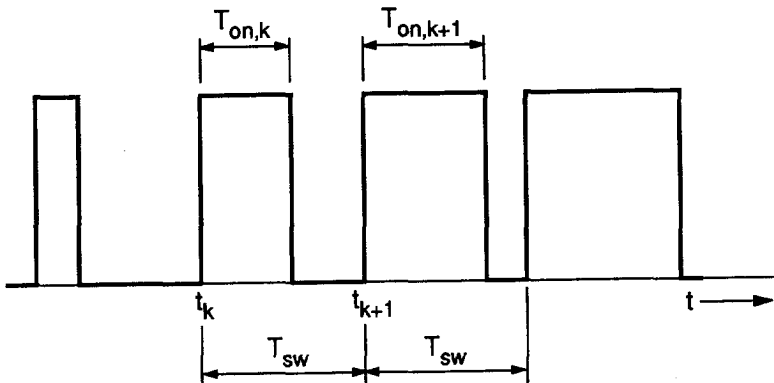


Fig. 1.5 Pulse-width modulated waveform

The degree of freedom that changes the pulse width is used to reach the required value of the electrical quantities such as the amplitude, frequency and phase-shift of the external waveforms of the converter.

Discrete-pulse modulated soft-switching resonant converters

For discrete-pulse modulated converters the width T_{on} of energy pulse is kept constant and equal to the half of the resonant link frequency period. The pulse time interval $T_{sw,k}$ and possibly the pulse amplitude change:

There are two variables (pulse frequency and amplitude) that determine the value

$$\begin{aligned} T_{on,k} &= T_{on,k+1} \\ T_{sw,k} &\neq T_{sw,k+1} \end{aligned} \quad (1.17)$$

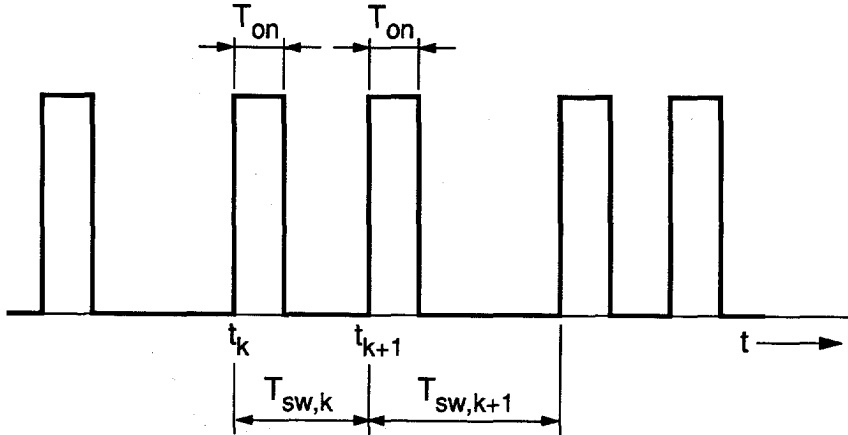


Fig. 1.6 Pulse frequency modulated waveform

of the transferred electrical quantities (voltage or current). The mentioned parameters depend in the most cases on each other, so a simple precalculation of the switching pattern is no longer possible. Therefore, this class of modulation is not used in an open-loop control. In soft-switching pulse-modulated converters, the feedback serves not only as a means of regulation but also as a means of synthesis of the low-frequency waveforms. Therefore, a different pulse modulation technique is applied compared with PWM converters.

The terminology "pulse frequency modulation" (PFM) is often used to identify this category of modulation techniques. It is due to the fact that this principle of modulation technique is similar to PFM, originally described for DC-to-DC converters but hardly used for AC conversion. In difference with the PFM modulated of resonant converters, in the case of discrete-pulse modulated soft-switching resonant converters, the amplitude of the pulses also varies. Therefore, it is not possible to precalculate a switching pattern.

An example of pulse frequency modulation is presented in Fig. 1.6. The pulses shown in Fig. 1.6 have a rectangular shape. Since the energy is transferred via a high-frequency resonant link, the shape of the modulated pulses is often sinusoidal with changing amplitudes. Soft-switching pulse-modulated converters are in fact resonant converters where each switching action depends on the instantaneous value of the state variables. Therefore, new approaches to the dynamic analysis and modelling should be considered.

Currently used modulation methods for soft-switched resonant converters can be also considered as sliding-mode control methods. They approach sliding-mode

control with a few differences which are referred to later. Polyphase, soft-switching resonant converters are in nature multi-input, variable-structure and discrete systems (discrete-pulse modulated).

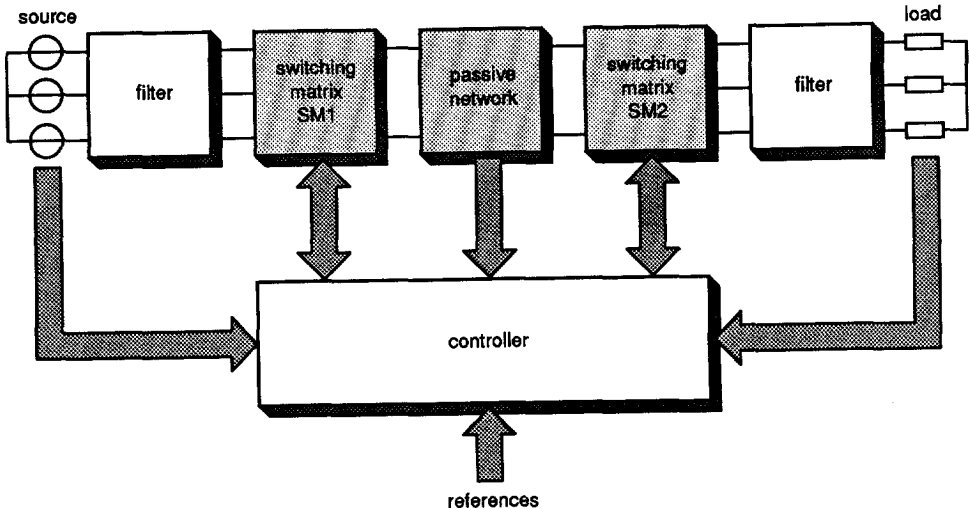


Fig. 1.7 Three-phase-to-three-phase power converter

Generalized conversion system

A general configuration of a three-phase-to-three-phase power converter is shown in Fig. 1.7. The used converter topology and the related control techniques depend on the character of the passive network located between the switching matrices and on the character of the filters as well.

The character of the passive network and the character of the filters provides the character of the converter (in terms of DC-to-DC power conversion: boost, buck, buck-boost topologies). In the case of DC link converters, the analysis is divided into two parts (AC-to-DC and DC-to-AC). This is because of the energy storage in the link (buffer), which makes power conversion twofold.

1.4 Conclusions

Power converters are mostly nonlinear systems because of their inherent switching operation. When looking at the averaging methods applied to the analysis of the DC-to-DC power converters, we see that the averaging method simplifies the nonlinear, time-varying, discontinuous model of a converter by creating a linear time-invariant (LTI) system (or by obtaining an LTI model from a piecewise LTI model). The averaging step is, however, not applicable to AC converters, so a different approach should be considered. We also concluded that the dynamic model cannot be obtained by linearization.

To enable the study of AC power converters, a generalized classification of the converter topology and their related modulation techniques are presented. Two basic groups according to the control configuration are defined: *pulse-width modulated converters* and *discrete-pulse modulated converters*. These groups are investigated separately. The focus is on soft-switching resonant power conversion since there were no methods for analysis available so far.

The DC-to-DC power converter topologies mostly consist of a single power semiconductor switch. The averaging operation is applied to the switching cycle of a switch during the switching period. The AC converter topologies consist of a considerably high number of semiconductor switches. Therefore, the first step in the analysis is the study of the mathematical model of a generalized converter.

2

**MATHEMATICAL MODEL
OF A CONVERTER**

2.1 Introduction

The study of three-phase-to-three-phase AC power converters for all modes of operation requires the establishment of a set of dynamic equations. In other words, it is essential to adopt a mathematical model that involves the dynamic effects in the physical quantities of the converter and relates them to each other. The selection of a mathematical model is a crucial point in the analysis of the converter operation. However, the selected mathematical model and the control mechanism are related to each other. As shown in Chapter 1, in the survey of the modelling techniques for DC-to-DC converters, the obtained models have reduced accuracy due to the introduced simplifications. The accuracy should normally be sufficient for practical purposes.

The dynamic equations of the system involving energy storage elements (inductors and capacitors) result in a set of differential equations. The order of the differential equations is equal to the number of independent state variables. The development of the differential equations for an electrical network containing active and reactive components is routine work that involves the application of the definition of circuit elements and the rules of network theory.

The conventional approach to the inspection of the converter network, including switches, is to analyse the operation from one time interval to another time interval. Each alteration of the topology results in a new configuration and another set of differential equations. A sampled-data model based on the solution of the equations for each individual interval has no practical solution because the number of topologies can be extremely large.

Another approach is to avoid the topological details by introducing a model that applies nonlinear discontinuous switching functions that perform the switching operation of semiconductor switches. Because of the switching action of the semiconductor power devices, the obtained differential equations are nonlinear with discontinuous excitation. Mathematical science does not offer a satisfactory solution for differential equations with discontinuous right side. Therefore, creating a mathematical model of switches and a model of the switching behaviour is the first step in the analysis.

The model of a *direct AC-to-AC converter* that is not involving energy storage elements is quite simple and straightforward [Gyugyi, Pelly, 1976]. The input and output of the converter are connected via semiconductor switches:

$$\mathbf{u}_o(t) = \mathbf{H}(t) \mathbf{u}_s(t) \quad (2.1)$$

$$\mathbf{i}_s(t) = \mathbf{H}^T(t) \mathbf{i}_o(t) \quad (2.2)$$

where:

\mathbf{u}_o -output voltage vector,

- i_o -output current vector,
 u_s -input voltage vector,
 i_s -input current vector,
 H -existence matrix,
 H^T -transferred existence matrix.

The output voltage u_o is a combination of input voltages u_s and the source current i_s is a combination of output load currents i_o . The existence matrix H defines the relationship between the input and output quantities of the converter and thus specifies the operation of the power switches. Similarly, equations (2.1) and (2.2) represent a transfer function. The existence matrix is a simple model for a switching matrix of semiconductor switches.

Compared to a direct converter, mathematical model of the converter shown in Fig. 1.7 results in a set of differential equations because it contains energy storing elements. The switching matrices SM1 and SM2 represent the switches in the bridge configuration (Fig. 2.1). The number of the possible network configurations in a three-phase system is large. The number of possible switching states for a network containing n switches is in general 2^n . However, not all possible switching states create an allowed and meaningful configuration. In fact, the number of meaningful and allowed switching states is small as shown later. A meaningful or active switching state is that in which energy transfer between the three-phase terminals and the one-phase side of the switching bridge takes place. The allowed switching state configuration is one that does not result in failure of the semiconductor switches. Depending on the network as connected to the three-phase side and the one-phase side of the bridge, there are only 6 meaningful and active states. The investigation is focused on the converter topologies using a three-phase bridge configuration.

Two approaches are discussed:

1. the *switching function* for each *single leg* of a *switching bridge SM*,
2. the *switching phasor* for a *switching bridge SM*.

Another possibility would be the assignment of a switching function for each single switch in the switching matrix. This possibility is not studied because switches in the switching bridge are functionally related to each other, which means that none of the switches operates separately.

2.2 Configuration

The general topology of a three-phase-to-three-phase converter is shown in Fig. 1.7. The source and the load are presented in a star configuration. The character of the input and output filters depends on the character of the passive network in the link. The switching matrices SM1 and SM2 are realized by a three-phase switching bridge. A scheme of such a switching bridge is shown in Fig. 2.1. In this figure, a DC side is shown although it does not need to be a DC link in the

classical way of understanding. The three-phase switching bridge generally performs a three-phase to single-phase conversion. In this thesis, the three-phase side is assigned as the AC side and the single-phase side will be assigned as the DC side or link.

In Fig. 2.1a, a rectifier (AC-to-DC) is depicted and in Fig.2.1b, an inverter (DC-to-AC) is depicted. Although, the topology of a rectifier is a mirror picture of an inverter, the control mechanism differs and depends on the configuration as it is explained further. Voltages of the three-phase AC side $u_{j,k}$ for $j=s,o$ and $k=a,b,c$ are defined with respect to the starpoint of a three-phase source or a three-phase load as defined in Fig. 1.7.

The character of the AC side or the DC side is described by the character of a voltage source or current source. The character of the AC side and the DC side are always complimentary. A three-phase AC current source or AC filters with inductive character are connected to a one-phase DC voltage source or filters with capacitive character via a switching bridge. A three-phase AC voltage source or AC filters with capacitive character are connected via a switching bridge to a one-phase DC current source or filters with inductive character.

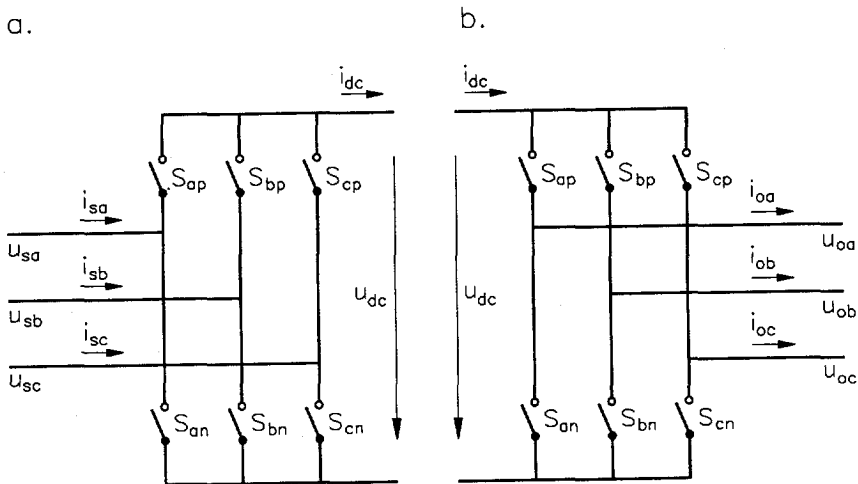


Fig. 2.1 Three-phase switching bridge
a, rectifier
b, inverter

Depending on the character of the filters and the passive network of the link, there are two different configurations:

1. *current configuration*, where a path is created for the current in each phase of the AC side. The impedance of a three-phase AC side is large compared to the impedance of one-phase DC side.

2. *voltage configuration*, where a line voltage is connected to the link. The impedance of a three-phase AC side is low compared to the impedance of a one-phase DC side.

Current configuration

An active configuration requires the creation of a path for the current of each individual phase and energy transfer between the AC and the DC sides. Current configuration means a configuration that creates nonzero currents in the switching bridge. This constraint on the switching functions is analytically expressed as:

$$\begin{aligned} S_{ap} + S_{an} &= 1 \\ S_{bp} + S_{bn} &= 1 \\ S_{cp} + S_{cn} &= 1 \end{aligned} \quad (2.3)$$

where:

$$\begin{aligned} S_{jk} &= 1 && \text{- closed switch,} \\ S_{jk} &= 0 && \text{- open switch,} \\ &&& \text{for } j=a,b,c \text{ and } k=p,n. \end{aligned}$$

The constraint (2.3) defines six active and two allowed switching states. This configuration for the three-phase switching bridge is identified as a *current configuration*.

Voltage configuration

The other active configuration requires two closed switches in the switching bridge. It is always one switch from the upper group (S_{ap} , S_{bp} , S_{cp}) and one switch from the lower group (S_{an} , S_{bn} , S_{cn}). This constraint on the switching functions is analytically expressed as:

$$\begin{aligned} S_{ap} + S_{bp} + S_{cp} &= 1 \\ S_{an} + S_{bn} + S_{cn} &= 1 \end{aligned} \quad (2.4)$$

The constraint (2.4) defines six active and three allowed switching states. Since only two switches from the switching bridge are closed, this configuration is a *voltage configuration*.

2.3 Switching function

One switching leg of a switching bridge is shown in Fig. 2.2. The canonical cell of one leg of the switching bridge connects one phase of the AC side of the converter to the DC side (or link) via two switches S_p and S_n .

A possible method to characterize the switching behaviour of a three-phase converter is a switching function or duty ratio concept. Similarly to DC-to-DC modelling techniques, the on and off states of a semiconductor switch are modelled by a switching function:

$$\delta(t) = S_p - S_n \quad (2.5)$$

where:

- $\delta(t)$ - switching function (duty cycle) of a bridge leg,
- $S_j = 1$ - closed switch ($j=p,n$),
- $S_j = 0$ - opened switch ($j=p,n$).

By applying the model to a switching leg, it is possible to establish a mathematical model for a three-phase switching bridge. The mathematical model shows that there is a relation between the AC and the DC sides.

The switching function $\delta(t)$ introduced in equation (2.5) has now three values:

- $\delta(t) = 1$ - if the phase is connected to the pole of the link,
- $\delta(t) = -1$ - if the phase is connected to the zero of the link,
- $\delta(t) = 0$ - if the phase is disconnected (switches S_j , $j=p,n$ are closed).

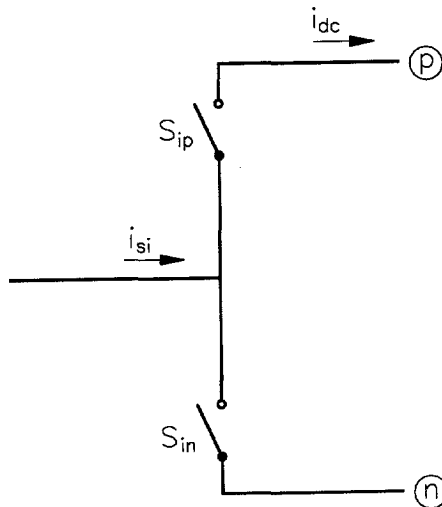


Fig. 2.2 One leg of a switching bridge ($i=a,b,c$)

The relation between the AC and the DC sides of one switching bridge leg is defined by equation:

$$u_{si} = \frac{1}{2} \left(\delta_i(t) - \frac{1}{3} \sum_{i=a,b,c} \delta_i(t) \right) u_{dc} \quad (2.6)$$

where:

- u_{si} - phase voltage of the AC side,
- u_{dc} - voltage of the DC link,
- $\delta_i(t)$ - switching function of i phase ($i=a,b,c$).

Equation (2.6) is valid for a current configuration of a rectifier and an inverter.

The term $\sum \delta_i(t)$ represents the influence of the actual switching position of the other two legs of a three-phase switching bridge. In the case of the voltage configuration, this term is always zero. This fact is derived from (2.4) and (2.5). The general expression valid for an inverter and a rectifier in a voltage configuration is:

$$u_{dc} = \sum_{i=a,b,c} \delta_i(t) u_{si} \quad (2.7)$$

The general expression valid for DC and AC currents of an inverter and a rectifier in the voltage and the current configuration follows:

$$i_{dc} = \frac{1}{2} \sum_{i=a,b,c} \delta_i(t) i_{si} \quad (2.8)$$

where:

- i_{dc} - current of the DC side of a bridge,
- i_{si} - current of the AC side of a bridge.

Because the DC link current for a voltage configuration flows through two connected phases, expression (2.8) can be simplified for a rectifier and an inverter:

$$i_{si} = \delta_i(t) i_{dc} \quad (2.9)$$

The *current configuration* offers another definition of the switching function. This is possible because of the complimentary switching of the switches in a switching bridge leg:

- $\delta(t) = 1$ - if the phase is connected to the pole of the link,
- $\delta(t) = 0$ - if the phase is connected to the null point of the link.

Equation (2.6) for a current configuration is then changed:

$$u_{si} = \left(\delta_i(t) - \frac{1}{3} \sum_{i=a,b,c} \delta_i(t) \right) u_{dc} \quad (2.10)$$

To summarize, a multi-terminal block of a three-phase switching bridge constructed from three individual switching bridge legs is shown in Fig. 2.3. The introduced mathematical model of the *switching function* is applicable in the case when each phase is modulated separately. A possible modulation method is the subs oscillation PWM method [Holtz, 1992].

Equations (2.6) and (2.7) yield that the currents and voltages at both sides of a switching bridge leg depend on all three switching functions $\delta_i(t)$ ($i=a,b,c$). This model is very useful for the analysis of existing classes of modulation but limited

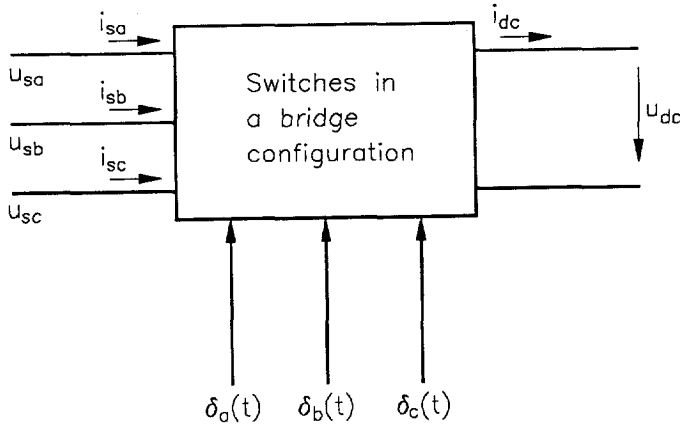


Fig. 2.3 Model of a switching bridge with switching function $\delta_i(t)$ ($i=a,b,c$)

for the process of synthesis, as shown in the following chapters.

It would be advantageous to develop a model where the switching action is prescribed by only one function. Therefore, an advanced mathematical model is introduced as a **space phasor** representation of a complex switching bridge. The fundamental harmonics of the steady-state values of the AC side currents and voltages of the converter circuits vary sinusoidally in time. These values can be found by means of the Cartesian projection of an oriented segment in a complex plane (time phasor).

When dealing with three-phase circuits, three sinusoidal waveforms are presented by phasors in a complex plane with an electrical phase shift of $2\pi/3$. A combined representation is possible by a space phasor prescription. A space phasor is defined as an oriented segment in the complex plane that characterizes at every moment the spatial distribution of an internal quantity of an electrical machine. Because the three-phase power converter is often loaded by three-phase electrical machines, a space phasor representation of a three-phase circuit is an advantageous choice. Thus is compatibility with the theory of electrical machines maintained.

2.4 Space phasor definition

The space phasor representation of three-phase circuits has been proved to have considerable advantages over conventional circuit analysis methods [Kovacs, Racz, 1959]. The complex notation of the state variables facilitates easy transformation into various coordinate systems as it is common practice in the dynamic analysis of AC machines. In the following, a space phasor definition is given. An analysis of a three-phase switching bridge enables the definition of a switching phasor \underline{g} which supervises the interaction between the AC side and the DC side of a bridge.

There is lot of misunderstanding in the literature related to the phasor-vector theory. Term *phasor* is used because of the complex notation of the function in this work.

For the three balanced time-varying functions $x_a(t)$, $x_b(t)$ and $x_c(t)$, the instantaneous space phasor $\underline{x}(t)$ is defined as:

$$\underline{x}(t) = \frac{2}{3} (x_a(t) + x_b(t)e^{j\rho} + x_c(t)e^{-j\rho}) \tag{2.11}$$

where:

- $\underline{x}(t)$ - instantaneous space phasor,
- $x_i(t)$ - (i = a,b,c) time-varying functions of a balanced three-phase system,
- $\rho = 2\pi/3$ - angle.

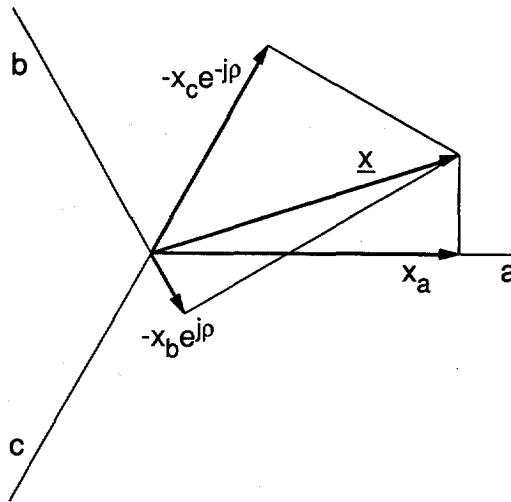


Fig. 2.4 Space phasor in a,b,c coordinate system in a two dimensional plane

If the sum of the three functions is zero (they are components of a balanced three-phase system), the inverse transformation exists and $x_a(t)$, $x_b(t)$ and $x_c(t)$ can be reconstructed from the space phasor representation (Fig. 2.4). The main assumption made in the analysis is that all three-phase variables are balanced so they can be uniquely represented by an instantaneous space phasor. A three-phase system is defined as balanced when both the currents and the voltages are symmetrical. Generally, a set of polyphase quantities (phase currents, phase voltages, etc.) is balanced, if they are sinusoidal in time, they have identical amplitudes and they are shifted in time with respect to each other by identical phase angles [IEEE Standard 100-1972].

By the projection of the resulting phasor $\underline{x}(t)$ in the direction of each axis, an instantaneous value of the components is given. The resulting space phasor is with

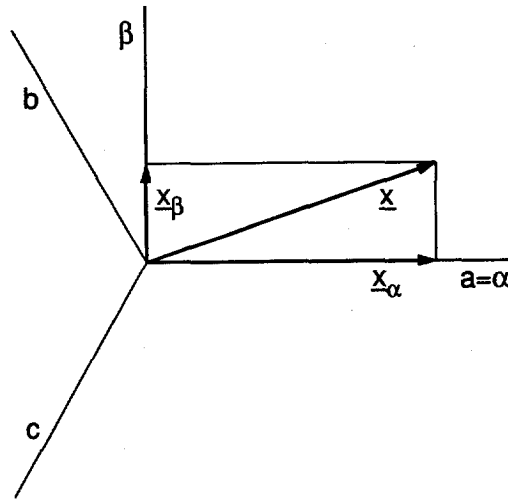


Fig. 2.5 Space phasor in α, β coordinate system

advantage expressed in α, β coordinate system. This coordinate system is linked with one of the axes of the a, b, c coordinate system. On Fig. 2.5, a and α axes are linked together.

The transformation of the coordinates between the a, b, c and the α, β frames of reference is defined by the transformation matrix $T_{\alpha, \beta}$ (2.13). This transformation is named *the Park transformation* known from the theory of AC electrical machines.

$$T_{\alpha, \beta} = \frac{2}{3} \begin{bmatrix} \cos(0) & \cos(\frac{2\pi}{3}) & \cos(\frac{-2\pi}{3}) \\ \sin(0) & \sin(\frac{2\pi}{3}) & \sin(\frac{-2\pi}{3}) \end{bmatrix} \quad (2.12)$$

By using a space phasor definition (2.11) for three-phase time-varying functions, the resulting phasor is also time varying. It is convenient to transform the obtained phasor to a coordinate system rotating with the same angular speed ω as the three-phase functions. This system is called the d, q coordinate system. It must be noted that the name of the coordinate system rotating with frequency ω comes from the theory of the electrical machine. The transformation of the phasor from the α, β to the d, q coordinate system shown in Fig. 2.6, is defined by the transformation matrix $T_{d, q}$:

$$T_{d,q} = \begin{bmatrix} \cos\theta & \sin\theta \\ -\sin\theta & \cos\theta \end{bmatrix} \tag{2.13}$$

where:

$$\theta = \int \omega dt \tag{2.14}$$

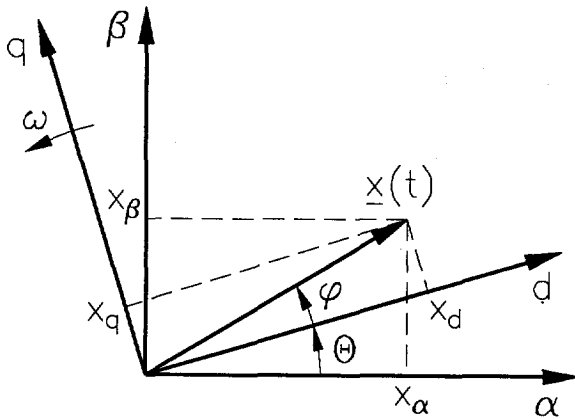


Fig. 2.6 Space phasor in d,q coordinate system

Transformation of the coordinates of the phasor from a,b,c to d,q coordinates is given by equation:

$$X_{d,q} = T_{d,q} T_{\alpha,\beta} X_{a,b,c} \tag{2.15}$$

The resulting space phasor appears in this new coordinate system as a stationary phasor (if x_i for $i=a,b,c$ is sinusoidal).

2.5 Switching space phasor

A *switching space phasor* is defined according to the definition of an instantaneous space phasor. This switching space phasor prescribes the configuration of a three-phase bridge:

$$\underline{s} = \frac{2}{3} [(S_{ap} - S_{an}) + (S_{bp} - S_{bn})e^{j\rho} + (S_{cp} - S_{cn})e^{-j\rho}] \tag{2.16}$$

The function S_{ij} for $i=a,b,c$ and $j=p,n$ prescribes the actual position of the switches in a three-phase switching bridge Fig. 2.1. Therefore, the resulting switching phasor \underline{s} (2.16) appears as stationary in the α,β coordinate system. The positions and amplitudes of the switching space phasors for current and voltage configurations are studied later.

The input and the output three-phase currents and voltages are also defined by space phasor definition:

$$\underline{u}_s = \frac{2}{3}(u_{sa} + u_{sb}e^{j\rho} + u_{sc}e^{-j\rho}) \quad (2.17)$$

$$\underline{i}_s = \frac{2}{3}(i_{sa} + i_{sb}e^{j\rho} + i_{sc}e^{-j\rho}) \quad (2.18)$$

$$\underline{u}_o = \frac{2}{3}(u_{oa} + u_{ob}e^{j\rho} + u_{oc}e^{-j\rho}) \quad (2.19)$$

$$\underline{i}_o = \frac{2}{3}(i_{oa} + i_{ob}e^{j\rho} + i_{oc}e^{-j\rho}) \quad (2.20)$$

where:

- \underline{u}_i - space phasor voltage,
 - \underline{i}_i - space phasor current,
 - u_{ij} - phase voltage,
 - i_{ij} - phase current,
 - s - AC side of rectifier (source),
 - o - AC side of inverter (output),
- for $i=s,o$ and $j=a,b,c$.

The obtained phasors of currents or voltages are in the α,β coordinate system rotary (rotating with an angular frequency of the three-phase voltages or currents) or stationary.

2.5.1 Current configuration

Using the notation of a switching bridge from Fig. 2.1 and considering the switching constraint defined in equation (2.3), a set of 7 switching space phasors can be defined. As stated in the introduction of this chapter, there are 6 active and meaningful switching states. The set of 6 switching phasors is presented in Table 2.1. The positions of the switching phasors in Table 2.1 are presented in Fig. 2.7.

The seventh phasor defined by the switching constraint (2.3) is a zero phasor \underline{s}_0 (Fig. 2.7), that means the real and imaginary values of the switching phasor are equal to zero. The zero phasor \underline{s}_0 prescribes two allowed switching states.

Table 2.1

n	Closed switches	Switching phasor \underline{s}_n	
1	S_{ap}, S_{cn}, S_{bp}	$\underline{s}_1 = 2/3 (1 + e^{j\rho} - e^{-j\rho})$	$2/3 (-2e^{-j\rho})$
2	S_{cn}, S_{bp}, S_{an}	$\underline{s}_2 = 2/3 (-1 + e^{j\rho} - e^{-j\rho})$	$2/3 (2e^{j\rho})$
3	S_{bp}, S_{an}, S_{cp}	$\underline{s}_3 = 2/3 (-1 + e^{j\rho} + e^{-j\rho})$	$2/3 (-2)$
4	S_{an}, S_{cp}, S_{bn}	$\underline{s}_4 = 2/3 (-1 - e^{j\rho} + e^{-j\rho})$	$2/3 (2e^{-j\rho})$
5	S_{cp}, S_{bn}, S_{ap}	$\underline{s}_5 = 2/3 (1 - e^{j\rho} + e^{-j\rho})$	$2/3 (-2e^{j\rho})$
6	S_{bn}, S_{ap}, S_{cn}	$\underline{s}_6 = 2/3 (1 - e^{j\rho} - e^{-j\rho})$	$2/3 (2)$

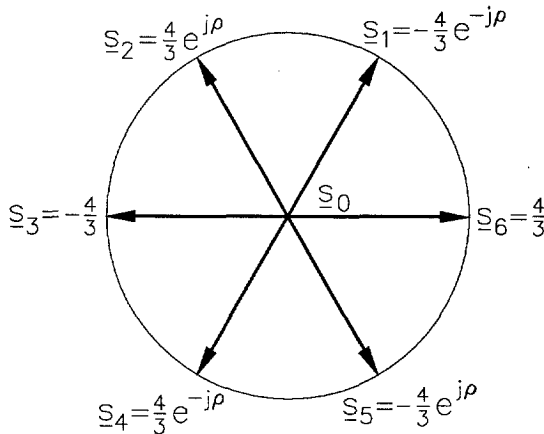


Fig. 2.7 Switching space phasors from Table 2.1 and zero phasor \underline{s}_0

The current configuration is applied for three-phase voltage source inverters and boost (current source) rectifiers, that means converters with current character of the AC side and voltage character of the DC side. The relation between the AC and the DC sides can be found in the case of an inverter (Fig. 2.1b) as a set of equations:

$$\underline{u}_o = \frac{1}{2} \underline{s} u_{dc} \tag{2.21}$$

$$i_{dc} = \frac{3}{4} \text{Re}\{\underline{s}^* \underline{i}_o\} \tag{2.22}$$

where:

- \underline{u}_o - space phasor of the AC voltages,
- i_{dc} - current in the DC link,

- i_o - space phasor of the AC current,
 u_{dc} - voltage of the DC side,
 \underline{s}_* - switching space phasor,
 \underline{s} - conjugate switching space phasor.

In the equations and the schematic shown in Fig. 2.1, the DC side is assigned although it is not a DC link as classically understood.

Proof of the equations (2.21) and (2.22):

In the following equations (2.21) and (2.22) are proved. If the switches S_{ap} , S_{bp} , S_{cn} of the three-phase switching bridge shown in Fig. 2.1b are closed, the adequate switching phasor $\underline{s}=\underline{s}_1$ according to Table 2.1 is:

$$\underline{s}_1 = -\frac{4}{3}e^{-j\rho} \quad (2.23)$$

According to the space phasor definition (2.12) the output voltage \underline{u}_o is:

$$\begin{aligned} \underline{u}_o &= \frac{2}{3}\left(\frac{1}{3}u_{dc} + \frac{1}{3}u_{dc}e^{j\rho} - \frac{2}{3}u_{dc}e^{-j\rho}\right) \\ &= -\frac{2}{3}e^{-j\rho}u_{dc} \\ &= \frac{1}{2}\underline{s}u_{dc} \end{aligned} \quad (2.24)$$

The result of equation (2.24) is identical to equation (2.21) which proves the validity of (2.21). The switching space phasor \underline{s} is a normalized phasor of the output voltages. Therefore, the graphic representation of the voltage phasor \underline{u}_o is in the same form as the graphic representation of the switching space phasor.

For the selected configuration, the link current is equal to the current in the odd phase, that means $i_{dc}=-i_{oc}$. Based on the defined equation (2.22) and the selected switching space phasor, equation (2.25) is obtained:

$$\begin{aligned} i_{dc} &= \frac{3}{4}\operatorname{Re}\{\underline{s}^*i_o\} \\ &= \frac{3}{4}\operatorname{Re}\left\{-\frac{4}{3}e^{j\rho}\frac{2}{3}(i_{oa}+i_{ob}e^{j\rho}+i_{oc}e^{-j\rho})\right\} \\ &= -\frac{2}{3}\operatorname{Re}\{i_{oa}e^{j\rho}+i_{ob}e^{2j\rho}+i_{oc}\} \\ &= -\frac{2}{3}\left(-\frac{1}{2}i_{oa}-\frac{1}{2}i_{ob}+i_{oc}\right) = -i_{oc} \end{aligned} \quad (2.25)$$

The graphic interpretation of equation (2.25) is depicted in Fig. 2.8. The position of the switching space phasors \underline{s} is in case of a current configuration identical with the position of the a, b, c axes. This is due to the fact that the a, b, c components of the switching space phasor in a current configuration are nonzero as summarized in (2.3). Then the phase of the switching space phasors $\underline{s}_1 \dots \underline{s}_6$ is equal to the integer multiple of ρ , which is identical to the phase of the a, b, c coordinates in α, β system. The phase of the switching phasors $\underline{s}_1 \dots \underline{s}_6$ is then the same as one of

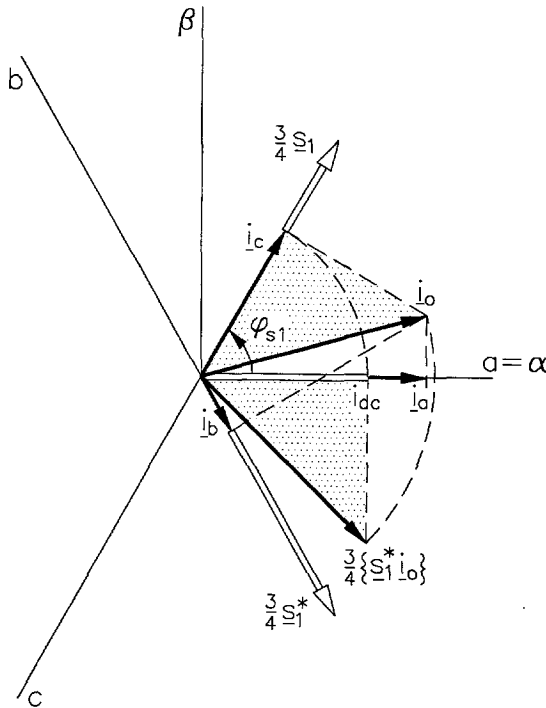


Fig. 2.8 Graphic interpretation of equation (2.25)

the coordinates a, b, c .

As a result of the multiplication, the space phasor of the current i_0 is rotated by the phase φ_{s1} of the conjugate of the selected switching space phasor s_1 . The switching space phasor s_1 is multiplied in Fig. 2.8 by the coefficient $3/4$ in order to obtain a phasor with a unity length. This coefficient is compensated in equation (2.22). Thus, the current space phasor i_0 is rotated by the phase of a conjugate of a switching space phasor but its amplitude stays the same. The real part of the resulting phasor $3/4\{s_1^* i_0\}$ performs the link current i_{dc} . In this particular case, the current i_{dc} is positive and equal to $-i_c$. The graphic solution automatically takes the right polarity because of the projection of the resulting phasor in the direction of each axis. By rotating the single triangle $i_c, i_0, 0$ by the phase angle φ_{s1} , the $i_c = -i_c e^{-j\varphi}$ enters the real axis.

The rotation of the current phasor i_0 with respect to the other switching phasors can be similarly documented. In Fig. 2.9, the current i_0 , switched by all possible switching phasors $s_1 \dots s_6$ for the current configuration, is depicted. Generally, by taking any space phasor of three-phase balanced currents, its components (phase currents) are projections in the a, b, c axes. By multiplying such a current phasor by the conjugate of any of the defined switching phasors, a projection to one of the

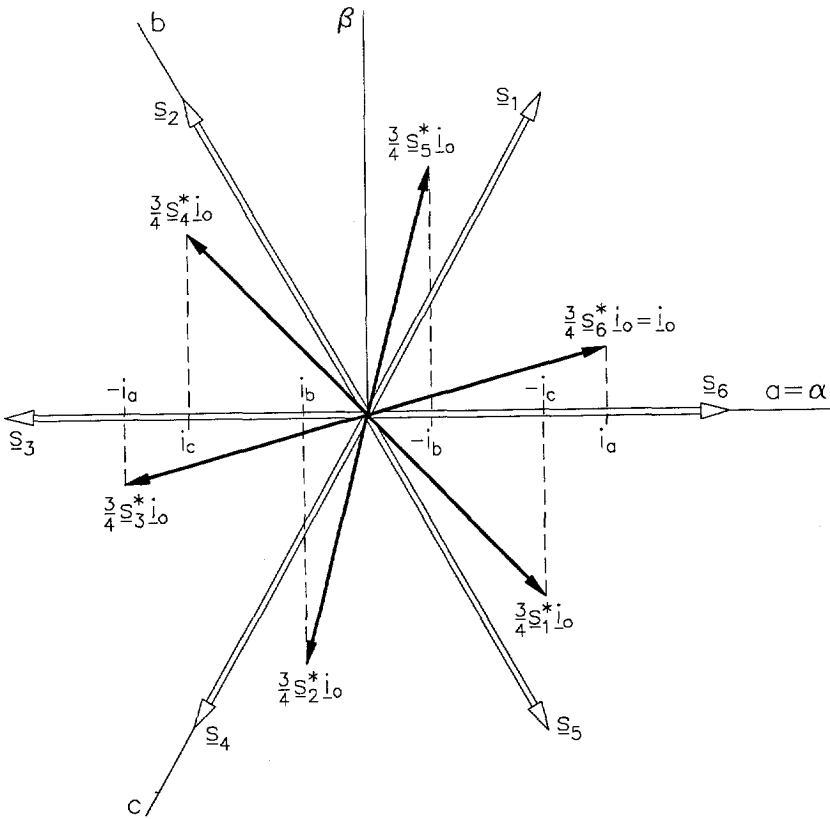


Fig. 2.9 Current i_{dc} with current configuration switching space phasors

coordinates a, b, c enters into a real axis. This is because the phase of the switching phasors is identical with the phase of the a, b, c coordinates. This means that the current i_{dc} is always equal to the absolute value of the current in one of the phases. This fact corresponds with the definition of a current configuration and proves the validity of the defined expressions for any current phasor.

In the case of a rectifier presented in Fig. 2.1a, the relation between the AC and the DC sides is as in equation (2.26):

$$i_{dc} = \frac{3}{4} \text{Re}\{\underline{s}^* \underline{i}_s\} \tag{2.26}$$

Because it is the same expression as in the case of an inverter, it does not require an additional proof.

2.5.2 Voltage configuration

A set of switching space phasors \underline{s}_n can be similarly defined also for voltage configuration. For the switching constraint defined in (2.4), it is the set of 6 switching space phasors of active states in Table 2.2.

Table 2.2

n	Closed switches	Switching phasor \underline{s}_n
1	S_{ap}, S_{cn}	$\underline{s}_2 = 2/3 (1 - e^{j\rho})$
2	S_{cn}, S_{bp}	$\underline{s}_3 = 2/3 (e^{j\rho} - e^{-j\rho})$
3	S_{bp}, S_{an}	$\underline{s}_4 = 2/3 (-1 + e^{j\rho})$
4	S_{an}, S_{cp}	$\underline{s}_5 = 2/3 (-1 + e^{-j\rho})$
5	S_{cp}, S_{bn}	$\underline{s}_6 = 2/3 (e^{-j\rho} - e^{j\rho})$
6	S_{ap}, S_{bn}	$\underline{s}_1 = 2/3 (1 - e^{-j\rho})$

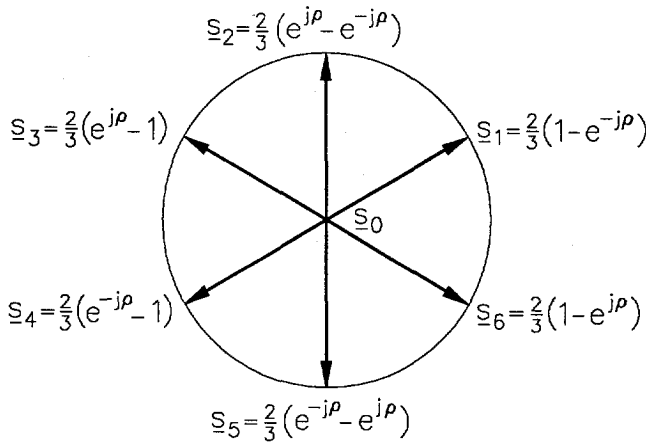


Fig. 2.10 Switching space phasors from Table 2.2 and zero phasor \underline{s}_0

The position of the switching space phasors from Table 2.2 is shown in Fig. 2.10. The seventh phasor defined by the switching constraint (2.4) is a zero phasor \underline{s}_0 (Fig. 2.10). The voltage configuration is applied for three-phase converters with a voltage character of the AC side and a current character of the DC side.

The relation between the AC and the DC sides of a rectifier in Fig. 2.1a can be found as:

$$u_{dc} = \frac{3}{2} \operatorname{Re}\{\underline{s}^* \underline{u}_s\} \quad (2.27)$$

$$\underline{i}_s = \underline{s} i_{dc} \quad (2.28)$$

Proof of equations (2.27) and (2.28):

Take for example the switching configuration with closed switches S_{ap} , S_{bn} . The resulting voltage u_{dc} in the link is then $u_{sa} - u_{sb}$:

$$\begin{aligned} u_{dc} &= \frac{3}{2} \operatorname{Re}\{\underline{s}^* \underline{u}_s\} \\ &= \frac{3}{2} \operatorname{Re}\left\{\frac{2}{3}(1 - e^{-j\rho}) \frac{2}{3}(u_{sa} + u_{sb}e^{j\rho} + u_{sc}e^{-j\rho})\right\} \\ &= (u_{sa} - \frac{1}{2}u_{sb} - \frac{1}{2}u_{sc} + \frac{1}{2}u_{sa} - u_{sb} + \frac{1}{2}u_{sc}) = u_{sa} - u_{sb} \end{aligned} \quad (2.29)$$

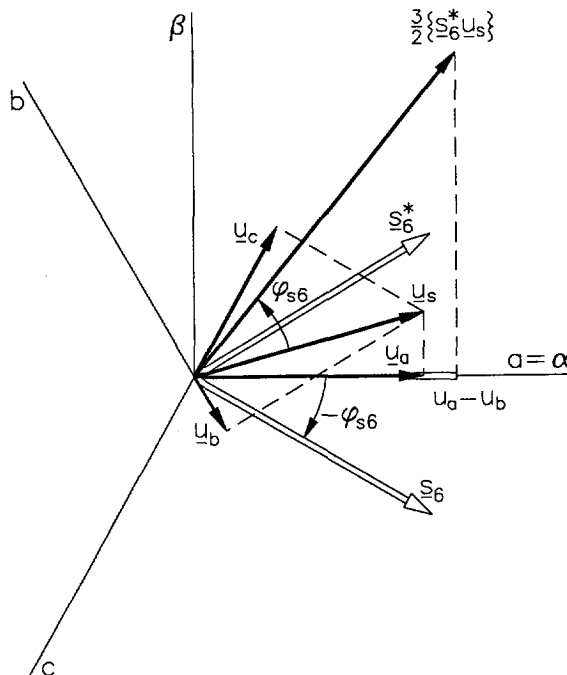


Fig. 2.11 Graphic interpretation of equation (2.29)

The graphic interpretation of equation (2.29) is depicted in Fig. 2.11. The phase of the switching space phasors is in the case of a voltage configuration different from the phase of the a, b, c axes. The modulus of the switching space phasor is $(2/3)\sqrt{3}$ (Table 2.2). The constant $2/3$ is compensated by the constant $3/2$ in

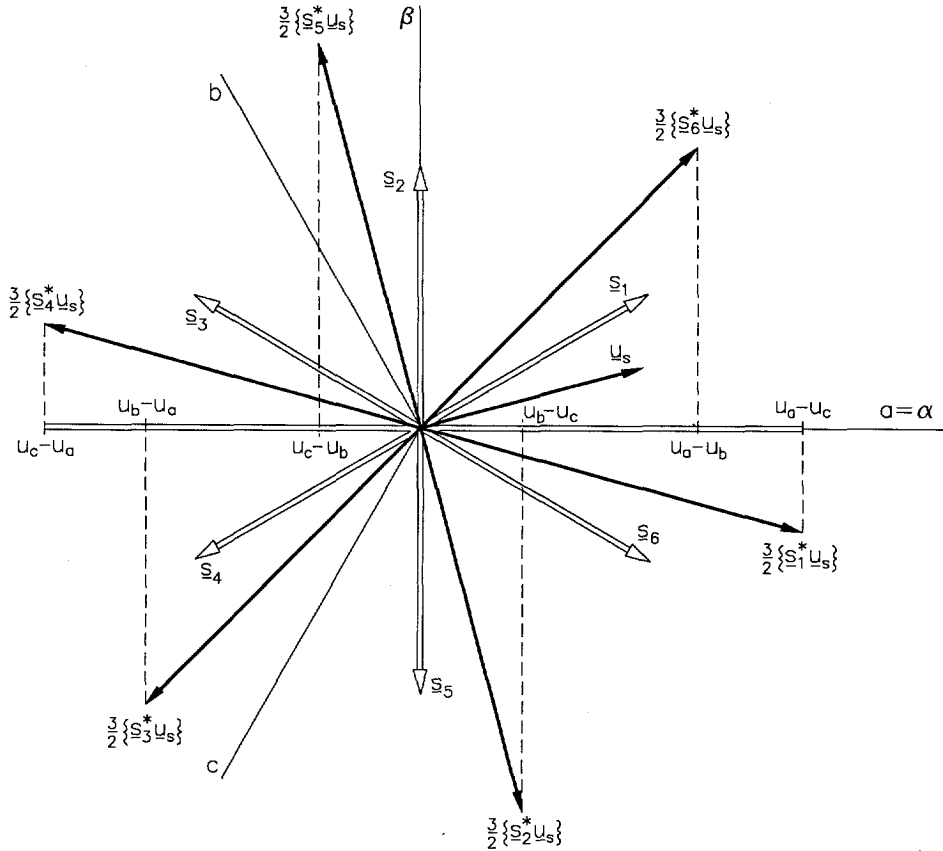


Fig. 2.12 Voltages of the link created from voltage \underline{u}_s with switching phasors of the voltage configuration

equation (2.27). The modulus of the switching space phasor shown in Fig. 2.11 is then $\sqrt{3}$. Thus the modulus of the voltage space phasor is increased by a factor $\sqrt{3}$. The switching space phasor modulus brings back the phase-line voltage relation. As known, the ratio between line and phase voltages for a three-phase system is equal to $\sqrt{3}$.

The phasor \underline{u}_s in Fig. 2.11 is rotated by the angle ϕ_{s6} of the conjugate of a selected switching space phasor \underline{s}_6 . The real part of the resulting phasor $\frac{3}{2}\{\underline{s}_6^* \underline{u}_s\}$ is the DC voltage of the link. The resulting voltage of a DC link using other switching phasors is depicted in Fig. 2.12. As in the previous case, the DC link voltage is given by projection of the resulting phasor in the real axis. In Fig. 2.11 all possibilities of creating a DC link voltage switching phasors $\underline{s}_1 \dots \underline{s}_6$ from a voltage source phasor \underline{u}_s are presented. As a result there are three DC voltages with positive polarity and three DC voltages with negative polarity.

The current in phase a and b is for the selected configuration identical to the current i_{dc} . The construction of the current space phasor \underline{i}_s according to the definition of the instantaneous space phasor results in:

$$\underline{i}_s = \frac{2}{3}(i_{dc} - i_{dc}e^{j\rho}) \quad (2.30)$$

According to equation (2.28), current phasor is equal to:

$$\underline{i}_s = \underline{s} i_{dc} = \frac{2}{3}(1 - e^{j\rho}) i_{dc} = \frac{2}{3}(i_{dc} - i_{dc}e^{j\rho}) \quad (2.31)$$

The obtained result is identical to equation (2.30) which proves the validity of equation (2.28). Since the switching space phasor is a normalized phasor of the source current \underline{i}_s , the graphic representation of the current phasor \underline{i}_s is identical to the switching space phasors from Fig. 2.10.

The same relations (2.27) and (2.28) between the AC and the DC sides are also valid for inverters with a current character of the DC side and a voltage character of the AC side. This is the case e.g. of a boost inverter. Let us investigate the case of an inverter (see Fig. 2.1b) with a voltage character of the DC side which applies a voltage configuration. The relation between the AC and the DC sides is as follows:

$$\underline{u}_o = \frac{1}{2} \underline{s} u_{dc} \quad (2.32)$$

$$i_{dc} = \frac{3}{4} \operatorname{Re}\{\underline{s}^* \underline{i}_o\} \quad (2.33)$$

Proof of equations (2.32) and (2.33):

For the same configuration of the switches S_{ap} , S_{bn} , the voltage phasor of the AC side is:

$$\underline{u}_o = \frac{2}{3} \left(\frac{1}{2} u_{dc} - \frac{1}{2} u_{dc} e^{j\rho} \right) \quad (2.34)$$

According equation (2.32) the voltage phasor is equal to:

$$\underline{u}_o = \frac{1}{2} \frac{2}{3} (1 - e^{j\rho}) u_{dc} \quad (2.35)$$

Once again, the graphical interpretation of the voltage phasors \underline{u}_o (2.32) is identical to the switching space phasors $\underline{s}_1 \dots \underline{s}_6$ from Fig. 2.7. The switching space phasor is a phasor of normalized voltages.

Similarly, the AC current with the closed switches S_{an} , S_{bn} is according to the space phasor definition equal to:

$$\underline{i}_o = \frac{2}{3}(i_{dc} - i_{dc}e^{j\rho}) \tag{2.36}$$

According to equation (2.33) the current in the link is equal to:

$$i_{dc} = \frac{3}{4} \operatorname{Re} \left\{ \frac{2}{3}(1 - e^{-j\rho}) \frac{2}{3} i_{dc}(1 - e^{j\rho}) \right\} = i_{dc} \tag{2.37}$$

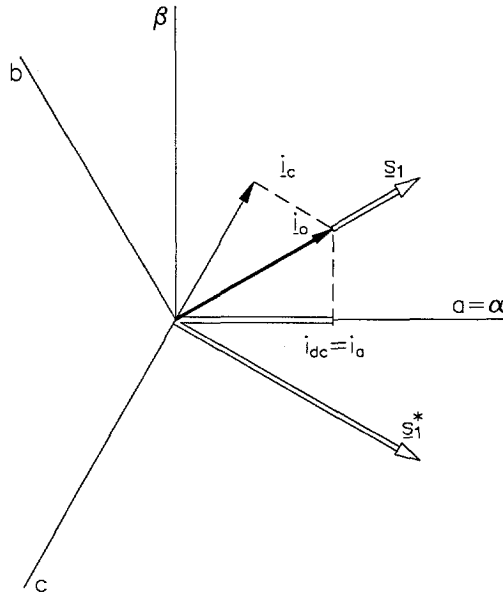


Fig. 2.13 Graphic interpretation of equation (2.37)

The phase of the current phasor \underline{i}_o is in this particular case equal to the phase of the switching phasor \underline{s}_1 (Fig. 2.13). The modulus of the phasor \underline{i}_o is $2/\sqrt{3}$ of the components of the phasor (phase currents). Since the modulus of the switching phasor is also $2/\sqrt{3}$, by multiplication, the resulting phasor has modulus $4/3$. This coefficient is compensated in equation (2.33) by coefficient $3/4$. The resulting phasor has a zero phase and the modulus is equal to the components of the phasor (phase currents). The phase of the selected switching space phasor is always identical to the phase of \underline{i}_o . Therefore, equation (2.33) can be rewritten in the form:

$$i_{dc} = \frac{3}{4} \underline{s}_1^* \underline{i}_o \tag{2.38}$$

Equation (2.38) is valid only for an inverter in a voltage configuration because the phase of the current phasor \underline{i}_o is identical to the phase of the selected switching phasor.

2.6 Instantaneous power in three-phase switching circuits

Nonlinear equations (2.21), (2.22), (2.26), (2.27), (2.28), (2.32) and (2.33) define the relation between the AC and the DC sides of a switching bridge with the use of a switching phasor. It is important to relate the obtained set of nonlinear equations to the power flow in the converter.

The conventional theory of active and reactive power in one phase of a three-phase system is based on an averaged value concept. It makes it impossible to define instantaneous active and reactive power in a real sense for three-phase circuits. Therefore, a new definition based on an instantaneous value concept has been proposed [Akagi, Nabae, 1984] and recently extended for nonsinusoidal conditions [Akagi, Nabae, 1993].

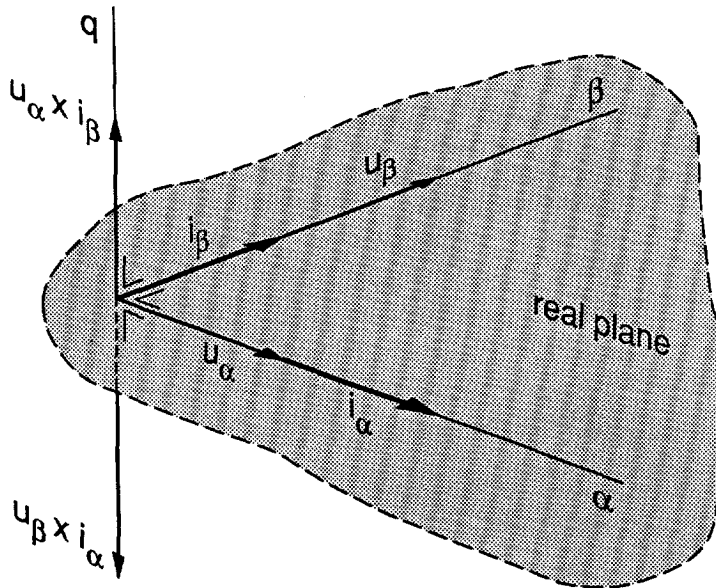


Fig. 2.14 Instantaneous space phasors of a three-phase system

The instantaneous power in a three-phase system is obtained from its three-phase voltages and currents as:

$$p = u_{sa}i_{sa} + u_{sb}i_{sb} + u_{sc}i_{sc} \quad (2.39)$$

The instantaneous power is defined in the α, β coordinates as:

$$p = \frac{3}{2}(u_{\alpha}i_{\alpha} + u_{\beta}i_{\beta}) \quad (2.40)$$

Similarly, in a d, q coordinate system the instantaneous power is equal to:

$$p = \frac{3}{2}(u_d i_d + u_q i_q) \quad (2.41)$$

Expressions coincide with the definition of the Park real component of the power [Ferrero, et.al., 1993].

The Park real component of the power and consequently the imaginary component of the power were introduced for the first time mainly to investigate the behaviour of a three-phase static compensator.

Fig. 2.14 shows the instantaneous space phasors of a power of a three-phase system in a vector diagram. The instantaneous imaginary part of the space phasor is defined as:

$$q = u_\alpha i_\beta - u_\beta i_\alpha \quad (2.42)$$

As shown in Fig. 2.14, the space phasor of the imaginary power is the imaginary axis phasor and is perpendicular to the real plane on the α, β coordinates. Considering that u_α is in parallel to i_α and u_β to i_β , and that u_α is perpendicular to i_β , and u_β to i_α , the conventional instantaneous power p and the instantaneous imaginary power q , which is the amplitude of space phasor \underline{q} , are expressed by:

$$\begin{bmatrix} p \\ q \end{bmatrix} = \frac{3}{2} \begin{bmatrix} u_\alpha & u_\beta \\ -u_\beta & u_\alpha \end{bmatrix} \begin{bmatrix} i_\alpha \\ i_\beta \end{bmatrix} \quad (2.43)$$

The instantaneous complex power is then defined as:

$$\underline{a} = \frac{3}{2} \underline{u}_{ac} * \underline{i}_{ac} \quad (2.44)$$

where:

\underline{u}_{ac} - Park voltage phasors of AC voltages (\underline{u}_s or \underline{u}_o),
 \underline{i}_{ac} - Park current phasors of AC phasors (\underline{i}_s or \underline{i}_o).

The instantaneous real power is defined as :

$$p = \text{Re}\{\underline{a}\} = \frac{3}{2} \text{Re}\{\underline{u}_{ac} * \underline{i}_{ac}\} \quad (2.45)$$

The physical interpretation of the instantaneous real and imaginary part is given in [Akagi, Nabae, 1993]. It is possible to prove that the instantaneous imaginary power, also identified as reactive power, does not contribute to the power flow between the input and output of the converter.

Equation (2.43) results into the following equation:

$$\begin{bmatrix} i_\alpha \\ i_\beta \end{bmatrix} = \frac{2}{3} \begin{bmatrix} u_\alpha & u_\beta \\ -u_\beta & u_\alpha \end{bmatrix}^{-1} \begin{bmatrix} p \\ q \end{bmatrix} \quad (2.46)$$

The instantaneous currents i_α and i_β in the α, β coordinate system are separated into two different instantaneous current components:

$$\begin{aligned} \begin{bmatrix} i_\alpha \\ i_\beta \end{bmatrix} &= \frac{2}{3} \begin{bmatrix} u_\alpha & u_\beta \\ -u_\beta & u_\alpha \end{bmatrix}^{-1} \begin{bmatrix} p \\ 0 \end{bmatrix} + \frac{2}{3} \begin{bmatrix} u_\alpha & u_\beta \\ -u_\beta & u_\alpha \end{bmatrix}^{-1} \begin{bmatrix} 0 \\ q \end{bmatrix} \\ &\equiv \frac{2}{3} \begin{bmatrix} i_{\alpha p} \\ i_{\beta p} \end{bmatrix} + \frac{2}{3} \begin{bmatrix} i_{\alpha q} \\ i_{\beta q} \end{bmatrix} \end{aligned} \quad (2.47)$$

$i_{\alpha p}$ is the α -axis instantaneous active current:

$$i_{\alpha p} = \frac{u_\alpha}{\frac{2}{u_\alpha} + \frac{2}{u_\beta}} p \quad (2.48)$$

$i_{\alpha q}$ is the α -axis instantaneous reactive current:

$$i_{\alpha q} = \frac{-u_\beta}{\frac{2}{u_\alpha} + \frac{2}{u_\beta}} q \quad (2.49)$$

$i_{\beta p}$ is the β -axis instantaneous active current:

$$i_{\beta p} = \frac{u_\beta}{\frac{2}{u_\alpha} + \frac{2}{u_\beta}} p \quad (2.50)$$

$i_{\beta q}$ is the β -axis instantaneous reactive current:

$$i_{\beta q} = \frac{u_\alpha}{\frac{2}{u_\alpha} + \frac{2}{u_\beta}} q \quad (2.51)$$

Let the instantaneous power in the α -axis and β -axis be p_α and p_β , respectively. They are given by the following expression:

$$\begin{bmatrix} p_\alpha \\ p_\beta \end{bmatrix} = \begin{bmatrix} u_\alpha & i_\alpha \\ u_\beta & i_\beta \end{bmatrix} = \begin{bmatrix} u_\alpha & i_{\alpha p} \\ u_\beta & i_{\beta p} \end{bmatrix} + \begin{bmatrix} u_\alpha & i_{\alpha q} \\ u_\beta & i_{\beta q} \end{bmatrix} \quad (2.52)$$

The instantaneous real power in the three-phase circuit p is expressed by equation

(2.53) by using the equations (2.47) and (2.52):

$$\begin{aligned}
 p &= p_{\alpha} + p_{\beta} \\
 &= \left[\frac{u_{\alpha}^2}{u_{\alpha}^2 + u_{\beta}^2} p + \frac{u_{\beta}^2}{u_{\alpha}^2 + u_{\beta}^2} p \right] + \left[\frac{-u_{\alpha} u_{\beta}}{u_{\alpha}^2 + u_{\beta}^2} q + \frac{u_{\alpha} u_{\beta}}{u_{\alpha}^2 + u_{\beta}^2} q \right]
 \end{aligned} \tag{2.53}$$

The sum of the third and fourth term on the right side of equation (2.53) is zero. We obtain then the following equations:

$$\begin{aligned}
 p &= u_{\alpha} i_{\alpha p} + u_{\beta} i_{\beta p} \equiv p_{\alpha p} + p_{\beta p} \\
 0 &= u_{\alpha} i_{\alpha q} + u_{\beta} i_{\beta q} \equiv p_{\alpha q} + p_{\beta q}
 \end{aligned} \tag{2.54}$$

Inspection of equation (2.54) leads to the following essential conclusions.

1. The sum of the instantaneous power $p_{\alpha p}$ and $p_{\beta p}$ coincides with instantaneous real power in a three-phase circuit. Therefore, $p_{\alpha p}$ and $p_{\beta p}$ are named instantaneous active power.
2. The instantaneous power $p_{\alpha q}$ and $p_{\beta q}$ cancel each other out and have no contribution to the instantaneous power flow from the source to the load. Therefore, $p_{\alpha q}$ and $p_{\beta q}$ are named instantaneous reactive power.

If there are neither storage components nor losses in the static power converter, the following relationship exists between the instantaneous imaginary power q_s on the input side and the instantaneous imaginary power on the output side q_o :

$$q_s \neq q_o \tag{2.55}$$

The instantaneous powers have no contribution to the instantaneous power flow from the source to the load. To the contrary, the following relationship is valid for the instantaneous real power p_s on the input side and instantaneous real power p_o on the output side of the converter:

$$p_s = p_o \tag{2.56}$$

With the use of equation (2.45), the following expression is valid for the power balance between the AC and the DC sides of the three-phase bridge:

$$\frac{3}{2} \operatorname{Re}\{ \underline{u}_{ac}^* \underline{i}_{ac} \} = \frac{3}{2} \operatorname{Re}\{ \underline{u}_{ac} \underline{i}_{ac}^* \} = u_{dc} i_{dc} \tag{2.57}$$

The model of the bridge is shown in Fig. 2.15.

Based on the power balance equation, all relations between the AC and DC sides can be reviewed. The relation between the AC and DC sides was defined for

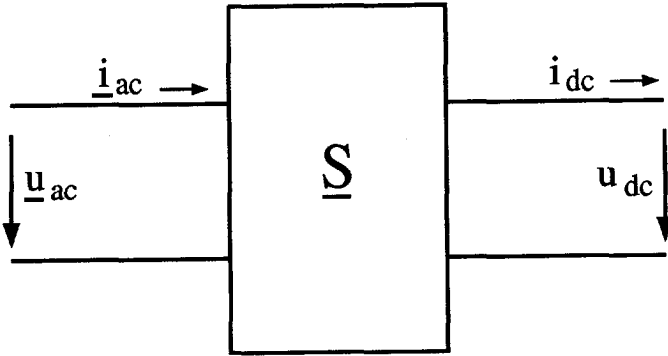


Fig. 2.15 Switching space phasor model of the switching bridge

current configuration as (2.21) and (2.20). By eliminating the switching space phasor \underline{s} , the power balance equation is obtained:

$$u_{dc}i_{dc} = \frac{3}{2} \operatorname{Re}\{\underline{u}_{ac}^* \underline{i}_{ac}\} \quad (2.58)$$

For a voltage configuration, the relation between the AC and the DC sides for a rectifier is (2.27) and (2.28) and for an inverter (2.32) and (2.33). Both sets are in coincidence with the power balance equation. The difference between the set of equations for a rectifier and an inverter is in the control mechanism. In the case of a rectifier, the given quantity is the AC line voltage \underline{u}_s . The DC voltage is a result of the action of the control phasor \underline{s} as well as the AC current. In the case of an inverter, the given input quantity is the DC bus voltage. The AC voltage and the DC current are obtained as the result of an action of the control phasor \underline{s} .

2.7 Relation between switching leg function and switching space phasor

Two different models of a three-phase switching bridge are defined. The model of a switching bridge leg represents the bridge with three *switching functions* $\delta_i(t)$ for $i=a,b,c$. The model of a *switching space phasor* represents the three-phase switching bridge with one space phasor \underline{s} .

The question remains as to whether there is a relation between these models. Let us assume that the design of a modulation process is provided on the base of both models. By determining three switching functions $\delta_i(t)$ ($i=a,b,c$) and with switching strategy applied to each switching function separately, the configuration of a three-phase switching bridge is determined. With the use of the transformation matrix $T_{\alpha,\beta}$ (2.13), a space phasor can be constructed. The obtained phasor will

be one from the set presented in Chapter 2.5. Derivation of a space phasor from three switching functions is thus straightforward and unique.

The model of a switching bridge with a switching space phasor assumes that a switching bridge configuration is represented by a space phasor. Let us assume that as a result of the dynamic equations, an arbitrary switching space phasor is calculated. The transformation matrix between a, b, c and d, q respectively α, β coordinates has two rows and three columns. The switching function for each switching leg is the subject of our interest. Calculating d, q respectively α, β coordinates of the arbitrary switching space phasor does not allow a unique selection of a switching space phasor and this way solution for $\delta_i(t)$ ($i=a, b, c$). When the switching strategy is decided (PWM, PFM, hysteretic control, sliding mode), there is no unique solution too, as will be shown in Chapter 6 for sliding mode. Additional constraints must be added to overcome this ambiguity in the switching pattern. This additional degree of freedom (or redundancy) explains why there is a possibility to create the required (calculated) switching space phasor in an unlimited number of ways. Comparing it to the model of the switching bridge leg, this results in a unique solution. The mentioned redundancy gives room for the switching pattern selection and optimization.

2.8 Conclusions

A mathematical model for the three-phase switching bridge has been recommended. Two different classes of configurations for a three-phase switching bridge have been defined:

- *current configuration*
- *voltage configuration.*

The switching constraint of the semiconductor switches defines the configuration. Two mathematical models have been described for both configurations.

The first mathematical model is a *switching function* of a switching leg. The switching leg contains two semiconductor switches and is a basic unit connecting one phase of a three-phase system with a link. The mathematical expression prescribing the relation between the AC and the DC sides of a switching leg contains the switching function of all three switching legs. Therefore, the operation of one leg is not completely independent and it is influenced by the position of the switches of two additional legs.

The second model is a *space phasor* representation for the three-phase switching bridge. The application of the space phasor representation for the three-phase switching bridge has been studied. Relations between the AC and the DC side of the three-phase switching bridge have been found and proved. The defined relations correlate with the power flow in the three-phase circuits and the power flow in the converter. The defined relations coincide with the power balance.

The link between the switching function model and the space switching phasor has been established. On the basis of the obtained equations, the dynamic equations for a three-phase-to-three-phase converter can be obtained as routine work. The defined relations allow the writing of a set of differential equations for the investigated topology without going into topological details. The required dynamic analysis and synthesis are based on the obtained set of equations.

3

PWM AC CONVERTERS

3.1 Introduction

Pulse-width modulation techniques (PWM) for AC power converters have been the subject of intensive research throughout the last two decades. A wide variety of methods, different in concept and performance, has been developed and described. Several authors have studied the aspects of PWM modulation in detail. The applied performance criterion is the harmonic spectrum of the implemented PWM: the harmonics content of the current and torque. A comprehensive review of PWM methods can be found in recent papers [Holtz, 1992, 1993]. The best known method is *the carrier modulation feedforward method*, which is treated in this chapter.

A method of dynamic analysis is provided. The setting up of the dynamic analysis of the converter with a three-phase switching bridge with the use of the mathematical model as defined in Chapter 2 is reported. Based on the obtained dynamic model, the process of modulation is analysed. It is shown that the modulations under study are open-loop. Transfer functions of a converter's behaviour are matters of interest. In the realized dynamic analysis there are two types of transfer functions that are interesting to know when designing a controller:

1. *control-to-output*
The *control-to-output* transfer function determines how the variation in the switching time influences the output waveforms.
2. *input-to-output*
The *input-to-output* transfer function determines how the variation of an independent source effects the output waveforms.

The terms output and input need a more precise explanation. Their interpretation is not so obvious as in the case of DC-to-DC power converters. Therefore, this problem is also treated later.

As stated in Chapter 1, two basic problems are recognized in the analysis of AC converters.

1. The system is discontinuous due to the switching behaviour. It is not possible to employ the method of averaging applied to DC-to-DC converter analysis.
2. The steady-state waveforms are time-varying waveforms. Therefore, the dynamic model cannot be obtained by linearization.

First, the topology of AC-to-DC and DC-to-AC power conversion and their basic control principles are explored. Then the solution for the above-stated problems is suggested and documented in examples.

3.2 AC-to-DC and DC-to-AC PWM converters

Topologies for AC-to-DC and DC-to-AC three-phase power converters

There are two basic topologies: the topology with the DC voltage link and the topology with the DC current link. The duality of the DC voltage link and the DC current link is well known. Only the DC voltage link converters are studied since the solution for a current link is dual.

Two conventional PWM converters widely used in three-phase AC-to-DC applications are: the three-phase buck rectifier with a second-order filter (Fig. 3.1) and the three-phase boost rectifier with a source-side inductor (Fig. 3.2). Depending on the pulse modulation process, both converters provide a source current with reduced low-frequency harmonics. In the boost topology, the continuous source current minimizes the requirements for additional filtering. In the buck converter a source filter is necessary to eliminate the switching frequency harmonics. The buck power converter shown in Fig. 3.1 applies a second-order filter but also higher order filters are applicable. The three-phase AC-to-DC buck converter applies a *voltage configuration* to transfer energy from the AC side to the DC side or vice versa. The three-phase AC-to-DC boost converter applies a *current configuration* to transfer energy from the AC side to the DC side or vice versa.

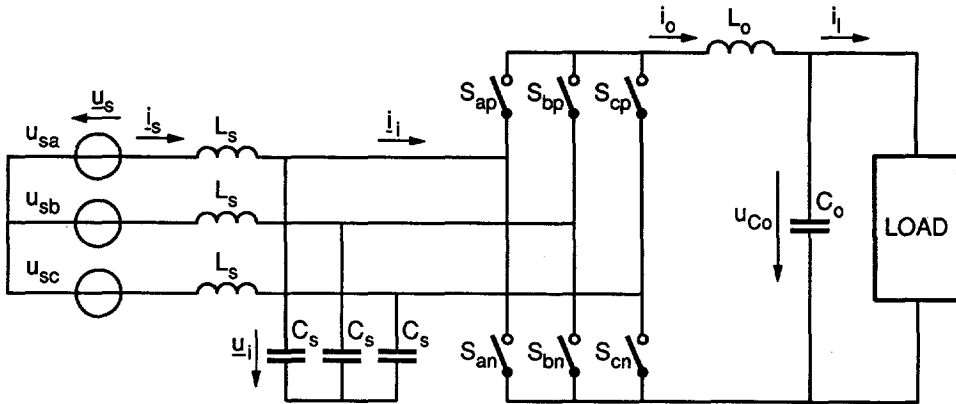


Fig. 3.1 Three phase AC-to-DC buck converter

The configuration of the DC-to-AC power converter is similar. A diagram of a voltage source inverter with output filters is shown in Fig. 3.3. A diagram of a current controlled voltage source inverter is shown in Fig. 3.4. The voltage phasor \underline{u}_o in both cases is defined with respect to the middle point of the load connected in the star configuration.

Control principles and definition of the input and output

Although a rectifier and an inverter have identical circuit topologies, the control mechanisms are different. In the inverter control scheme, the input quantity is the

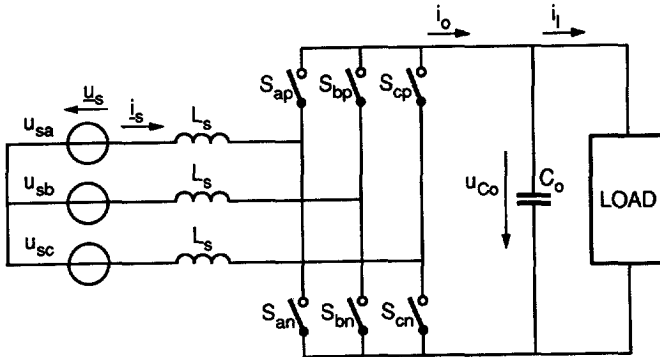


Fig. 3.2 Three phase AC-to-DC boost rectifier

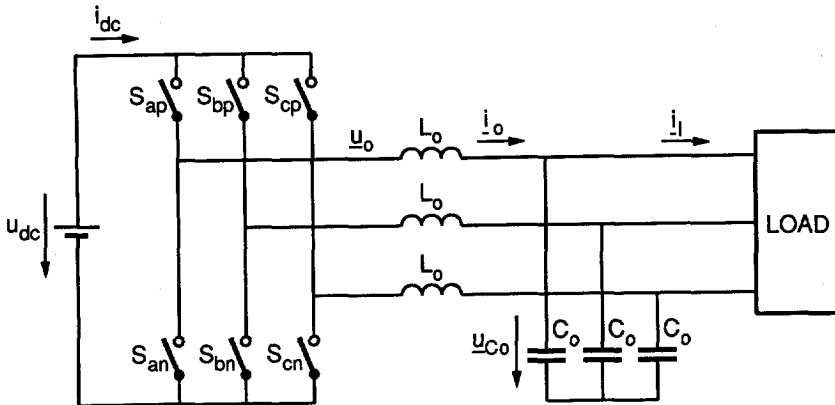


Fig. 3.3 Voltage source inverter

DC-bus voltage (voltage of the DC link) and the controlled quantity is the AC side voltage (or current). Consequently, the output quantities are defined as the harmonic components of the AC voltage and current. In a rectifier, the input quantity is the AC line voltage and the controlled quantity is usually the DC-bus voltage and the harmonic content of the AC line current. This means that the input quantity is the AC voltage and the output is the DC voltage or current and the harmonic contents of AC currents. In both cases the control is performed by the function of the pulse modulator. Due to the large number of existing modifications of PWM, it serves no purpose to make a survey of PWM methods. The first selection criteria of a PWM method are the possible power of an applied converter and the related switching frequency. The harmonic distortion of the AC currents reduces almost linearly with the switching frequency. Yet the switching frequency cannot deliberately be increased for the following reasons:

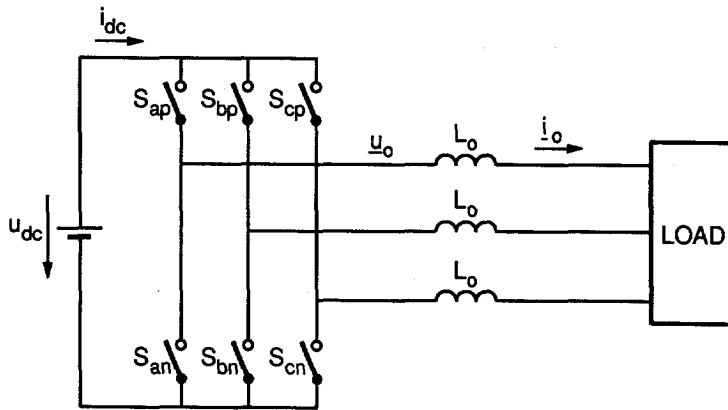


Fig. 3.4 Current controlled voltage source inverter

1. The switching losses of semiconductor devices increase proportionally to the switching frequency.
2. Semiconductor switches for higher power generally produce higher switching frequency losses. This limits the switching frequency for bipolar transistors and IGBT modules for higher power rating to a few kHz. The maximum switching frequency for GTOs is only a few 100 Hz. The problem of switching losses is treated in detail in Chapter 4.

The investigated PWM methods are feedforward modulation methods operating at switching frequencies up to 10 kHz and applied for low and medium power levels. The situation differs at power levels above 1 MW, where the harmonic elimination method is used almost exclusively and the switching frequency is maintained well below 500 Hz.

The most popular control strategies for PWM feedforward modulated converters are methods based on *carrier modulation*:

- *suboscillation carrier PWM*,
- *space phasor PWM*.

3.2.1 Suboscillation carrier PWM

Many PWM techniques have been presented and the sinusoidal PWM has become quite common. The analog implementation of the suboscillation carrier PWM is realized by a triangular carrier waveform u_{saw} that is being compared with a sinusoidal reference signal u_{ref} . The crossover points determine the instants of commutation of the semiconductor switches as shown by the voltage u_o in Fig. 3.5.

The amplitude of the fundamental output voltage varies according to the modulation index. Modulation index is defined as the ration of the reference sinusoid u_{ref} and the fundamental voltage of the six step waveform [Holtz, 1992]. If the modulation index is less than unity, except the basic harmonics, only carrier frequency harmonics with fundamental related side bands appear at the output. The voltage can be increased beyond the modulation index of unity until the maximum voltage is obtained in the square wave mode.

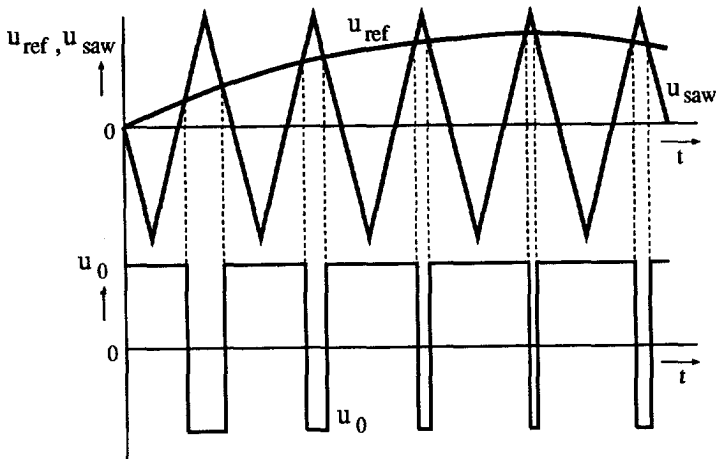


Fig. 3.5 Suboscillation carrier PWM

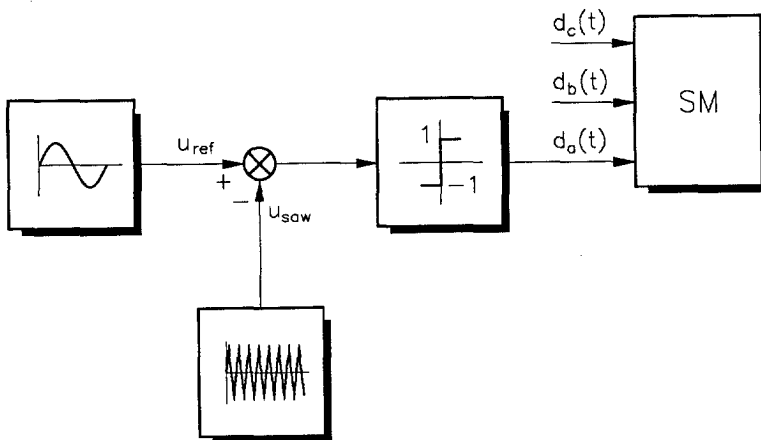


Fig. 3.6 Signal flow diagram for PWM modulator of one phase

The suboscillation method employs individual modulators for each of the three

phases as shown in Fig. 3.6. Due to the individual modulation, asymmetry can arise in a three-phase circuit but this is not studied here.

Since the modulator for each phase works independently, the model of a switching leg defined in Chapter 2 is suitable. The carrier reference u_{ref} can be modulated in several ways and the presented example illustrates only the principle.

3.2.2 Space phasor PWM

A different approach to PWM modulation is based on the space phasor presentation of the reference and inverter (rectifier) voltages. Since this method of modulation is also identified as *space vector modulation*, this terminology can also be used. However, the term *phasor* is more appropriate since the results are presented in a d, q reference frame. The name *vector* commonly used in literature is therefore not really appropriate.

PWM modulation generated in a space phasor representation has the advantage of lower harmonics and a possible higher modulation index than the three-phase suboscillation PWM method [Holtz, 1992]. Since the space phasor modulation is more suitable for a digital implementation than the carrier modulation, it is gaining more popularity.

Because of the space phasor representation of AC voltages and currents, the model of a switching bridge with a switching space phasor is suitable. The space phasor modulation technique averages three consecutive switching state phasors over an interval of a switching cycle T_{sw} . The reference switching phasor \underline{s}_{ref} is realized by computing the duty ratios (fraction of the switching period) for two switching phasors \underline{s}_k and \underline{s}_{k+1} :

$$\underline{s}_{ref} T_{sw} = \underline{s}_k T_k + \underline{s}_{k+1} T_{k+1} \tag{3.1}$$

where:

- \underline{s}_{ref} - reference switching phasor for PWM,
- $\underline{s}_k, \underline{s}_{k+1}$ - switching phasor of k and $k+1$ switching interval,
- T_k, T_{k+1} - time interval spent on \underline{s}_k and \underline{s}_{k+1} , respectively.

To keep the switching frequency constant, the remaining part T_0 of the switching period T_{sw} is spent on the zero state. This means:

$$T_0 = T_{sw} - T_k - T_{k+1} \tag{3.2}$$

where:

- T_{sw} - switching period of PWM,
- T_k - interval with phasor \underline{s}_k ,
- T_{k+1} - interval with phasor \underline{s}_{k+1} ,
- T_0 - interval with zero phasor.

The reference switching phasor $\underline{s}_{\text{ref}}$ composed of two adjacent switching phasors $\underline{s}_1, \underline{s}_2$ is depicted in Fig. 3.8. The decomposition of the reference switching phasor $\underline{s}_{\text{ref}}$ into existing phasors is possible in general in unlimited number of ways.

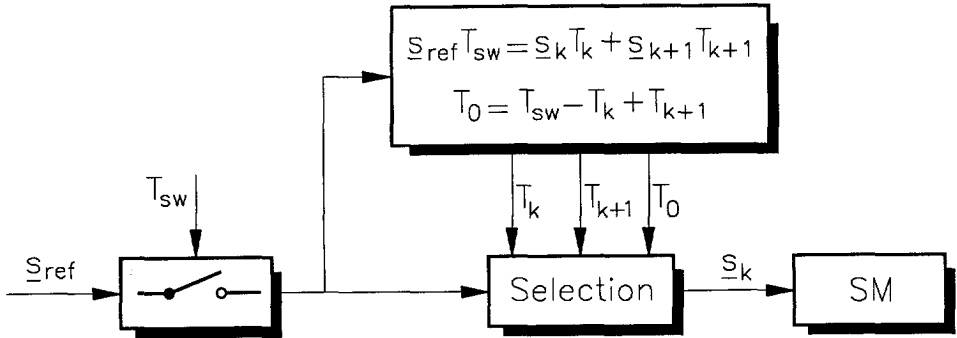


Fig. 3.7 Space switching phasor modulation principle

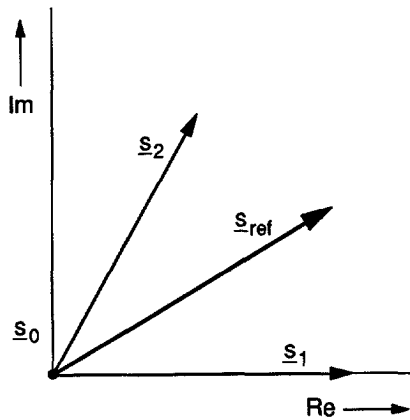


Fig. 3.8 Space phasor PWM

In the literature [Holtz, 1992], [Profumo, 1992], the space phasor modulation is explained with the use of voltage phasors. This means that not a *reference switching phasor* is accomplished by modulation, but an inverter *voltage phasor* or rectifier *current phasor*. Further explanation of the modulation process in the above-mentioned literature does not differ from the method defined in Fig. 3.7.

The inverter voltage phasors for current configuration are:

$$\begin{aligned} \underline{u}_0 &= \frac{2}{3} U_{dc} e^{\frac{jk\pi}{3}} & k=1,2,\dots,6 \\ \underline{u}_0 &= 0 & k=0,7 \end{aligned} \quad (3.3)$$

where:

\underline{u}_0 - voltage phasor of the inverter output,
 U_{dc} - inverter DC link voltage.

The obtained phasors coincide with equation (2.21) and Table 2.1 as presented in Chapter 2. In practice, there is no difference if the switching phasor or current or voltage phasors are modulated. The model of the switching bridge links the switching phasor with current or voltage phasor. However, the modulation as it is defined here is more general and is valid for all configurations (current and voltage) and rectifier and inverter as well. Therefore, Fig. 3.7 and Fig. 3.8 illustrate all space phasor methods.

3.2.3 Summary of control principles

A survey of topologies for the three-phase AC-to-DC and DC-to-AC power converters is presented. Pulse-width modulation methods are applied to modulate AC waveforms. The best known PWM methods are revealed: *suboscillation carrier PWM* and *space phasor PWM*.

For the method *suboscillation carrier PWM*, the mathematical model for a switching leg is suitable, because each individual phase of a three-phase system operates individually.

For *space phasor modulation*, a space phasor model of a three-phase bridge is eligible.

Because the mathematical models differ for two modulation methods, a further analysis is now separately executed.

First, a space phasor modulation is studied. Two problems concerning the analysis of AC power converters are defined in Introduction 3.1: the discontinuous switching behaviour of power converters and time varying waveforms in the steady state. To perform a dynamic analysis and to develop the required transfer functions, the mentioned problems must be solved. First, a general theoretical solution is given and then it is documented with reference to an example of a space phasor modulated AC-to-DC power converter.

The same steps are performed for the modulation methods based on a mathematical model of a switching bridge leg.

3.3 Space phasor PWM in rotating reference frame

The mathematical model of a space phasor modulated PWM AC converter with the use of a switching space phasor as defined in Chapter 2 is established. AC voltages and currents of the converter are presented by space phasors.

In general, the behaviour of the AC power stage of any converter with space phasor modulation is represented by a nonlinear state equation:

$$\frac{d\underline{x}}{dt} = F(\underline{x}, \underline{u}, \underline{s}(t)) \quad (3.4)$$

where:

- \underline{x} - phasor of the state variables usually formed by inductor currents and capacitor voltages,
- \underline{u} - phasor of AC voltages,
- $\underline{s}(t)$ - discontinuous switching phasor,
- $F()$ - function of the variables.

The general form of equation (3.4) depends on the converter topology. Since the modulation of the converter waveforms is an open-loop modulation and $\underline{s}(t)$ is a precalculated function, expression (3.4) can be expanded into a Fourier series:

$$\underline{s}(t) = \sum_{k=-\infty}^{\infty} \underline{s}_k e^{jk\omega t} \quad (3.5)$$

$$\underline{s}_k = \frac{1}{T} \int_0^T \underline{s}(t) e^{-jk\omega t} dt \quad (3.6)$$

$$\omega = \frac{2\pi}{T} \quad (3.7)$$

where:

- T - period of modulated fundamental harmonics,
- \underline{s}_k - Fourier coefficient of the k th harmonics ($k = -\infty, \dots, 0, \dots, \infty$),
- ω - angular frequency of modulated fundamental harmonics.

By substituting (3.5) in (3.4), the obtained model contains a continuous Fourier series representation of a switching phasor $\underline{s}(t)$. The dominant coefficient is observed for the frequency ω , which is the low-frequency component of the PWM. In the following, only the fundamental harmonics term $s_1 e^{j\omega t}$ is considered.

The phasor of the state variables $\underline{x}(t)$ of the AC side and the phasor of the AC

voltages are periodic functions of the angle ωt in the steady state:

$$\underline{x}(t) = X e^{j\omega t} \tag{3.8}$$

$$\underline{u}(t) = U e^{j\omega t} \tag{3.9}$$

This property allows the rotation of the set (3.4) into a complex d,q reference frame rotating with an angular speed ω . The defined space phasor modulation is open-looped with a possible use of feedforward. The modulation is based on the assumption that the system is in the cyclic steady-state. The reference switching phasor is calculated by inserting equations (3.8) and (3.9) into (3.4). The derivative of the phasor \underline{x} contains only the steady-state term:

$$\frac{d\underline{x}(t)}{dt} = j\omega X e^{j\omega t} \tag{3.10}$$

After transformation to the d,q reference frame, a linear equation is obtained and the reference switching phasor can be calculated from:

$$\underline{s}_{ref} = F(X, U, \omega) \tag{3.11}$$

The term of the input source U performs feedforward. After changing the source voltage, the reference phasor reach another values.

To perform the dynamic analysis and to develop the transfer functions, the phasors cannot be considered in the steady-state. The space phasor is therefore defined as:

$$\underline{x}(t) = \underline{X}(t) e^{j\omega t} \tag{3.12}$$

where:

$\underline{X}(t)$ - time-varying complex quantity.

The derivative of the phasors is then performed in a rotating reference frame as introduced in Chapter 2:

$$\frac{d\underline{x}(t)}{dt} = \frac{d}{dt} (\underline{X}(t) e^{j\omega t}) = \frac{d\underline{X}(t)}{dt} e^{j\omega t} + j\omega \underline{X}(t) e^{j\omega t} \tag{3.13}$$

where :

$\underline{X}(t)$ - phasor \underline{x} in a complex d,q coordinate system.

Derivation of the phasor (3.12) contains a steady-state term that is also present in the equation (3.10) and a transient term. It means, that a dynamic model of the converter in the d,q reference frame can be obtained. The steady-state term is constant and the model reflects the dynamics of the converter parameters. The

state equation (3.4) is changed by the explained procedure into equation:

$$\frac{d\underline{X}(t)}{dt} = F(\underline{X}(t), \underline{U}(t), \underline{S}(t)) \quad (3.14)$$

After splitting the complex quantity into a real and an imaginary part, we get :

$$\begin{aligned} \frac{dx_d(t)}{dt} &= F(x_d(t), x_q(t), u_d(t), u_q(t), s_d(t), s_q(t)) \\ \frac{dx_q(t)}{dt} &= F(x_d(t), x_q(t), u_d(t), u_q(t), s_d(t), s_q(t)) \end{aligned} \quad (3.15)$$

All terms at the right hand side of equation (3.15) are functions of the time and they are constant for the steady state. This equation is equivalent to the state space equation of a DC-to-DC power converter on which a method of averaging was performed. This means that both analysis methods for AC power converters and DC-to-DC power converters are calculated equivalently. After linearization of equation (3.15) around the steady-state point of operation, the small-signal dynamic model is obtained and the required transfer function is calculated. This procedure is documented on the example of a three-phase AC-to-DC buck power converter.

3.4 AC-to-DC buck converter

The three-phase AC-to-DC buck converter as shown in Fig. 3.1 is introduced to study the proposed method in a practical way. The converter is constructed as a full-bridge configuration complete with a three-phase input filter and a DC output filter. Both filters contain passive elements in the form of inductors and capacitors. The input source voltages and currents are represented by the instantaneous space phasors (with the assumption of balanced three-phase variables):

$$\underline{u}_s = \frac{2}{3}(u_{sa} + u_{sb}e^{j\rho} + u_{sc}e^{-j\rho}) \quad (3.16)$$

$$\underline{i}_s = \frac{2}{3}(i_{sa} + i_{sb}e^{j\rho} + i_{sc}e^{-j\rho}) \quad (3.17)$$

$$\underline{u}_i = \frac{2}{3}(u_{ia} + u_{ib}e^{j\rho} + u_{ic}e^{-j\rho}) \quad (3.18)$$

$$\underline{i}_i = \frac{2}{3}(i_{ia} + i_{ib}e^{j\rho} + i_{ic}e^{-j\rho}) \quad (3.19)$$

An equivalent circuit of a three-phase AC-to-DC buck converter from Fig. 3.1 is shown in Fig. 3.9.

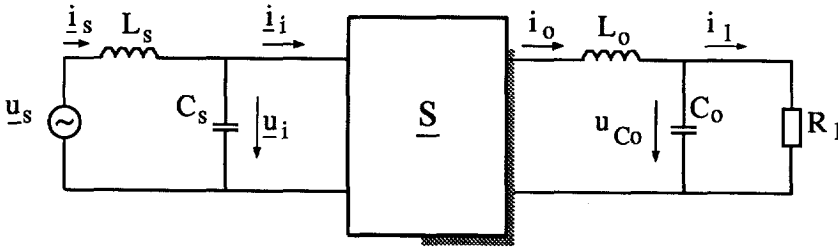


Fig. 3.9 Three-phase AC-to-DC power converter

Equations describing the input source filter using the notation presented in Fig. 3.1 and Fig. 3.9 are:

$$\frac{di_s}{dt} = \frac{1}{L_s}(u_s + u_i) \tag{3.20}$$

$$\frac{du_i}{dt} = \frac{1}{C_s}(i_s - i_i) \tag{3.21}$$

The buck converter implies the application of a *voltage* configuration. For this configuration applied as a rectifier (Chapter 2), the following equations are obtained:

$$\frac{di_o}{dt} = \frac{1}{L_o} \left(\frac{3}{2} \text{Re}\{s^* u_i\} - u_{C_o} \right) \tag{3.22}$$

$$i_i = s i_o \tag{3.23}$$

$$\frac{du_{C_o}}{dt} = \frac{1}{C_o}(i_o - i_1) \tag{3.24}$$

Equations (3.20)...(3.24) entirely describe the instantaneous operation of a three-phase AC-to-DC converter. Since the input voltages u_{sa} , u_{sb} and u_{sc} are sinusoidally time-varying functions, the phasor of the voltages is also time-varying. Similarly, the phase component of all three-phase variables varies sinusoidally with the same angular speed ω_s of the source.

The development of a small-signal dynamic model is now reported. According to (3.12), a space phasor is not in the steady-state and the phasor amplitude is not constant.

$$\underline{u}_s = \underline{U}_s(t)e^{j\omega_s t} \qquad \underline{u}_i = \underline{U}_i(t)e^{j\omega_s t} \tag{3.25}$$

$$\underline{i}_s = \underline{I}_s(t)e^{j\omega_s t} \quad \underline{i}_i = \underline{I}_i e^{j\omega_s t} \quad (3.26)$$

Additionally, the switching phasor \underline{s} is approximated by its low frequency component:

$$\underline{s} = \underline{S}_1 e^{j\omega_s t} \quad (3.27)$$

This property allows the performance of the derivation in the d, q reference frame and the transfer of the set of equations (3.20)...(3.24) into the d, q reference frame. For reasons of simplicity the subscript d, q is omitted. The transformed equations into the d, q reference frame rotating with an angular speed ω_s are:

$$\frac{d\underline{I}_s}{dt} = -j\omega_s \underline{I}_s - \frac{1}{L_s} \underline{U}_i + \frac{1}{L_s} \underline{U}_s \quad (3.28)$$

$$\frac{d\underline{U}_i}{dt} = -j\omega_s \underline{U}_i + \frac{1}{C_s} \underline{I}_s - \frac{1}{C_s} \underline{S}_1 i_o \quad (3.29)$$

$$\frac{di_o}{dt} = -\frac{1}{L_o} u_{Co} + \frac{1}{L_o} \frac{3}{2} \operatorname{Re}\{\underline{s}^* \underline{u}_i\} \quad (3.30)$$

$$\frac{du_{Co}}{dt} = \frac{1}{C_o} i_o - \frac{1}{C_o} i_l \quad (3.31)$$

The obtained set of equations is split into the d and q complex components:

$$\frac{di_{sd}}{dt} = \omega_s i_{sq} + \frac{1}{L_s} (u_{sd} - u_{id}) \quad (3.32)$$

$$\frac{di_{sq}}{dt} = -\omega_s i_{sd} + \frac{1}{L_s} (u_{sq} - u_{iq}) \quad (3.33)$$

$$\frac{du_{id}}{dt} = \omega_s u_{iq} + \frac{1}{C_s} (i_{sd} - i_o s_d) \quad (3.34)$$

$$\frac{du_{iq}}{dt} = -\omega_s u_{id} + \frac{1}{C_s} (i_{sq} - i_o s_q) \quad (3.35)$$

$$\frac{di_o}{dt} = \frac{1}{L_o} \left[\frac{3}{2} (u_{id} s_d + u_{iq} s_q) - u_{C_o} \right] \tag{3.36}$$

$$\frac{du_{C_o}}{dt} = \frac{1}{C_o} (i_o - i_l) \tag{3.37}$$

Variables in the obtained set of equations are now perturbed around the steady-state operation point. A small perturbation is superimposed on the steady-state component of each input and output:

$$\begin{aligned} \underline{s} &= \underline{S} + \underline{\tilde{s}} \\ i_o &= I_o + \tilde{i}_o \\ \underline{u}_s &= \underline{U}_s + \underline{\tilde{u}}_s \end{aligned} \tag{3.38}$$

The obtained DC equations define a steady-state operating point. The steady-state operating point gives a reference phasor:

$$\underline{s}_{ref} = \frac{(1 - \omega_s^2 L_s C_s) \underline{I}_s - j \omega_s C_s \underline{U}_s}{I_o} \tag{3.39}$$

The locus of the reference phasor is a circle in the complex plane. Its radius and phase angle depend on the load. The parameters of a reference phasor are parameters of the filter. By switching the switching bridge with a reference phasor \underline{s}_{ref} calculated on the basis of required values of currents \underline{I}_s and I_o , open-loop control with feedforward is realized. Feedforward compensates the phase shift created by the filter and compensate the changes of source voltage \underline{U}_s .

After neglecting the higher order terms in perturbed equations (3.32)...(3.37), small-signal equations are written in matrix form:

$$\frac{d}{dt} \begin{bmatrix} \tilde{i}_{sd} \\ \tilde{i}_{sq} \\ \tilde{u}_{id} \\ \tilde{u}_{iq} \\ \tilde{i}_o \\ \tilde{u}_{Co} \end{bmatrix} = \begin{bmatrix} 0 & \omega_s & -\frac{1}{L_s} & 0 & 0 & 0 \\ -\omega_s & 0 & 0 & -\frac{1}{L_s} & 0 & 0 \\ \frac{1}{C_s} & 0 & 0 & \omega_s & -\frac{S_d}{C_s} & 0 \\ 0 & \frac{1}{C_s} & -\omega_s & 0 & -\frac{S_q}{C_s} & 0 \\ 0 & 0 & \frac{3S_d}{2L_o} & \frac{3S_q}{2L_o} & 0 & -\frac{1}{L_o} \\ 0 & 0 & 0 & 0 & \frac{1}{C_o} & -\frac{1}{C_o R_1} \end{bmatrix} \begin{bmatrix} \tilde{i}_{sd} \\ \tilde{i}_{sq} \\ \tilde{u}_{id} \\ \tilde{u}_{iq} \\ \tilde{i}_o \\ \tilde{u}_{Co} \end{bmatrix} \quad (3.40)$$

$$+ \begin{bmatrix} \frac{1}{L_s} & 0 & 0 & 0 \\ 0 & \frac{1}{L_s} & 0 & 0 \\ 0 & 0 & -\frac{I_o}{C_s} & 0 \\ 0 & 0 & 0 & -\frac{I_o}{C_s} \\ 0 & 0 & \frac{3U_{id}}{2L_o} & \frac{3U_{iq}}{2L_o} \\ 0 & 0 & 0 & 0 \end{bmatrix} \begin{bmatrix} \tilde{u}_{sd} \\ \tilde{u}_{sq} \\ \tilde{s}_d \\ \tilde{s}_q \end{bmatrix}$$

The set of equations (3.40) can be written as:

$$\frac{d\tilde{x}}{dt} = A\tilde{x} + B\tilde{u} \quad (3.41)$$

where:

- \tilde{x} - matrix of state variables,
- \tilde{u} - input vector.

The obtained matrix equation can be Fourier transformed and rearranged:

$$\tilde{X}(j\omega) = (j\omega I - A)^{-1} B \tilde{U}(j\omega) \tag{3.42}$$

where:

I - unity matrix.

The required transfer function can be obtained from equation (3.42).

3.4.1 Transfer function of AC-to-DC buck converter

Calculation of the transfer function

It is possible to calculate the transfer function analytically or numerically. The calculation requires the computation of an inverse matrix. This possibility is offered by mathematical software Mathematica. Equation (3.42) is developed into a symbolic form. The obtained expressions for the transfer function have many terms and are of no practical importance. Therefore, the transfer function is calculated by Mathcad in a numerical way.

As stated in the introduction, the main objective is the transfer function of the control input to an output waveform. The output waveform is now proposed as the voltage u_{C_0} as well as the input current harmonics. Thus, the calculated transfer

functions are $\frac{\tilde{u}_{C_0}}{\underline{\tilde{s}}}$, $\frac{\tilde{i}_{sd}}{\underline{\tilde{s}}}$, $\frac{\tilde{i}_{sq}}{\underline{\tilde{s}}}$. These calculated transfer functions are presented

in Fig. 3.10, Fig. 3.11 and Fig. 3.12 altogether with the measured points of transfer function,

where:

- calculated transfer function,
- x—x—x measured for $f_{sw} = 5$ kHz,
- measured for $f_{sw} = 10$ kHz.

Measured points of transfer function

The calculated transfer functions are compared with the measured results obtained from the simulated model of a converter. Generally, when a transfer function is derived theoretically, its validity is checked by comparing it with experimental results obtained by measurements using a gain/phase analyzer. The analyzer injects a sinusoidal signal into the circuit under measurement and evaluates the magnitude and phase of the injected frequency component in the output spectrum. The same procedure is followed here during simulation in the time domain. The perturbations are sinusoidal waveforms with a small amplitude.

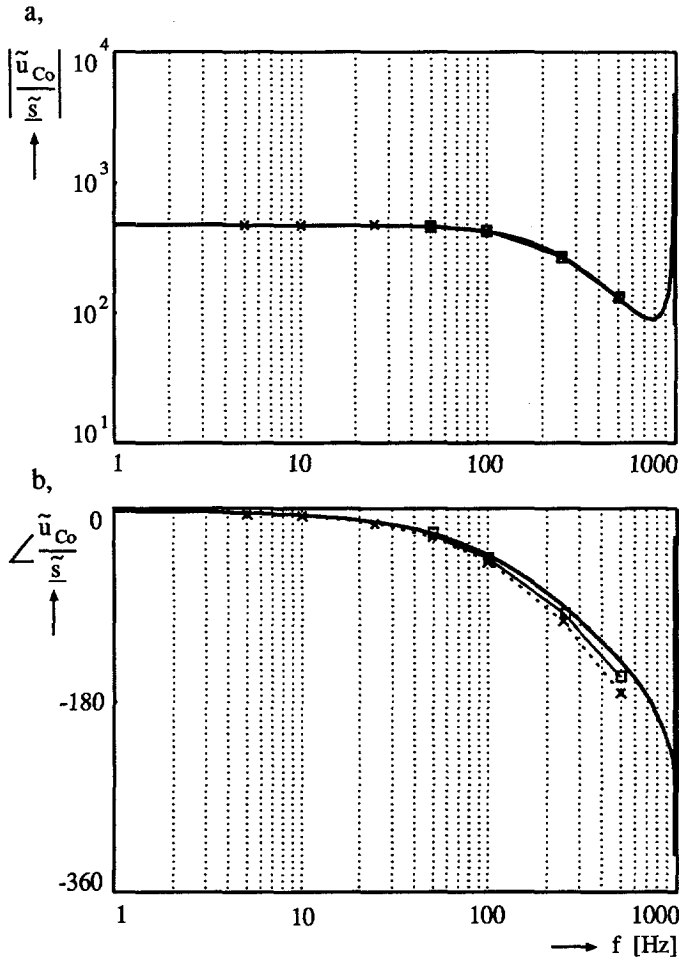


Fig. 3.10 Frequency response of transfer function \tilde{i}_{Co}/\tilde{s} :
 a. amplitude,
 b. phase.

The model of a three-phase AC-to-DC buck power converter (Fig. 3.1) is applied in a software simulation tool (Caspoc). The reference phasor that characterizes the ideal operation of the switching network is sampled with a fixed frequency f_{sw} . The sampled phasor \underline{s}_{ref} is created by the time averaging of two adjacent active states $\underline{s}_k, \underline{s}_{k+1}$ and zero state as explained in Chapter 3.2.2.

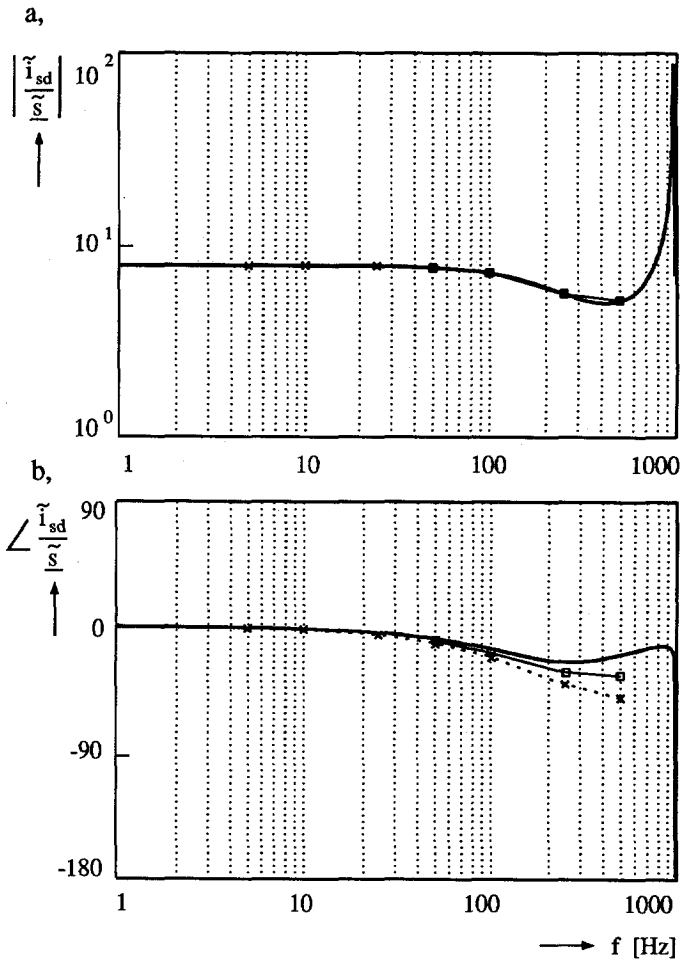


Fig. 3.11 Frequency response of transfer function \tilde{i}_{sd}/\tilde{s} :
 a. amplitude,
 b. phase.

From equation (3.1) we obtain:

$$T_k = \frac{\text{Im}(s_{k+1})\text{Re}(s_{ref}) - \text{Re}(s_{k+1})\text{Im}(s_{ref})}{\text{Re}(s_k)\text{Im}(s_{k+1}) - \text{Im}(s_k)\text{Re}(s_{k+1})} T_{sw} \tag{3.43}$$

$$T_{k+1} = \frac{\text{Re}(s_k)\text{Im}(s_{ref}) - \text{Im}(s_k)\text{Re}(s_{ref})}{\text{Re}(s_k)\text{Im}(s_{k+1}) - \text{Im}(s_k)\text{Re}(s_{k+1})} T_{sw} \tag{3.44}$$

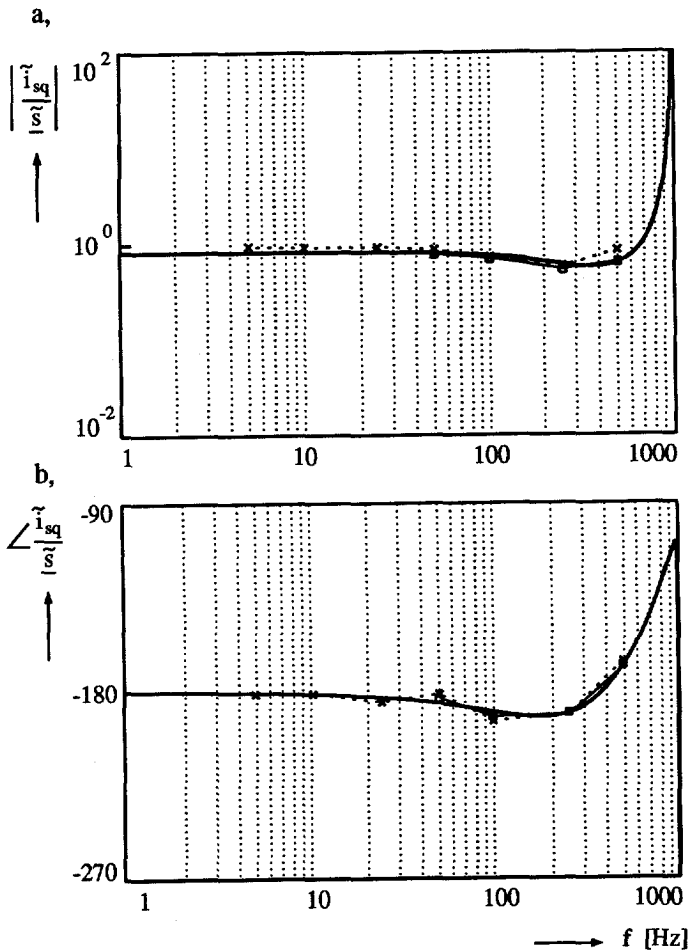


Fig. 3.12 Frequency response of transfer function $\bar{i}_{sq}/\underline{s}$:

- a. amplitude,
b. phase.

Equation (3.2) gives:

$$T_0 = T_{sw} - T_k - T_{k+1} \quad (3.45)$$

The three states are switched on for the calculated time intervals sequentially as shown in Fig. 3.13.

The reference switching phasor \underline{s}_{ref} (3.39) is sampled with switching period T_{sw} . To decrease the influence of a finite T_{sw} , an averaged switching phasor \underline{s} is created in the switching network. This phasor leads over an angle α with respect

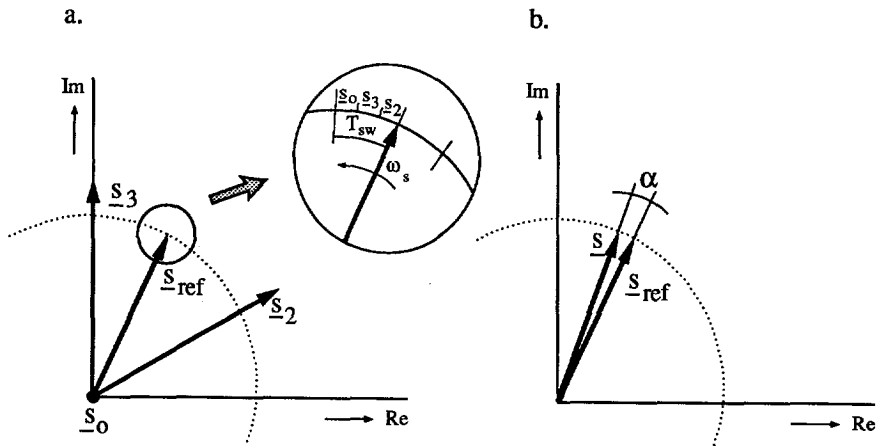


Fig. 3.13 Phasor control in complex plane

to \underline{s}_{ref} (Fig. 3.13.b). The established phasor is the sampled reference phasor while the reference phasor itself continues to rotate. Thus, the steady-state value of the established switching phasor \underline{s} is rotated by an angle α with respect to \underline{s}_{ref}

$$\underline{s} = \underline{s}_{ref} e^{-j\alpha} \quad \alpha = \frac{\pi}{n_{sw}} \quad n_{sw} = \frac{\omega_{sw}}{\omega_s} \quad (3.46)$$

where :

n_{sw} - ratio of the switching frequency ω_{sw} and the source frequency ω_s .

The three-phase-to-DC buck power converter with following parameters is simulated:

$$\begin{array}{lll} \underline{U}_s = U_{sd} = 311 \text{ V} & U_{C_0} = 400 \text{ V} & R_1 = 100 \text{ } \Omega \\ L_s = 10 \cdot 10^{-3} \text{ H} & C_s = 2.5 \cdot 10^{-6} \text{ F} & \omega_s = 2\pi \cdot 50 \text{ s}^{-1} \\ L_o = 100 \cdot 10^{-3} \text{ H} & C_o = 2.5 \cdot 10^{-6} \text{ F} & \omega_{sw} = 2\pi \cdot 5 \cdot 10^3 \text{ s}^{-1} \end{array}$$

Examples of simulated waveforms are given in Fig. 3.14 and Fig. 3.15, where the switching bridge switches with sampled reference phasor (3.39) rotate with angle α (3.46). The reference of the source current \underline{I}_s in equation (3.39) is calculated on the basis of the power balance equation:

$$\text{Re}\{\underline{u}_s^* \underline{i}_s\} = \frac{2}{3} u_{C_0} i_l \quad (3.47)$$

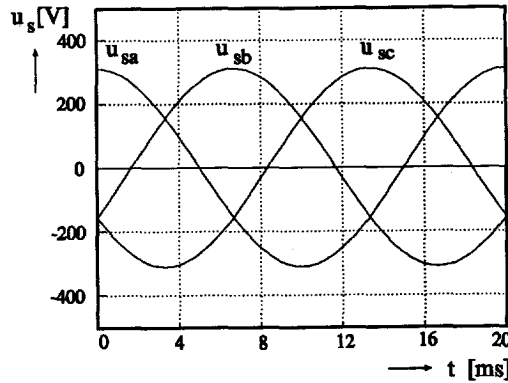


Fig. 3.14 Example of the simulated source voltages \underline{u}_s

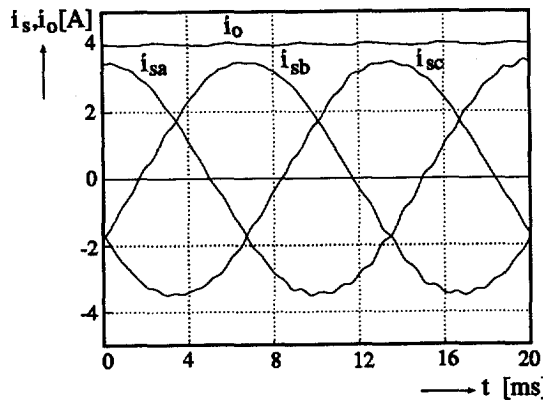


Fig. 3.15 Example of the simulated source current \underline{i}_s and \underline{i}_l

Wanting \underline{i}_s and \underline{u}_s in phase, the reference source current is given by:

$$I_{sd} = \frac{2}{3} \frac{u_{C_0} i_l}{U_{sd}} \quad (3.48)$$

The reference switching space phasor \underline{s}_{ref} and the actual switching space phasor in the α, β coordinates are shown in Fig. 3.16. The reference switching space phasor creates a circle in the α, β plane. The actual switching space phasor \underline{s} is a fictive quantity calculated on the basis of equation (3.39), but with the measured current phasor \underline{i}_s and current \underline{i}_0 :

$$\underline{s} = \frac{(1 - \omega^2 L_s C_s) \underline{i}_s - j\omega C_s \underline{u}_s}{\underline{i}_0} \quad (3.49)$$

The task of the actual switching space phasor is to show, how the switching

operation represented by an actual switching space phasor \underline{s} follows its template \underline{s}_{ref} . Due to the nature of PWM modulation and the fact that the high order filters are employed, the actual switching space phasor is distorted and contains unwanted higher harmonics.

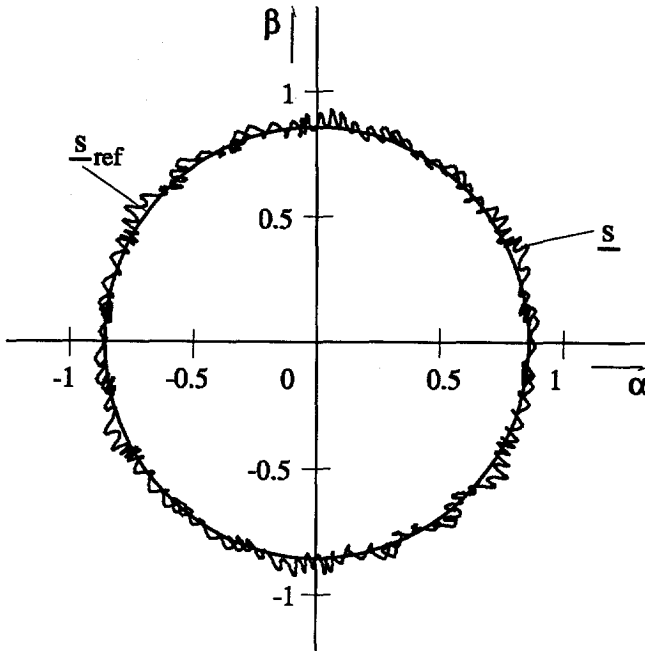


Fig. 3.16 Reference switching space phasor \underline{s}_{ref} and actual switching space phasor \underline{s}

The simulated waveforms show good agreement with the theoretical assumptions. The three-phase source currents \underline{i}_s are in phase with voltage the \underline{u}_s as expected. The sinusoidal waveforms of the three-phase source currents \underline{i}_s and the output current i_o are shown in steady state. The simulated model also serves for practical measurements of the theoretical transfer functions reported in Chapter 3.4.1. The measured points of transfer functions shown in Fig. 3.10, Fig. 3.11 and Fig. 3.12 are obtained by injecting a 3% perturbation on the switching phasor \underline{s} and the source voltages \underline{u}_s at different frequencies (5, 10, 25, 50, 100, 250 and 500 Hz). The influence of the perturbations with the different frequencies on the harmonic spectra of the source currents \underline{i}_s and the load current i_l determines the measured points of the transfer functions. Since the transfer function points marked by \times measured by simulation differ for the higher frequency range from the calculated ones, another measurement is performed with a switching frequency twice as high as the original switching frequency. The second simulation is provided at perturbation frequencies 100, 250, 500 Hz and the obtained points are marked by \square . From Fig. 3.10 and Fig. 3.11 we see that the curves simulated at the higher switching frequency are closer to the theoretical curves. This fact corresponds with

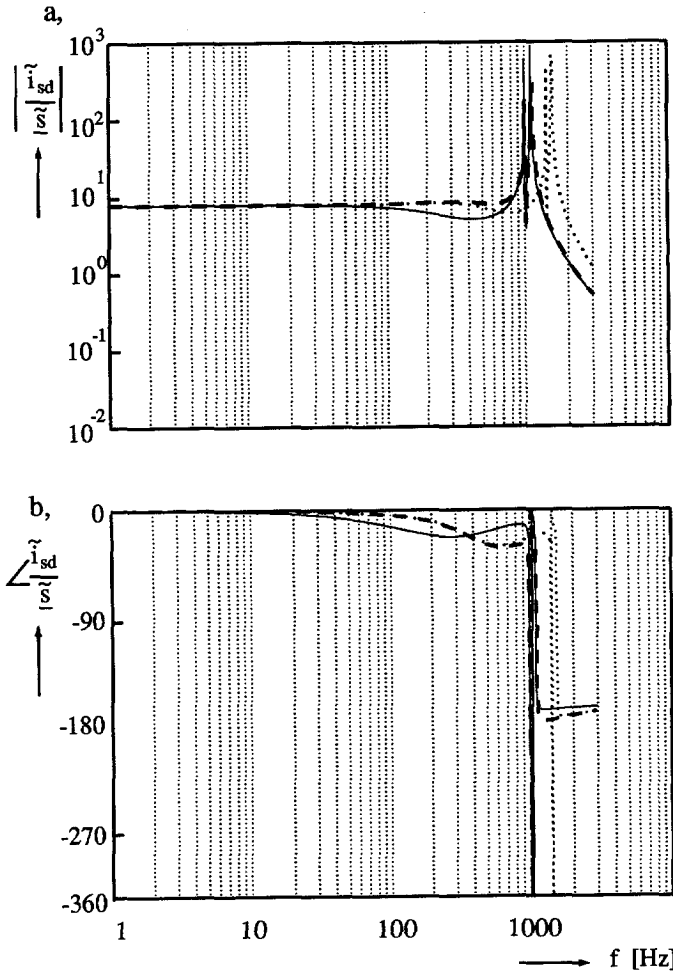


Fig. 3.17 Frequency response of transfer function $\frac{\tilde{i}_{sd}}{s}$
 with varying filters parameters
 a.magnitude, b.phase

the expectation that the theoretical curve assumes an ideal switching process. For an increased switching frequency, the influence of the higher harmonics is reduced.

Fig. 3.17 plots open-loop response of $\frac{\tilde{i}_{sd}}{s}$ for the parameters mentioned in this section (solid line) as well as for varying parameters (dashed line and dotted line). The filter elements L_s and C_s of the source filter create a peak close to the

resonant frequency. In the z -plane, this peak corresponds to one pair of the complex poles. This resonance causes the AC line current distortions under the steady-state operating conditions. The pole placement method might be used to improve the dynamic performance characteristics. The decrease of the output inductor filter value $L_o = 40$ mH results in a linearized transfer function in a high frequency region (dashed line). The impact of the source filter inductor change is shown by the dotted line. By decreasing the source inductor value L_s , the peak of the resonance is shifted towards higher frequencies.

The theoretical method studied in Chapter 3.3 is here documented using an example of an AC-to-DC buck power converter. The model based on a switching space phasor prescription serves to determinate a steady-state operating point as well as small-signal transfer functions. The steady-state operating point and the transfer functions calculated on the basis of a mathematical model are verified by independent simulation.

3.5 Carrier suboscillation PWM in rotating reference frame

Another mathematical model defined in Chapter 2 is the model of a switching bridge leg. Each switching leg is controlled separately and individually in the case of carrier suboscillation PWM as reviewed in 3.2.1. Therefore, a model of a switching leg with the switching function $d(t)$ is suitable for the analysis of this PWM method. Next, the mathematical model of a converter based on a switching bridge leg is studied theoretically and then documented on an example.

Similar to the case of the model with switching space phasor, also here, two basic problems defined in Chapter 3.1 have to be solved: the discontinuous switching behaviour and the varying nature of the AC waveforms.

Using the state space concept, the system equation is presented by:

$$\dot{\mathbf{x}} = \mathbf{A}(d(t))\mathbf{x}(t) + \mathbf{B}(d(t))\mathbf{u}(t) \quad (3.50)$$

The matrices \mathbf{A} and \mathbf{B} contain a discontinuous switching function $d_i(t)$. Since the switching pattern is precalculated similar to the space phasor modulation, a Fourier transformation can be applied to the switching pattern.

For a carrier pulse-width modulation, the switching points within one switching period are not symmetrical. However, for a high ratio of the utility frequency (frequency of the reference) and the switching frequency, the modulating waveform can be regarded constant in each switching period. Therefore, the switching pattern is close to a symmetrical waveform as shown in Fig. 3.18.

The Fourier series of the periodical time function is:

$$f(\omega t) = a_0 + \sum_{n=1}^{\infty} a_n \sin(n\omega t) + \sum_{n=1}^{\infty} b_n \cos(n\omega t) \quad (3.51)$$

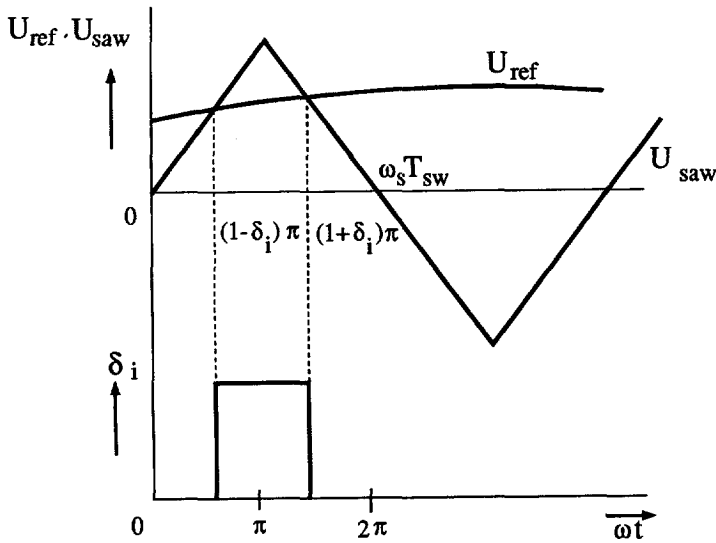


Fig. 3.18 Method of pulse width modulation.

The switching function within one switching cycle is expressed as (see also Fig. 3.18):

$$\begin{aligned} \delta_i &= 0 & 0 \leq \omega_s t \leq (1-\delta_i)\pi \\ & & (1+\delta_i)\pi \leq \omega_s t \leq 2\pi \\ \delta_i &= 1 & (1-\delta_i)\pi < \omega_s t < (1+\delta_i)\pi \end{aligned} \quad (3.52)$$

Therefore, next equations are valid:

$$a_0 = \frac{1}{2\pi} \int_{(1-\delta_i)\pi}^{(1+\delta_i)\pi} \delta(\omega_s t) = \delta_i \quad (3.53)$$

$$a_n = 0$$

$$b_n = (-1)^n \frac{2}{n\pi} \sin(n\delta_i\pi)$$

$$\delta_i^* = \delta_i + \sum_{n=1}^{\infty} (-1)^n \frac{2}{n\pi} \sin(n\delta_i\pi) \cos(n\omega_s t) \quad (3.54)$$

Similar to the case of space-phaser modulation, only the fundamental harmonic components are considered.

Matrices \mathbf{A} and \mathbf{u} are time functions of the utility frequency ω for AC-to-DC power converters and matrices \mathbf{A} and \mathbf{B} are time functions of the utility frequency ω for

DC-to-AC power converters. To make the system time invariant, a rotating reference frame is applied. The rotating frame always refers to the AC side of a converter.

The next step is the transformation into the rotating reference frame that is synchronized with the utility frequency (input or output modulated frequency). A transformation makes the system time invariant. For a three-phase balanced system the transformation matrix is:

$$T = \frac{1}{\sqrt{3}} \begin{bmatrix} 1 & e^{-j\omega t} & e^{j\omega t} & 0 \\ 1 & e^{-j(\omega t - 2\frac{\pi}{3})} & e^{j(\omega t - 2\frac{\pi}{3})} & 0 \\ 1 & e^{-j(\omega t + 2\frac{\pi}{3})} & e^{j(\omega t + 2\frac{\pi}{3})} & 0 \\ 0 & 0 & 0 & \sqrt{3} \end{bmatrix} \tag{3.55}$$

In an AC-to-DC PWM system, the input vector $u(t)$ consists of a three-phase voltage system. The PWM pattern is synchronized to the utility frequency of the three-phase system (the duty cycle is also a function of the utility frequency). After applying the transformation, the system becomes time-invariant:

$$x = Tx_r \quad x_r = T^{-1}x \tag{3.56}$$

$$u = Tu_r \quad u_r = T^{-1}u \tag{3.57}$$

The state space equation becomes:

$$\dot{T}x_r + T\dot{x}_r = ATx_r + BTu_r \tag{3.58}$$

$$\dot{x}_r = (T^{-1}AT - T^{-1}\dot{T})x_r + T^{-1}BTu_r \tag{3.59}$$

Because the coefficients of matrix A are functions of the utility frequency, the result is a time-invariant model.

The procedure for a small-signal analysis is the same as performed for DC converters. It has to be noted that the high-frequency behaviour was neglected and the rotating reference frame transforms the part equal to the utility frequency. An example of a dynamic analysis of an AC-to-DC step up power converter is shown in reference [Wu et.al., 1991].

The dynamic analysis applied to the resulting LTI system captures the low-frequency behaviour of such a system. The boundary of this behaviour is set by the switching frequency. A natural question about the transformation matrix and its

influence on the system here arises. Let us compare the rotating frame transformation with a more generally defined Lyapunov transformation [Chen, 1984]. Under certain conditions, the equivalent transformation can be named Lyapunov because it preserves the property of stability of the system. Finally, we recognize that the rotating frame transformation is nothing else but a Lyapunov transformation [Bauer, Klaassens, 1992]. This fact gives an answer to the question how the transformation should be designed to meet the individual properties of the system.

3.6 Conclusions

For carrier suboscillation PWM modulation and space phasor modulation, a dynamic model with the mathematical tools defined in Chapter 2 has been developed. This model contains a discontinuous time function $\delta(t)$ that presents the action of a switching leg in a three-phase bridge configuration. For space phasor modulation, it is a discontinuous switching phasor \underline{s} that represents the action of the switching bridge as a whole.

The simplest way to reduce the complex problem of a switching network is the application of a Fourier transformation at the resulting switching pattern. This application is possible to establish because the switching pattern is precalculated. In fact, the averaging methods, where we consider one-cycle average, are nothing else than a calculation of the DC coefficient in the Fourier series representation:

$$x(t) = \frac{1}{T} \int_t^{T+t} x(s) ds \quad (3.60)$$

This fact offers a clear relation between the averaging methods applied to DC-to-DC power converters reviewed in Chapter 1 and the method suggested here. The suggested method is a generalization of an averaging method. By using a state-space description and by calculating the zero Fourier component, the state-space averaging method is obtained. This means that the state-space averaging is a special case of the proposed method. The proposed method is applicable to any open-loop modulated converter.

**MODULATION OF SOFT-
SWITCHING POWER
CONVERTERS**

4.1 Introduction

A group of discrete-pulse modulated converters is defined in Chapter 1. The applied method of modulation and the converter topology are strongly related, so is the discrete-pulse modulation connected to the soft-switching resonant link topology. The various methods of soft switching are reviewed to understand this relation.

To develop power converters with improved characteristics for a specific volume, the quality of the external waveforms, the reliability, the efficiency and the costs, further increase of the internal switching frequency are desired. Soft switching is a possible method to increase the internal switching frequency by reducing the dynamic losses in the power semiconductor switches. To study the dynamic behaviour of soft-switching converters, first, the topological rules and relations are examined in this chapter. A survey of topologies and related basic control principles is accomplished.

In the first part, problems concerning soft-switching converters are identified and analyzed. Two different approaches are used to modulate the external low frequency waveforms: pulse-width modulation (PWM) and discrete-pulse modulation (pulse-frequency modulation (PFM)). Because a resonant circuit is usually the timing element of the internal waveforms, PFM is often used to control the power flow. However, PWM applied in combination with soft switching has advantages over the currently used PFM methods as can be demonstrated. PFM applied to AC-to-AC converters requires unconventional power factor control and filter design.

The modelling and dynamic analysis of the introduced converters is demanding because of the complexity of the networks and their related control techniques. While PWM is state of the art, the control of three-phase-to-three-phase PFM modulated converters is far from that. Dynamic analysis is an important step towards improving the control.

4.2 Hard switching and soft switching

The converter processes power by interrupting the power flow from the source to the load by control of the duty cycle of each switching interval. This operation results in pulsating currents and voltages. A typical operation of a hard-switching semiconductor switch is shown in Fig. 4.1.

A forced interruption of the current through a semiconductor switch in combination with a substantial voltage over the device (*hard switching*) will lead to excessive momentary values of the power during switching (P_{on} and P_{off}) compared to the conduction losses during the current conduction interval P_{cond} .

The losses are dissipated in the switching elements during the turn-on and turn-

off intervals. These switching losses (*dynamic losses*) are the fundamental reason for the increase in the total losses in the semiconductor switches at an increased switching frequency. It can be shown that there is a maximum value for the switching frequency for which the dissipated energy in the semiconductor switch can no longer be transmitted to its environment when there is a limited temperature rise (thermal barrier). For semiconductor switches suited for high voltages and/or high currents, the pulse repetition frequency is in the order of a few kHz. Also, the necessary complex snubber and protection networks lower the efficiency and reliability of the converter.

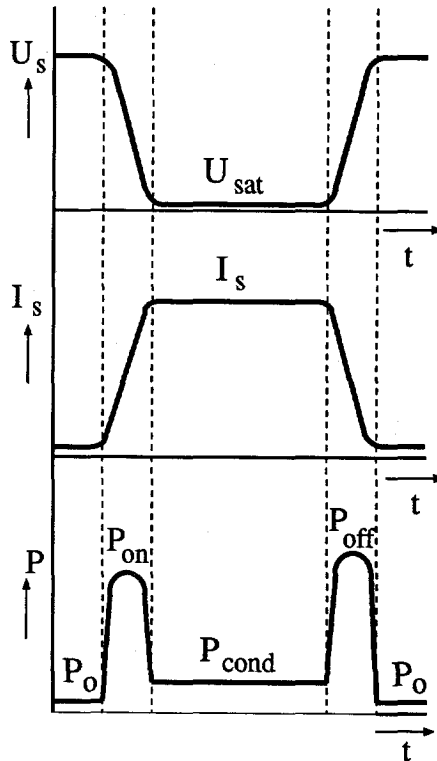


Fig. 4.1 Voltage over and current through a semiconductor switch and their related switching losses

4.2.1 Soft switching

The development of power converters with improved characteristics is based on a further increase of the switching frequency. In the case of hard switching as used in the basic topologies of choppers and inverters with forced turn-off, the switching losses are reduced by applying fast-switching power semiconductors such as IGBTs, FETs, MCTs. It is necessary to include a complex and lossy protection

networks to counteract the effects of hard switching that result from the presence of parasitic components in the converter, e.g. parasitic inductances in series with the switch. Depending on the selected type of switching device, it is necessary to reduce the rate of voltage rise over the switch. This will often result in significant losses at higher switching frequencies.

The application of *soft-switching* methods will minimize or eliminate these disadvantageous phenomena by a suitable control of the waveforms over and in the semiconductor switches. Therefore, the rate of current rise through the switch or the voltage over the switch or both during the turn-on and turn-off interval have to be reduced at such a rate that the turn-on and turn-off losses become acceptable. By placing a nondissipative electric network NS in series with the switch or a non-dissipative network NP in parallel to the switch as shown in Fig. 4.2, one can realize a method of control for the waveforms of the current or voltage of the switch.

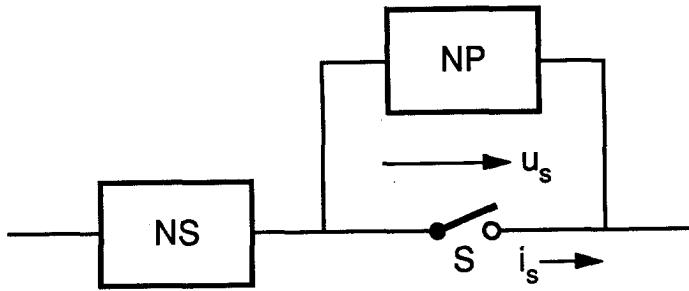


Fig. 4.2 A switch and its accompanying electric networks

This method of controlled switching waveforms is often called *soft switching*.

4.2.2 Hard switching

The load-line trajectory of PWM switches shown in Fig. 4.3 depends on the loading of the semiconductor switches. The load-line trajectory *a* crosses the high-stress region in which the device is subjected simultaneously to high voltage and high current for inductive load turn-off and capacitive turn-on. This method of switching is introduced as *hard switching*. The example of inductive load turn-off and capacitive turn-on is chosen because it induces the high stress on the switching device.

The load-line trajectory of a soft-switching device shown as curve *b* in the same figure moves along the axis. Since high voltage and high current are not excited simultaneously, the switching stresses are minimized.

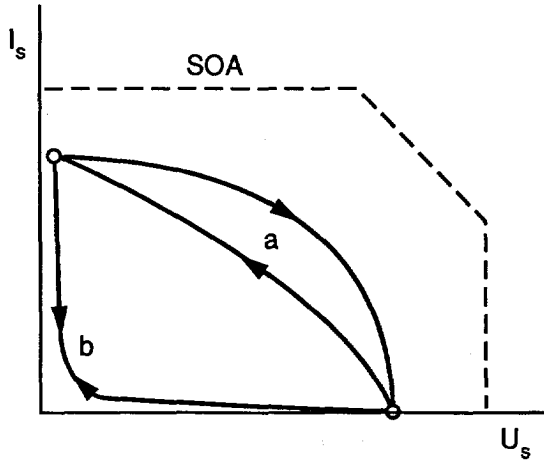


Fig. 4.3 Switching load line for:
 a. hard-switching converter
 b. soft-switching converter

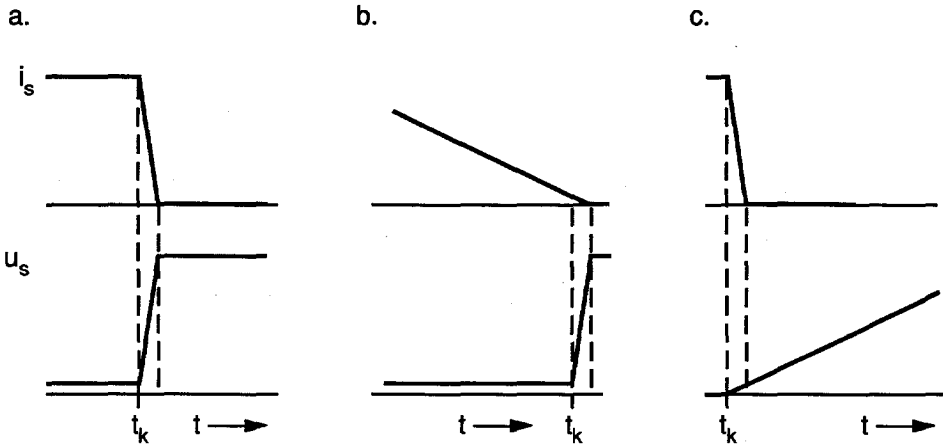


Fig. 4.4 Illustration of the turn-off process
 a. hard switching,
 b. soft switching (zero-current turn-off),
 c. soft switching (zero-voltage turn-off).

Fig. 4.4 illustrates the switching waveforms in the time domain at the turnoff of the semiconductor device. Fig. 4.4a illustrates the method of hard switching. The methods of soft switching are illustrated in the time domain in Fig. 4.4b and Fig. 4.4c for zero-current and zero-voltage turn-off, respectively.

The combination of a semiconductor switch and an inductor or capacitor makes it practical to program the waveforms of the switch. To allow a recurrent operation

of the switch, the circuit is completed as a resonant network.

Resonant converters and PWM soft switching

The soft-switching technique is applied in two basically different ways: as resonant converters or as soft-switching PWM converters. Resonant converters process power by using sinusoidal or quasi-sinusoidal internal waveforms. There is a reduction in switching losses and stresses on the power semiconductors in comparison with hard-switched PWM converters.

Due to the resonant nature of the current and voltage waveforms, however, a resonant converter operation usually involves high circulating energy that increases switch voltage/current stresses and results in a substantial increase in conduction losses.

Various soft-switching techniques are proposed to combine the advantages of soft switching and a constant switching frequency as characteristic of pulse width modulation (PWM). A soft-switching converter uses a resonant circuit to soften the switching process. The resonant circuit is the timing element of the internal waveforms. While resonant converters use PFM, this family of soft-switching converters uses the familiar PWM techniques to modulate voltages and currents at the external ports of the converter.

4.3 Topologies of the soft-switching power converters

To improve the switching conditions for the semiconductor devices, resonant techniques which are based on the implementation of parallel-resonant or series-resonant circuits are proposed. The application of a particular resonant network creates zero-voltage or zero-current conditions for the semiconductor devices at the switching instants. The dynamic losses are reduced or abandoned. The increase in the switching frequency allowed by eliminating switching losses by soft switching has shown distinctive advantages such as high power density, low EMI, low acoustic noise and high dynamic performance. The use of a resonant circuit to achieve soft switching unfortunately involves penalties such as circulating energy in the converter which produces high values of the internal resonant waveforms.

During the past several years, many topologies have been suggested and evaluated. Soft-switching converters received considerable attention for high-frequency DC-to-DC conversion, including high power applications. They are increasingly replacing the conventional hard-switched converters in applications where the demands are high. The attention is now focused on the polyphase AC-to-AC power converters.

The classification of resonant converters was introduced in Chapter 1 in Fig. 1.4. A survey of the soft-switching resonant topologies is presented in the literature [Klaassens, van Weesenbeek, Bauer 1993]. Switching schemes for the resonant

link converters can be classified according to whether they involve a resonant AC voltage or AC current impressed on the link and/or include a pulsating DC voltage or current component (resonant DC link).

In the case of an AC link, the resonant circuit impresses both polarities of AC voltage and current in the link. The switches at the input and output sides of the converter carry both positive and negative current and block both polarities of the voltage. The switches applied in this class of converters should therefore be bidirectional switches. These switches are usually realized by two inverse parallelled BJTs, IGBTs, FETs or thyristors for the parallel or series resonant circuit. The recent development of the MCT, however, may lead to the realization of a truly bidirectional switch.

Two different categories of soft-switching converters are introduced as resonant DC link converters and pole commutated converters. Resonant AC-to-AC converters are characterized by a passive circuit in the link (Fig. 1.7) including a resonant tank that is placed at the DC bus of the switching matrix. The DC bus connected to the switching matrix is forced to oscillate to set up a possible commutation instant for the semiconductor devices. The result is a zero-voltage or a zero-current condition at turn-on and/or at turn-off. An example of a resonant link converter with a series-resonant circuit in the link, is shown in Fig. 4.5.

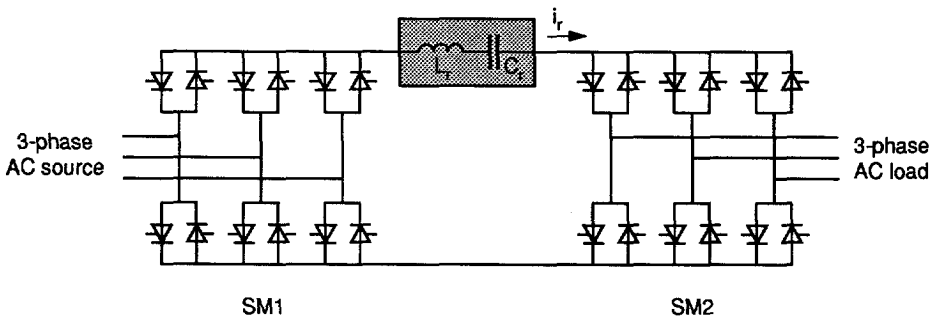


Fig. 4.5 Series-resonant AC-to-AC converter

The resonant pole inverter features one resonant commutation circuit for each pole of the switching matrix. In contrast to the resonant link converter, it enables each phase to operate independently from the other, thus providing PWM capability.

The diagram of a resonant pole commutated converter is shown in Fig. 4.6.

The general topology of a three-phase-to-three-phase converter is presented in Fig. 1.7. The passive network in the link is for resonant converters performed by a resonant network. The character of the input and output filters coincide with the nature of the resonant link. This resonant network placed in series or in parallel to a switch or a group of switches gives the potential of soft switching.

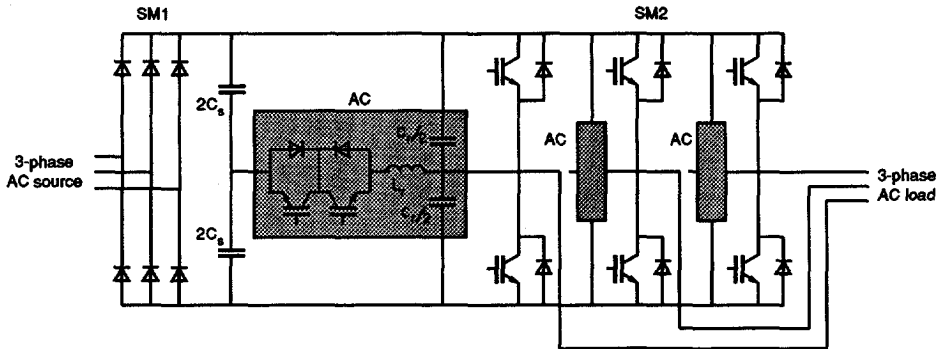


Fig. 4.6 The resonant pole inverter

The basic classification of soft-switching resonant converters in the series-resonant, the parallel-resonant or the multi-resonant converter was presented in Chapter 1 (see also Fig. 1.4). As defined in Chapter 2, the switching bridge can appear in two possible configurations: *current configuration* or *voltage configuration*. We now investigate the relation between the characteristics of the resonant link and the possible configuration of the switching bridge.

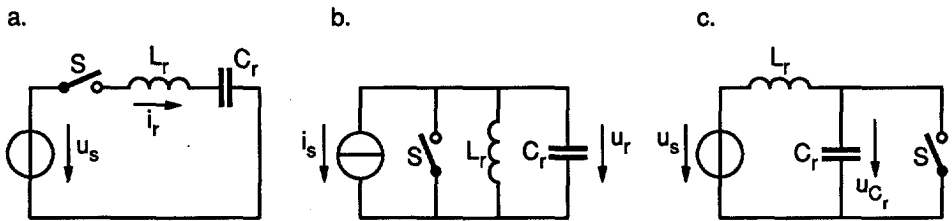


Fig. 4.7 Resonant link variations:
 a. series-resonant AC link
 b. parallel-resonant AC link
 c. resonant DC link

The series-resonant circuit is excited by a voltage source (Fig. 4.7a) to create a resonant current (Fig. 4.8a). Therefore, the switching bridge with a series-resonant circuit in the link uses a voltage configuration while the filters have the characteristics of a voltage source (capacitor).

The parallel-resonant circuit is excited by a current source (Fig. 4.7b) to create a resonant voltage (Fig. 4.8b). Therefore, the switching bridge with a parallel-resonant circuit in the link uses a current configuration while the filters have the characteristics of a current source (inductor).

The third type shown in Fig. 4.7c is, in fact, a parallel-loaded series-resonant circuit. The switch is placed in parallel to the resonant capacitor and allows an independent control of the energy stored in the resonant tank, thus creating

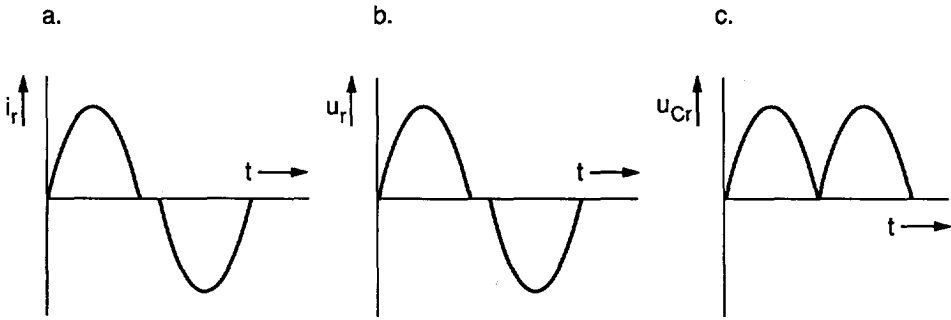


Fig. 4.8 Typical voltages and currents in the link:
 a. current of the series-resonant AC link
 b. voltage of the parallel-resonant AC link
 c. voltage of the resonant DC link

another degree of freedom. Since the switch S is actually one leg of the switching bridge, it has no additional requirements on hardware. The topologies with this configuration of resonant elements are shown in literature as the resonant DC voltage link converters. Typical voltage of the resonant DC link is shown in (Fig. 4.8c). There are also possibilities to establish a resonant DC current link. The series- or parallel-resonant DC link configurations are reviewed in Fig. 4.9. In Fig. 4.9a the inductor L_d provides a DC bias to the resonant link current while in Fig. 4.9b the capacitor C_d provides a DC bias to the resonant link voltage. The link voltage or link current is a DC-biased sinusoidal waveform (Fig. 4.10 a, b).

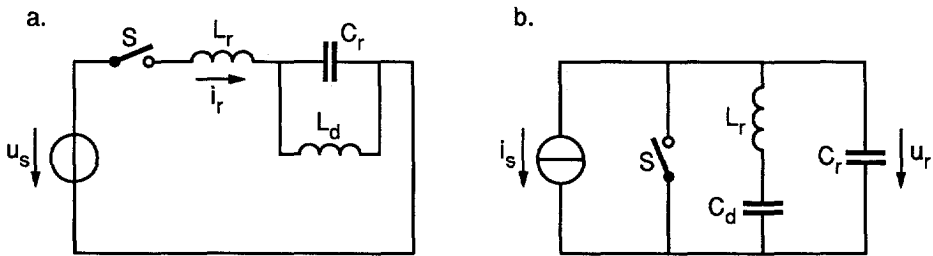


Fig. 4.9 a. series-resonant DC link
 b. parallel-resonant DC link

An extra switch added to the series- or parallel-resonant circuit allows the independent control of the energy stored in the resonant link. The control of the energy in the resonant link is one of the basic problems encountered in the resonant link converter. At the cost of additional complexity of the resonant network, the control of the zero-crossing of the resonant voltage or current can be provided as will be shown later. The capability of PWM can be thus provided.

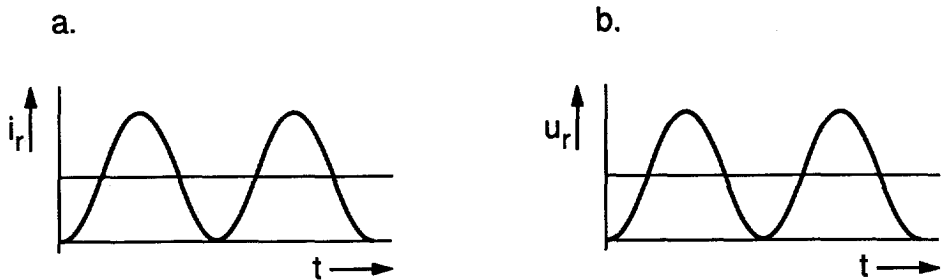


Fig. 4.10 Typical voltages and currents of the resonant link:
 a. current of the series-resonant DC link,
 b. voltage of the parallel-resonant DC link.

As usual for the operation of resonant converters, two basic problems have to be dealt with:

1. the control of the power flow from the source to the load or vice versa, and the generation of the external waveforms at the input and output terminals of the converter (*external control shell*),
2. the stabilization of critical waveforms and the control of the energy level in the high-frequency link (*internal control shell*).

4.4 Methods of modulation

To control the external waveforms, two basically different approaches are recognized:

1. *pulse-width modulation (PWM)*
2. *discrete-pulse modulation (pulse frequency modulation: PFM)*

Typical waveforms of the reference and modulated voltages (or currents) are shown in Fig. 4.11.

The converter topologies differ also according to the way the *external* waveforms are controlled. The use of a high-frequency resonant circuit, where the voltages or currents (almost) periodically reach zero, evokes the discrete-pulse modulation. This means that a pulse modulation technique uses the natural properties of the resonant circuit. To be able to change the width of a pulse, an additional action has to be implied. Generally, by the extension of the power part of a resonant pulse-modulated converter, the PWM capability is obtained. In other words, the power part of a PFM soft-switching converter is always simpler than the power part of the PWM soft-switching converter.

Variations of a resonant link are presented in Fig. 4.12. Circuit a1 in Fig. 4.12

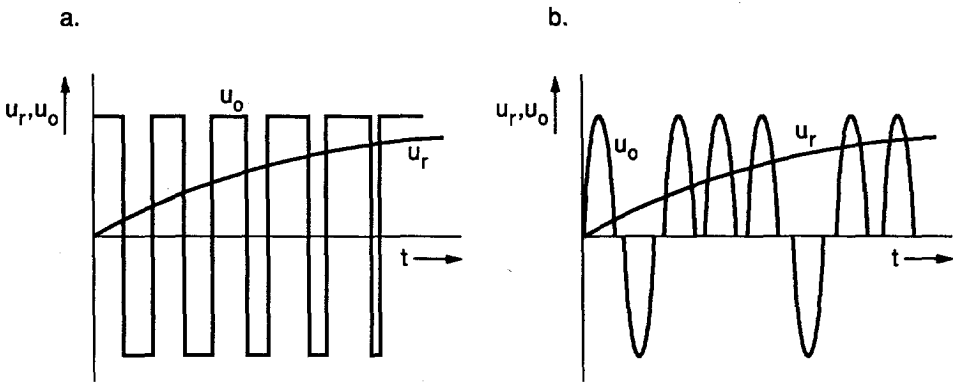


Fig. 4.11 PWM (a) and PFM (b) modulation
 U_r - reference voltage,
 U_o - unfiltered voltage.

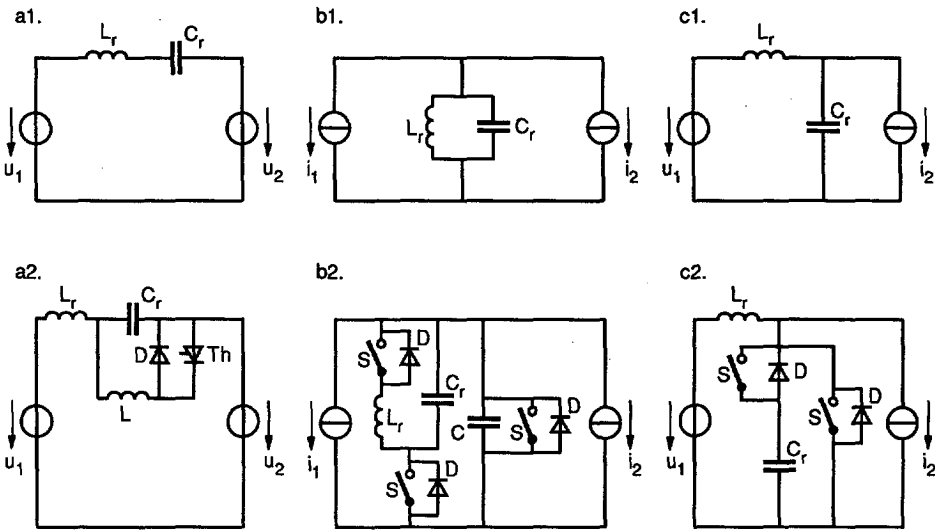


Fig. 4.12 Resonant link with pulse frequency modulation (a1, b1, c1) and resonant link with pulse-width modulation (a2, b2, c2)

shows the series-resonant link and circuit a2 shows the same link extended for PWM techniques. Circuits b1 and b2 describe the similar circuits for a parallel-resonant link and circuits c1 and c2 for a parallel-loaded series-resonant circuit utilized as applied in the resonant DC-link converter.

The tendency is to decrease the complexity of the power part on the account of an

increase in the complexity of the control. For this reason, it is more attractive to employ PFM modulation. The applied PFM modulation is by far not so well developed as PWM, and always employs additional current or voltage sensors. This can be also a reason of lower popularity of PFM compared to PWM.

However, the comparison PWM-PFM shows that PWM has certain advantages. In the case of PWM converters, the harmonic components in the low-frequency waveforms are found only at the side bands around the multiples of the switching frequency because of the switching with constant frequency. The unwanted harmonics are thus well constrained and simple to filter. In contrast, the PFM modulation creates the unwanted harmonics below the resonant link frequency. The harmonic content of the unwanted harmonics changes with the modulation index because of the constant duration of the resonant pulse and variable frequency which changes to enable a modulation of a time-varying signal. A classical filter design does not improve the harmonic content of the external waveforms.

Pulse-width modulation

The performance and cost criteria mainly determine the choice of a PWM method in a specific application. The conclusion is that PWM is a state-of-the-art method which is easily applicable and available. The dynamic and static behaviour has been studied and is understood. It typically operates with an open-loop control (the modulation itself is an open loop). In Chapter 2, the dynamics of PWM converters are studied in detail.

Discrete-pulse modulation

PFM converters use single resonant pulses to synthesize the low-frequency waveforms at the terminals of the converter. The switching process is synchronized with the (almost) periodically zero-crossings of the resonant waveforms. With this constraint on the switching operation of the converter, one half-cycle of the resonant operation becomes the basic unit for the synthesis of the low-frequency waveforms.

Pulse modulation techniques are applied to synthesize the low-frequency waveforms. An *ASDTIC* controller (Analog-Signal-to-Discrete-Time Interval-Converter) [Schwarz, 1974] was the first pulse modulation technique applied. The controller continuously integrates the current error and fires the next resonant pulse to decrease this error. The ASDTIC created a modulation philosophy that was modified later by many engineers and used to control external waveforms of pulse-modulated converters.

Delta-modulation or *area comparison-integral PWM* is the best known. The *Synchronous-Sigma-Delta-Modulation* system is based on a feedback of the output signal. The filtered error signal is fed to a comparator the output of which is sampled at a constant clock frequency f_c .

The output of the modulator $s(t)$ determines the state of the switches of the

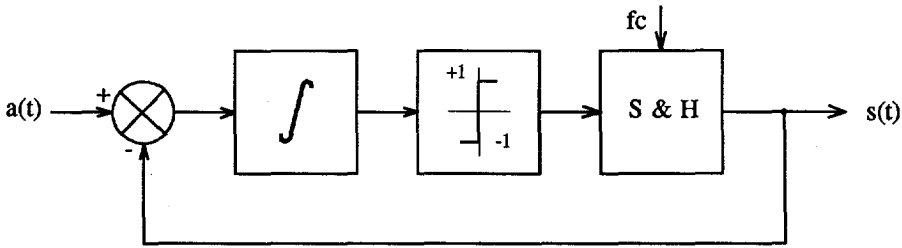


Fig. 4.13 Single-phase sigma-delta modulator.

respective inverter phase leg and is only changed at instants synchronous to the internal clock. Using the resonant link as a clock, the modulators are perfectly suited to control resonant link converters. The modulator has also been used in combination with a conventional hard-switching inverter. The performance analysis of a three-phase inverter controlled by delta modulation is provided in [Mertens, 1992,a] and the performance of a delta modulator in terms of harmonic distortion is given in [Mertens, 1992,b]. Delta modulation is applied in converters using a current configuration.

The fact, that the modulator in Fig. 4.13 utilizes the feedback of the output signal and compares it with a reference, makes the modulation resemble to a sliding mode control principle. Variable structure systems and sliding mode control are well defined subjects [Utkin, 1978]. To explore the relation between pulse-modulation techniques and sliding mode control, this relation is investigated in next chapter.

There are topologies for which a choice has to be made between the phases to select the conducting phase for the next cycle. This selection process is typical for converter topologies using a voltage configuration as defined in Chapter 2.

The commonly suggested control philosophy is based on the static error. This error is defined as a difference between the line voltage or current and a reference value of this voltage or current, respectively. The phase with a positive or negative maximum error is selected to conduct in the next cycle. First, the errors between the reference voltages and the capacitor voltages of a three-phase converter are calculated. Then phases with a positive and negative error are determined. In this case the positive maximum error phase is the one in which an error is maximum among the three phases and similarly, the negative maximum error phase is the one in which the error is maximum with negative polarity. The next resonant pulse is created the way to compensate the created errors. This philosophy is suggested in [Kim, Cho, 1990], [Woo, et.al., 1990]. In the examples referred to, the resonant link energy is independently controlled and the pulse width is varying. A similar approach for the selection of the input/output bridge was also taken in [De Beer, Klaassens, 1991]. The control principles suggested in the mentioned

paper resemble the fuzzy logic control.

A discussion over AC-to-AC converter control with a series-resonant link has to consider the evolution of the resonant capacitor voltage. The maximum voltage over the resonant capacitor is physically limited and the selection of the input and output phases is then even more complex.

Finally two problems of soft-switching resonant AC power conversion can be encountered:

1. **Filtering problem**

The conventional design of a filter is not very effective since the harmonics are not very well located. Therefore, it is preferable to include the filter behaviour in the dynamic model. The modulation process has to be based on this model. Thus, the passive filter becomes a part of an active filter process.

2. **Selection problem**

The selection of the conducting phase is based on the static error (current or voltage). The AC-AC pulse-modulated resonant converter can be compared to a matrix converter, where the energy is transferred by high-frequency pulses only. The selection of a conducting phase in the input bridge SM1 has a direct influence on the current at the output of the converter.

The same problem occurs in the opposite situation. The selection of an output conducting phase has a direct influence on the input. In addition, the selection of the input and output determines what is called the mirror voltage, which has a direct impact on the energy in the resonant link.

To solve the encountered problems, a modulation process based on a mathematical description of the entire converter has to be studied. The suggested way is a space phasor description.

4.5 Conclusions

The soft-switching converter topologies and control principles have been reviewed. Two strategies: PWM and PFM are applied for the modulation of the external waveforms. The dynamic analysis of the PWM converter is essentially the same as for the hard-switched converters studied in Chapter 3. Therefore, the PWM soft-switched converters do not need further attention. The group of pulse-modulated resonant converters are addressed in the following chapters. The dynamic synthesis with the use of model defined in Chapter 2 is documented. Two typical examples: a *zero-current switching* series-resonant converter and a *zero-voltage switching* parallel-resonant converter are selected as typical representatives.

Filtering problems and selection problems concerning soft-switching resonant

pulse-modulated converters have also been encountered. A state-of-the-art modulation process for AC-to-AC resonant converter is based on the static error. So far, there is no method that could prescribe the dynamic behaviour of pulse-modulated converters. The modulation process based on the mathematical model of the complete converter has to be studied. The behaviour of the filter has to be included in that model to explore active filtering. The suggested method is to investigate the dynamic behaviour by the application of a mathematical model defined in Chapter 2. It is recognized that the pulse-modulation process of soft-switching resonant converters is approaching the sliding mode principle. To understand this relation, the variable structure control and the sliding mode are studied in the following chapter.

5

**PULSE-MODULATION
TECHNIQUES AND VARIABLE
STRUCTURE CONTROL**

5.1 Introduction

As indicated in Chapter 4, most of the currently used control methods for pulse modulated soft-switching resonant-link converters are based on the principles of the sliding mode control. However, they are not designed as sliding mode controllers as will be explained in Chapter 5.3. In fact, the methods fulfil the conditions and the characteristics of a sliding mode control for discrete systems.

Sliding mode control is reviewed in the first part of this chapter. It is recognized that the AC-to-AC pulse modulated converter is a multiple-input/multiple-output discrete, nonlinear system. In the following part, the link between sliding mode control and existing control methods is established. An ASDTIC controller, a philosophy applied to modulate the external waveforms of a series-resonant converter, is compared with sliding mode control. The possibility to design a pulse modulator based on a sliding mode control with the use of a switching bridge model defined in Chapter 2 is investigated.

5.2 Variable structure control - survey

Variable structure control (VSC), including sliding mode [V.Utkin,1978], has been extended into a general design method applied for a wide spectrum of systems including nonlinear systems, multiple-input/multiple-output systems, discrete time models, etc. [J.Y.Hung, 1992].

The most distinguished feature of VSC is its ability to establish very robust control systems: in many cases invariant control. The term "invariant" indicates that the system is insensitive to parametric uncertainties and external disturbances.

In AC-to-AC pulse modulated resonant converters we are considering a multiple-input/multiple-output system. Further, the system has a discrete nature where discretization is originated from the generation of repetitive pulses. It is known that a discrete system can only undergo the *quasi-sliding* mode: the state of the system can only *approach* the switching surface but cannot *stay* on this surface. This is because the control action can only be activated at sampling instants and the control effort is constant over each sampling period. However, this is not totally valid for pulse modulation techniques. In spite of the discrete nature of resonant pulse modulation, the possibility to change the pulse position adds a continuous variable to discrete processes.

Next, a definition of a variable structure control follows. A given control system is represented by state equation:

$$\dot{x} = A(x,t) + B(x,t)u \quad (5.1)$$

with:

n - dimension of state variable x ,

m - dimension of control input u .

The task of sliding mode control is to find:

1. m switching surface functions presented in vector form as $s(x)$,
2. a variable structure control input:

$$u(x,t) = u^+(x,t) \quad \text{when } s(x) > 0,$$

$$u(x,t) = u^-(x,t) \quad \text{when } s(x) < 0,$$

so that the reaching modes satisfy the reaching condition. The physical interpretation of the statement above is:

1. to design a switching surface $s(x)=0$ which represents the desired system dynamics that is of a lower order than the given plant.
2. to design a variable structure control $u(x,t)$ so that any state x outside the switching surface is driven to reach the surface in a finite time. The sliding mode follows the desired system dynamics on the switching surface. In this way the complete VSC system is globally asymptotically stable.

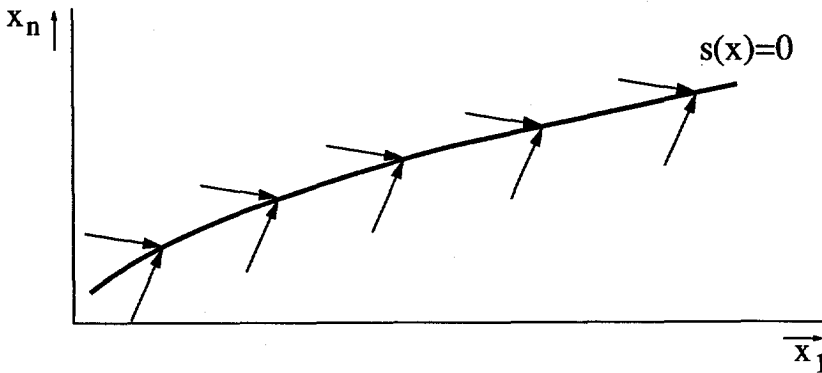


Fig. 5.1 Sliding mode and the sliding surface

For the existence of the sliding motion, it is necessary that the state trajectories near the switching surface point towards the surface $s(x)=0$ shown in Fig. 5.1. The condition for the existence of a sliding mode for switch (i) is:

$$\lim_{s_i(x) \uparrow 0} \dot{s}_i(x) > 0 \tag{5.2}$$

and:

$$\lim_{s_i(x) \downarrow 0} \dot{s}_i(x) < 0 \tag{5.3}$$

or:

$$\dot{s}_i(x)s_i(x) < 0 \quad (5.4)$$

Once the system is in the sliding mode, the system satisfies two conditions. First, the state of the system in sliding mode moves on the switching surface:

$$s(x) = 0 \quad (5.5)$$

Secondly, the state will not leave the switching surface. This means that for the sliding mode, the following equation is valid:

$$\dot{s}(x) = 0 \quad (5.6)$$

Conditions (5.5) and (5.6) are valid for ideal sliding mode. In the case of a *quasi-sliding mode*, the state of the system does not move strictly on the sliding surface.

5.2.1 Multiple-input variable structure system

For a multiple-input system, more than one switching surface can be defined, each acting on a single switch. The sliding movement can start in a different number of ways called a switching scheme. Since a resonant pulse modulated three-phase resonant converter performs according to a multiple-input variable structure control, it is important to investigate a possible switching scheme. Next, different switching schemes are summarized.

Fixed-order switching scheme

In this scheme, the sliding mode takes place in a preassigned order as the system state traverses the state space. For example, the state can first move from the initial state x_0 to the switching surface S_1 that has the dimension $n-1$. Then the sliding mode moves to the surface $S_{12}=(S_1 \cap S_2)$ which has a dimension $n-2$.

The sliding mode moves to progressively lower dimensional sliding surfaces and eventually reaches the surface S_E that has a dimension $n-m$:

$$x_0 \rightarrow S_1 \rightarrow (S_1 \cap S_2) \rightarrow (S_1 \cap S_2 \cap S_3) \rightarrow \dots \rightarrow S_E \quad (5.7)$$

where:

S_E - sliding mode surface.

This early scheme has been called the *hierarchical VSC scheme*. The VSC scheme has several weaknesses: a slow and poor transient response in general which necessitates a large control effort and gives difficulty in its solution.

Free-order switching scheme

The order of sliding modes is not preassigned but follows a natural trajectory for a first-reach-first-switch scheme. Switching takes place according to the location

of the initial state in the state space. This scheme is more plausible than the fixed-order scheme for three reasons. Firstly, this solution of VSC is easy to find. Secondly, the reaching mode possesses better dynamic characteristics. Finally, the resulting control effort is smaller in magnitude so saturation is less likely to occur.

Eventual sliding mode switching scheme

In this scheme the state is driven from any initial state to the eventual sliding surface S_E on which the sliding mode control takes place. However, this method does not guarantee good transient characteristics [J.Y.Hung, 1992].

Decentralized switching scheme

The system is treated as a subsystem with m -single inputs, where each has a scalar switching function and the associated switching mode. This scheme is suitable for the synthesis of the modulator based on the switching function model of a switching leg for current and voltage configuration [J.Y.Hung, 1992].

State-of-the-art control and switching scheme

The comparison between the sliding mode switching scheme and a state-of-the-art pulse modulation for three-phase resonant converters shows that the fixed-order and the free-order schemes are applied. The switching scheme is related to the source and load sliding surfaces and sliding surfaces of a three-phase system of currents or voltages.

The *fixed-order* switching scheme in the state-of-the-art methods means that first currents and voltages of one side (either source or load) are investigated. There is thus preference given to one side of a three-phase-to-three-phase converter. The *free-order* switching scheme is applied in cases where the source or load side is switching in dependence of which the sliding surface is reached first.

The switching scheme can be related to the three-phase system of currents or voltages. In the case of an application of a switching leg model, each phase current or voltage creates a sliding line. In the case of application of a model of a space switching phasor, d, q coordinates of a three-phase system of currents or voltages create a sliding surface. Different switching schemes can also be applied.

5.3 Resonant pulse modulation techniques and sliding mode

The control of resonant converters and the sliding mode surveyed in the previous section have a strong relation. The first known modulator for a resonant converter *ASDTIC* (*Analog-Signal-To-Discrete-Time Interval Converter*) is based on the integral of the difference between the reference current and the actual resonant current. The zero state ASDTIC was originally developed for DC-to-DC converters [Schwarz, 1974], [Schwarz, 1976] and later extended to DC-to-AC and AC-to-DC applications [Klaassens, 1986], [Klaassens, 1987], [Klaassens, 1991].

The integral of the resonant current i_{ri} in i -phase over one cycle $[x_k, x_{k+1}]$ is

compared to a reference signal i_{ref} :

$$\varepsilon = \int_{x_k}^{x_{k+1}} i_{ref} dx - \int_{x_k}^{x_{k+1}} i_{r1} dx = 0 \quad (5.8)$$

where:

- i_{ref} - reference current,
- i_r - resonant current,
- ε - error signal.

Firing pulses for the switch are generated at the instants in which the average resonant current i_r is equal to the prescribed value of the control signal i_{ref} . The integral of the resonant inductor current presents, in fact, the transferred charge. The sliding surface is created as a difference between the reference charge and the actual charge transferred to the required terminal of the converter.

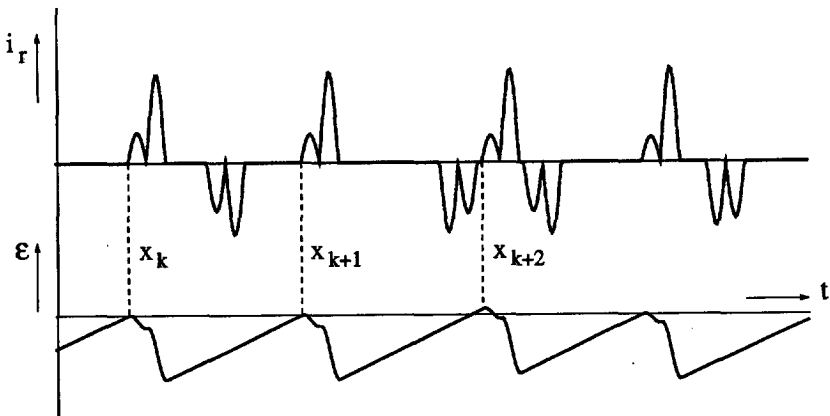


Fig. 5.2 Simulation of a resonant link current i_r and the error signal ε of an ASDTIC modulator

Simulated waveforms of a DC-to-three-phase series-resonant converter with ASDTIC regulation [Weesenbeek, Klaassens, 1993] are shown in Fig. 5.2. To maintain the energy in the resonant link on a required level, a pair of resonant pulses is used. In Fig. 5.2, a resonant link current i_r and error signal ε of the ASDTIC modulator are shown. One can see that whenever the difference of two integrals from (5.8) reaches zero, resonant pulses are initiated to reduce the error that arises. However, it can happen that the resonant pulse is initiated with time delay because the resonant pulse in the different phase is still on, as shown in Fig. 5.2 at the pulse in the time instant x_{k+2} . Because the modulator is applied to each phase of a three-phase AC system, it is in fact a free-order switching scheme. In the mentioned reference, the ASDTIC is applied for each phase separately. During the time interval of the resonant pulse, the controller cannot influence the

energy transfer. The sliding mode, thus, operates with a sampling frequency twice as big as the resonant-pulse frequency. The ASDTIC philosophy is inherently identical to a sliding mode control with the limitation of a discrete sampling instant during a resonant pulse. Therefore, the control is considered to be a quasi-sliding control mode. The application of ASDTIC and the related modulation philosophy for polyphase resonant converters is limited. ASDTIC, originally developed for single-phase converters, does not directly offer a solution for the *selection problem* defined in Chapter 4.

The dynamic analysis for resonant converters investigated in the following chapters can be considered as an extension of the ASDTIC philosophy based on a sliding mode control. It is shown, that a control design based on the sliding mode contains ASDTIC elements.

Next, the utilization of a design of a modulator for a three-phase soft-switching resonant power converter based on the quasi-sliding mode is investigated. The topologies under consideration are the ones with a three-phase switching bridge. As mentioned in Chapter 4, further attention is paid to a three-phase-to-three-phase series-resonant converter and a parallel-resonant converter. The application of a three-phase switching bridge for a quasi-sliding mode control is studied.

5.4 Quasi-sliding mode modulators and models of a three-phase switching bridge

To design a modulator based on a quasi-sliding mode, a switching surface $s(x)$ and a control input for a three-phase switching bridge have to be defined. In the case of a power converter, the switching surface is usually defined as the difference between the reference and the actual values of currents or voltages.

The switching action of a variable structure system is prescribed by its control input $u(x,t)$. Let us relate the control input $u(x,t)$ to the switching action of a three-phase switching bridge. In Chapter 2, two different models of the switching action of switches in the bridge configuration are defined.

The following discussion is meant for the design of quasi-sliding mode modulators for resonant pulse-modulated converters and sliding mode modulators for PWM converters. The AC PWM converter topologies were discussed in Chapter 3. Let us summarize the ultimate goal of the control action of a quasi-sliding mode modulator. The investigated topologies use switches in a bridge configuration as defined in Chapter 2. The goal of a switching action is to transfer the energy from the AC side of a bridge to the DC side or vice versa. The electrical quantities (voltages and currents) at the AC side are usually required with sinusoidal shape to achieve desired power factor. The control action of the modulator has to assure that the AC and the DC side voltages (or currents) track their reference. At the same time the required energy should be transferred from the AC to the DC side or vice versa.

Switching function model of a switching leg

The switching function $\delta_i(t)$ defined for a switching leg is in the case of the *current configuration* identical to a sliding mode control input. The switching function $\delta_i(t)$ obtains values +1 and -1 that coincide with the definition of the control input $u(x,t)$ for sliding mode. By defining a sliding switching surface $s(x)$ for each switching leg terminal a quasi-sliding mode is defined. The switching surface of the sliding mode is created by three reference currents of a three-phase system. The power balance of a three-phase switching bridge (equation (2.58)) shows that by selecting the AC reference current (voltage), DC values are determined. The actual position of the switching leg is calculated on the basis of equation (2.6). The term $\sum \delta_i(t)$ in this equation represents the actual position of two other legs and makes the calculation of the switching function cumbersome. The result of the term $1/3 \sum \delta_i(t)$ is a constant equal to 1/3 or 2/3 with positive or negative sign. However, the sign of the resulting calculated switching function $\delta_i(t)$ does not change with the value or sign of the term $1/3 \sum \delta_i(t)$. Based on the calculated value of the switching function $\delta_i(t)$, a discrete value of the switching function $\delta_1(t)$ (+1 or -1) is selected. The value of the selected switching function $\delta_1(t)$ depends on the sign of the calculated switching function which is not influenced by the term $1/3 \sum \delta_i(t)$. The switching function model is, thus, easy to apply for the dynamic synthesis of a quasi-sliding modulator of converter with current configuration of a switching bridge as shown in Chapter 7.

In the case of a *voltage configuration*, the application of a switching function is more complicated. Since the constraint (2.4) is imposed on the switches, the switching function $\delta_i(t)$ can have 3 values: +1, 0, -1. This time, the selection of the switching function $\delta_i(t)$ for $i=a,b,c$ cannot be based only on the signum of the calculated switching function as in case of a current configuration. The design of the quasi-sliding modulator is possible only with the use of a fuzzy terms and fuzzy logic control. It is not advantageous to derive a switching function from equations defined in Chapter 2 for a voltage configuration.

Switching space phasor model

The switching space phasor model is more suitable for the design of a quasi-sliding modulator for current or voltage configuration than the switching function model of a switching leg. The reason is that the switching phasor represents the position of the switches in all three phases at the same time. The problem is to find a suitable strategy since the selection of a switching space phasor from the sets defined in Table 2.1 and Table 2.2 is a complex problem. The selected switching space phasor has to drive the currents and voltages of the system towards its templates to fulfil the condition expressed in equation (5.4). This problem is studied in details on an example of a three-phase-to-three-phase series-resonant converter in Chapter 6. The control input $u(x,t)$ for a sliding mode is in this case performed by d,q or α,β coordinates of the switching space phasor \underline{g} . The switching surface of a sliding mode $\underline{g}(x)$ is performed by d,q or α,β coordinates of the reference current or voltage space phasor.

5.5 Conclusions

The application of a sliding mode control for discrete systems such as resonant pulse-modulation converters has been discussed. A three-phase-to-three-phase resonant link converter is considered to be a multiple-input/multiple-output system. An eventual sliding mode switching scheme is requested for modulation of desired waveforms at the source and the load sides of a converter. In transforming this condition (an eventual sliding mode scheme) into a switching philosophy of a three-phase-to-three-phase resonant converter, the sliding mode must occur at the source and the load sides of the converter simultaneously.

The discrete nature of the resonant pulse modulator results in a quasi-sliding mode. The disadvantage of a quasi-sliding mode is that the system does not stay on the sliding surface as it does in the case of ideal sliding motion. The deviation from the ideal sliding surface arises within the sampling period of the sliding modulator. The chattering which is a disadvantageous property of the ideal sliding motion does not occur in the case of a quasi-sliding motion.

There is a relation between existing resonant pulse-modulation techniques and sliding mode. It is proved that an ASDTIC is in fact a quasi-sliding mode modulator. The ASDTIC modulator, that was originally developed for single phase converters, however, does not solve the selection problem. Therefore, it is suggested to solve the modulation process of a three-phase-to-three-phase power converter by introducing a sliding mode principle.

The usefulness of the models defined in Chapter 2 for the design of a quasi-sliding mode modulator is investigated. It is concluded that the switching function model of a switching leg is eligible for converters with use of a current configuration. The switching space phasor model is more general and it is applicable for converters using either a current or a voltage configuration.

6

**SERIES-RESONANT
CONVERTER**

6.1 Introduction

The series-resonant converter that was originally developed for DC-to-DC applications has recently also been applied for AC-to-AC power conversion.

Conventional series-resonant converters are classified according to their method of control. One method is a frequency control where the external waveforms are controlled by the ratio of the switching frequency and the frequency of the resonant circuit. The other method is a phase-domain control where the control is achieved by the difference in phase between two switching matrixes while the switching frequency of each matrix is fixed.

The resonant converters with fixed frequency control and zero-phase are designed for AC applications. Soft-switching is achieved by the occurrence of the zero-crossing of the resonant current. Since the switching occurs at the zero-crossing instants of the link current, the current via the semiconductor switch drops below the holding current (when a thyristor is used as a switch). The natural turn-off ability is, thus, used for commutation (*zero-current turn off*). Thus, high power thyristors can be used with a minimal switching loss. The switching frequency of a thyristor is, however, limited by the reverse recovery time. Therefore, for applications where high-frequency operation is required, IGBTs or MCTs are appropriate. The principle of operation remains the same. The resonant current pulse becomes a basic unit for the transfer of energy.

The converter dynamics and converter modelling are crucial for the study of the application of a suitable feedback algorithm for closed loop modulation of the converter voltages and currents. Modelling of resonant converters is a difficult task because of the nonlinear characteristics of a switched resonant circuit. To understand the operation of the converter, its analysis is crucial. The dynamic synthesis of a converter modulation leads to improved control and modulation design as shown in this chapter.

The analysis of single-phase converters is straightforward. For polyphase series-resonant converters, the problems of the *filtering* and the *selection of switches* are serious. As explained in Chapter 4, the analysis of a polyphase series-resonant converter is based on a single-phase model. There is no extended model prescribing the dynamics of this converter. Its analysis is considered to be a demanding job. Modulation methods based on a single-phase model do not guarantee the solution for the described *filtering* and *selection* problem.

In this chapter, we develop a dynamic model of a series-resonant converter. This model is also the first dynamic model for polyphase resonant converters with switches in a bridge configuration.

6.2 A three-phase-to-three-phase series-resonant converter

The schematic of a three-phase-to-three-phase series-resonant converter is shown in Fig. 6.1.

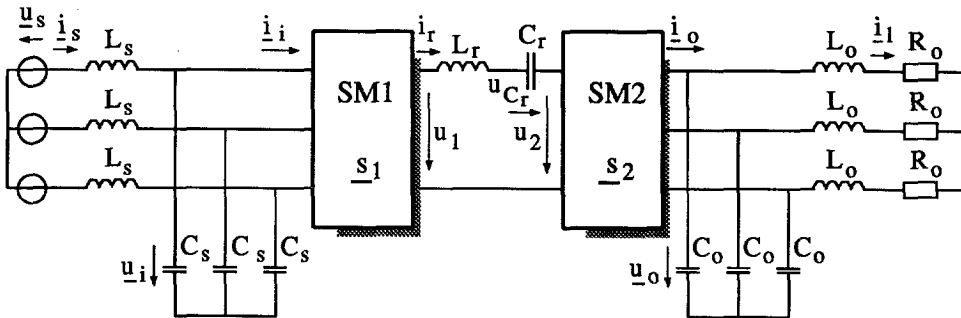


Fig. 6.1 Three-phase-to-three-phase series-resonant converter

The schematic corresponds with the general schematic of a three-phase-to-three-phase power converter scheme as mentioned in Chapter 1. The passive network from Fig. 1.7. is realized with a series-resonant circuit composed of the passive elements L_r and C_r . The switching matrices SM1 and SM2 are realized by three-phase switching bridges. The second order filter $L_s C_s$ is used at the source side and capacitors C_o are placed at the output (load) side. In Fig. 6.1 an inductive-resistive load R_o, L_o is depicted.

The converter is characterized as an AC series-resonant link converter. Bidirectional switches in the three-phase switching bridge are therefore required. Second-order filters with capacitive characteristics are applied. According to the definitions in Chapter 2, the switching matrices SM1 and SM2 employ the voltage configuration. Due to the complexity of the schematic and the lack of mathematical tools, there is no dynamic model available. The switching philosophy is developed on the base of a simple model as reviewed in Chapter 4. The usefulness of the models defined in Chapter 2 is documented on an example of a three-phase-to-three-phase series-resonant converter. As stated previously, dynamic effects must be included to obtain an accurate model. The usefulness of a dynamic analysis and a dynamic model is shown on an example of a converter which modulation and the control is a matter of intensive research,

In Chapter 2, two different models for a three-phase switching bridge are suggested. Now, based on these models, the *selection* problem defined in Chapter 4 has been solved. The filtering problem (Chapter 4) requires the insertion of the used passive filters in the model. Therefore, the model with the use of a switching space phasor is obviously suitable. Using the switching space phasor model from Chapter 2, a set of dynamic equations for the three-phase-to-three-phase series-resonant converter can be established.

6.3 Dynamic equations of a three-phase-to-three-phase series-resonant converter

A set of differential equations is presented for a three-phase-to-three-phase series-resonant converter shown in Fig. 6.1. The switching behaviour of the switching matrices SM1 and SM2 is represented by a space-switching phasor \underline{s}_I and \underline{s}_{II} respectively. The switching matrix is presented by the switches in a bridge configuration. In Chapter 2, the nonlinear equations relating the voltages and the currents between the AC and the DC sides of a switching bridge are defined. With the use of these relations, a set of differential equations describing a dynamic model is now created as routine work. Only the voltage configuration defined in Chapter 2 is applied for the investigated converter topology because of the character of the filters and the resonant link. Because the switching bridge SM1 behaves as a rectifier, equations (2.27) and (2.28) are valid. These equations define the relation between the AC and the DC sides of the bridge. The relations between the voltage u_1 and the voltage phasor \underline{u}_1 , and the current i_r and the current phasor \underline{i}_r are:

$$u_1 = \frac{3}{2} \operatorname{Re}\{\underline{s}_I^* \underline{u}_1\} \quad (6.1)$$

$$\underline{i}_1 = \underline{s}_I i_r \quad (6.2)$$

The selection of the equations for the switching matrix SM2 needs an additional explanation. The amplitude and polarity of the resonant current depend on the selected voltage u_o . The output current per phase i_o results from a resonant current pulse i_r and the selected switching phasor \underline{s}_{II} . This means that a switching matrix SM2 behaves as a current source inverter. Because of the principle of duality, the same relation for SM1 can be used.

After the selection of the equation is achieved, the construction of a dynamic model is elementary. The set of equations is as follows:

$$C_o \frac{du_o}{dt} = i_o - \underline{i}_1 = \underline{s}_{II} i_r - \underline{i}_1 \quad (6.3)$$

$$L_s \frac{di_s}{dt} = u_s - u_i \quad (6.4)$$

$$C_s \frac{du_i}{dt} = i_s - \underline{i}_1 = i_s - \underline{s}_I i_r \quad (6.5)$$

$$u_2 = \frac{3}{2} \operatorname{Re}\{\underline{s}_{II}^* \underline{u}_o\} \quad (6.6)$$

$$\frac{1}{C_r} \int i_r dt + L_r \frac{di_r}{dt} = u_1 - u_2 \quad (6.7)$$

The dynamic model of the three-phase-to-three-phase series-resonant converter is shown in Fig. 6.2.

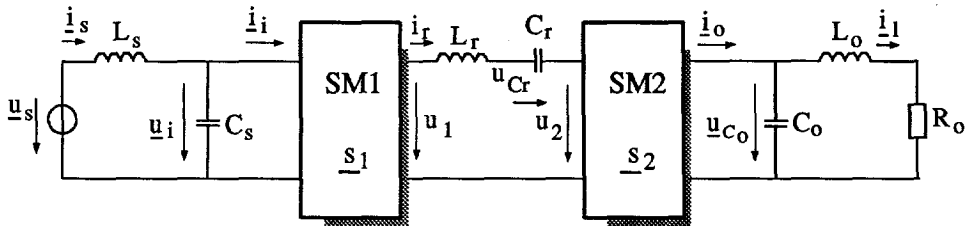


Fig. 6.2 Dynamic model of a series-resonant converter

The definition of the problem is simple. We have to find a switching phasor \underline{s}_I and \underline{s}_{II} in such a way that the currents \underline{i}_s and \underline{i}_l follow their references within the required degree of accuracy.

Another criterium that has to be considered is the value of resonant current i_r and the value of resonant capacitor voltage u_{Cr} . These quantities are physically limited by the current and voltage limitations of the applied components of the converter. The set of equations (6.1)...(6.7) is difficult to solve analytically. Therefore, these equations are analyzed and, as for all previous modelling methods, simplifications are introduced. At first glance it is obvious that the difficulties of obtaining a solution begin with the integrodifferential equation (6.7) prescribing the dynamics of the resonant link current. Therefore, further attention is paid to the resonant link current.

6.4 Resonant link current and quantum transformation

Each resonant current pulse is generated by the resonant circuit by excitation by one or two voltage sources. The voltages u_1 and u_2 are the results of the switching action of the switching matrices SM1 and SM2. The connection of two sources u_1 and u_2 to a single resonant circuit transfers electrical energy from one source to another. The simple single-phase model shown in Fig. 6.3 represents this circuit.

The control of polyphase resonant converters mentioned in literature is based on this simple model that reflects the evolution of the resonant current. This model is not suitable for calculation of the external waveforms of the converter. However, as already explained in Chapter 4, the state-of-the-art control is based on such a model.

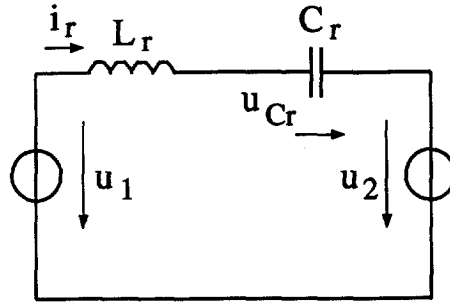


Fig. 6.3 One-phase model of a series-resonant converter

The set of dynamic equations of a three-phase-to-three-phase series-resonant converter involves fast varying quantities: voltages and currents of the resonant circuit. However, the natural frequency of the resonant link is half of the switching frequency. The natural frequency of the input and output filters is below the switching frequency. The external waveforms present slowly varying waveforms compared to the internal waveforms with the switching frequency, which is inherently double of the resonant frequency. Consequently, it is possible to consider the system of equations on two different time scales. The time scale t is the actual time scale. The phasors of input and output quantities are presented in this time scale. Time scale t' is related to the start of a resonant pulse and is reset whenever a resonant pulse is completed.

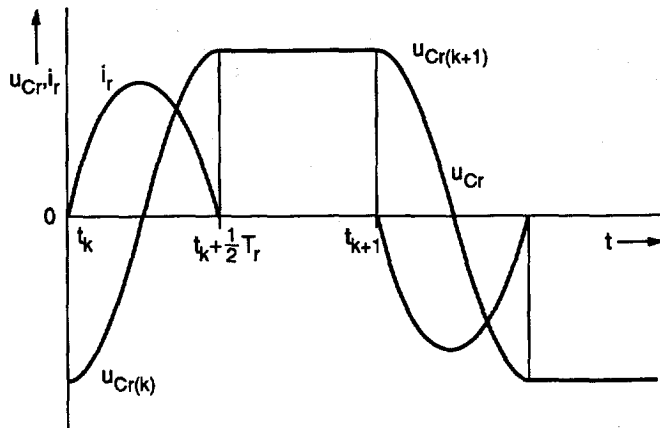


Fig. 6.4 Resonant current and resonant capacitor voltage

The voltages u_1 and u_2 are time-varying waveforms. The usual approximation for the analysis of the series-resonant converter assumes that these voltages are constant during the length of one resonant pulse. This approximation is justified by the fact that the frequency of the resonant current is several orders of

magnitude higher than the frequency of the external waveforms.

By solving equation (6.7) for u_1 and u_2 quasi constant, we obtain the dynamic relations that establish the evolution of the resonant voltage and the shape of the resonant current as shown in Fig. 6.4.

$$i_r(t') = \frac{-u_{Cr}(0) + u_1 - u_2}{Z_r} \sin(\omega_r t') \quad (6.8)$$

$$u_{Cr}(t') = -(-u_{Cr}(0) + u_1 - u_2) \cos(\omega_r t') + u_1 - u_2 \quad (6.9)$$

where:

Z_r - characteristic impedance of the resonant circuit:

$$Z_r = \sqrt{L_r/C_r} \quad (6.10)$$

ω_r - angular resonant frequency:

$$\omega_r = \frac{1}{\sqrt{L_r C_r}} = \frac{2\pi}{T_r} \quad (6.11)$$

$u_{Cr}(0)$ - resonant capacitor voltage at the beginning of resonant pulse $t'=0$.

Equations (6.8) and (6.9) provide an exact solution of equation (6.7) assuming that the voltages u_1 and u_2 are constant during the resonant pulse. The voltage $u_1 - u_2$ that are applied to the resonant $L_r C_r$ circuit is called in literature *the mirror voltage*. Voltage $u_{Cr}(0)$ is the resonant capacitor voltage at $t'=0$ being the initial condition for the differential equation (6.9). The current at $t'=0$ is zero. The time interval between two resonant pulses $t_{k+1} - (t_k + 1/2T_r)$ is called the *interpulse time* (Fig. 6.4). Assuming that the voltages u_1 and u_2 are constant during a resonant pulse, a sampled model is obtained for the resonant capacitor voltage and resonant inductor current for the k -th pulse (Fig. 6.4):

$$u_{Cr}(k+1) = -u_{Cr}(k) + 2(u_1 - u_2) \quad (6.12)$$

$$i_r(k) = \frac{-u_{Cr}(k) + u_1 - u_2}{Z_r} \sin(\omega_r t') \quad (6.13)$$

where:

$u_{Cr}(k)$ - the resonant capacitor voltage at the beginning of the k -th pulse.

Equations (6.12) and (6.13) prescribe the change in the resonant current. The exact shape of the resonant capacitor voltage u_{Cr} is not important. The initial

values of the resonant capacitor voltage for each successive phase are simple to calculate on the basis of equation (6.12).

The sampled model is obtained by replacing equation (6.7) by the obtained solution (6.12) and (6.13). The resonant link current is approximated by a sinusoidal waveform and the influence of the slowly varying voltages u_1 and u_2 is neglected.

Quantum transformation

The second approximation used for the analysis of the resonant converter is a *linearization* of the charge transferred by the resonant current.

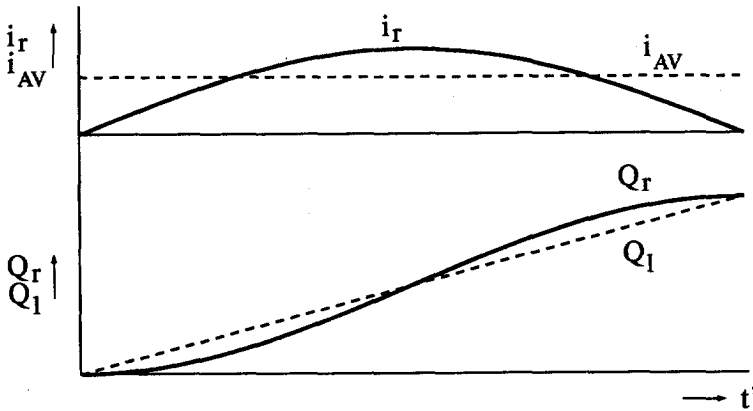


Fig. 6.5 Resonant current i_r and charge Q_r transferred by the resonant current

In Fig. 6.5, the resonant current i_r and the transferred charge of the resonant circuit are depicted. The dotted line Q_1 is the result of the approximation obtained by linearization $Q_r(t)$. The linearization of the transferred charge means that the sinusoidal waveform i_r is approximated by its average value i_{AV} . Thus, the influence of the wave shape of the resonant current on the external waveforms is neglected. The approximation is also justified by the difference in frequency between the external waveforms and the resonant current. The sampled equation (6.12) is, however, still the cause of the existence of a discontinuous dynamic model.

Therefore next, the quantum transformation [Joung et al., 1992], that partially solves the problem of the discontinuity, is studied. The amplitude of the resonant capacitor voltage is related to the stored energy in the resonant capacitor C_r . The average value of the inductor current i_{AV} is related to the stored energy in the resonant inductor L_r . Now, the state variables u_r^* and i_r^* are selected as new variables for the linearized circuit:

$$\begin{aligned} u_{Cr}^*(k) &= |u_{Cr}(k)| \\ i_r^*(k) &= |i_{AV}(k)| \end{aligned} \quad (6.14)$$

where:

- $u_{Cr}(k)$ - peak value of the resonant capacitor voltage at the beginning of the k^{th} cycle,
- $i_{AV}(k)$ - average value of the resonant current during the k^{th} cycle.

The value of the averaged resonant current throughout half of a period of a resonance is equal to:

$$i_r^*(k) = \frac{2}{\pi} \frac{u_{Cr}^*(k) + (u_1 - u_2)_k (-1)^{k+1}}{Z_r} \quad (6.15)$$

where $(u_1 - u_2)_k$ is mirror voltage in k^{th} cycle.

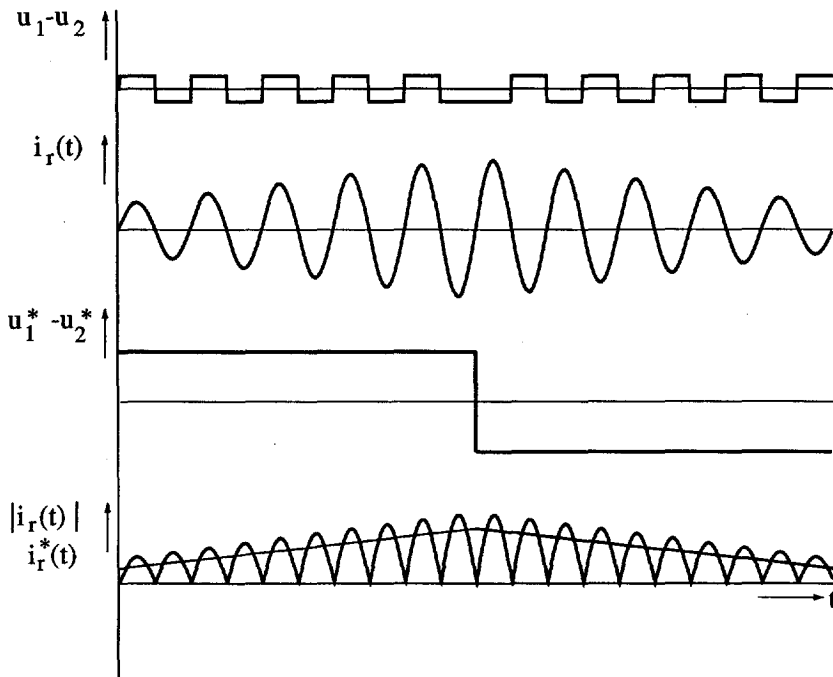


Fig. 6.6 Simulated waveforms of the resonant circuit

The sampled value of the resonant capacitor voltage (6.12) with the use of the new state variable $u_{Cr}^*(k)$ is equal to:

$$u_{Cr}^*(k+1) = u_{Cr}^*(k) + 2(u_1 - u_2)_k (-1)^{k+1} \quad (6.16)$$

The resonant current $i_r(t)$ excited by the mirror voltage u_1-u_2 is depicted in Fig. 6.6. The mirror voltage u_1-u_2 is in this case synchronized with the zero-crossing points of the resonant current. The time interval between two pulses $t_{k+1}-(t_k+1/2T_r)$ is here equal to zero. The quantum transformation investigates how the increase of the energy of the resonant circuit or the amplitude of the resonant current depends on the applied mirror voltage. The energy of the resonant circuit and the amplitude of the resonant current are independent of interpulse time. So, the quantum transformation is not influenced by this time interval. As said before, the interpulse time is neglected in Fig. 6.6. During the time intervals when the mirror voltage u_1-u_2 is in phase with the resonant current $i_r(t)$, the peak value and the average value of the resonant current rise as shown in Fig. 6.6. Energy is added to the resonant $L_r C_r$ circuit. Whenever the mirror voltage u_1-u_2 has the opposite polarity to the resonant current $i_r(t)$, the energy stored in the resonant circuit decreases. The amplitude of the resonant current and the averaged value of the resonant current $i_r^*(k)$ also decrease. Knowing this, the resonant $L_r C_r$ link is modelled as a single inductor L_{eq} in Fig. 6.7.

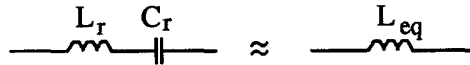


Fig. 6.7 Series-resonant $L_r C_r$ link and equivalent inductor L_{eq}

The mirror voltage u_1-u_2 in phase with the resonant current is equivalent to the positive voltage u_1-u_2 applied to the inductor L_{eq} (see Fig.6.6). The mirror voltage in opposite phase to the resonant current is equivalent to a negative voltage u_1-u_2 applied to inductor L_{eq} . The derivative of the discrete current value $i_r^*(k)$ from pulse to pulse expressed analytically at the sampling instants is the same as the derivative of the current $i_r^*(t)$, (Fig.6.8):

$$\begin{aligned} \frac{di_r^*(t)}{dt} &= \frac{i_r^*(k+1)-i_r^*(k)}{\frac{T}{2}} = \left(\frac{2}{\pi}\right)^2 \frac{(u_1-u_2)_k (-1)^{k+1}}{L_r} \\ &= \left(\frac{2}{\pi}\right)^2 \frac{u_1^*-u_2^*}{L_r} \end{aligned} \quad (6.17)$$

where:

$$\begin{aligned} i_r^*(t) & \text{ - current of an equivalent inductor,} \\ u_1^*-u_2^* & \text{ - equivalent mirror voltage.} \end{aligned}$$

The equivalent inductance then has the value:

$$L_{eq} = \left(\frac{\pi}{2}\right)^2 L_r \quad (6.18)$$

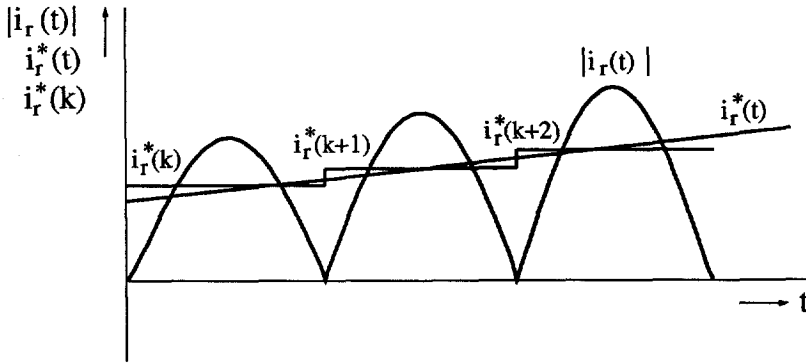


Fig. 6.8 Absolute value of the resonant current $i_r(t)$, its average value $i_r^*(k)$ and current of the equivalent inductor $i_r^*(t)$

The defined quantum transformation allows the replacement of the resonant $L_r C_r$ circuit with nonlinear characteristics (voltages and currents) by a linear inductance L_{eq} . By this procedure, a step of lowering the order of the switching circuit is provided. The equation (6.7) is replaced by:

$$L_{eq} \frac{di_r^*(t)}{dt} = (u_1^* - u_2^*) \tag{6.19}$$

In the further analysis, the current of the equivalent inductor $i_r^*(t)$ represents the absolute value of the mean pulse current of the resonant circuit. The replacement of the second order differential equation (6.7) by the first order differential equation (6.19) offers further simplification of the analysis and a better understanding of the operation of a three-phase-to-three-phase series-resonant converter. In further analysis the resonant current $i_r(t)$ is replaced by current of the equivalent inductor $i_r^*(t)$.

6.5 Phasor transformation

A three-phase-to-three-phase series-resonant converter is represented by a set of equations of the dynamic model (6.1)...(6.7) and (6.19). The three-phase voltages and currents are represented by space phasors, and the switching operation of the switches in the bridge configuration is represented by switching space phasors.

The conventional phasor represents the magnitude and phase of a sinusoidal waveform in the steady state. The space phasor presentation represents a three-phase sinusoidal system for which the formal mathematical prescription is the same. However, a conventional phasor description cannot represent circuit quantities in a transient state. For voltage or current space phasors, the solution in the form of equation (6.20) is assumed:

$$\underline{x}(t) = \underline{X}(t)e^{j\omega t} \quad (6.20)$$

where:

ω - angular frequency of the rotating phasor $\underline{X}(t)$.

The first derivation to time of the phasor $\underline{x}(t)$ in a transient state is equal to:

$$\dot{\underline{x}}(t) = \dot{\underline{X}}(t)e^{j\omega t} + j\omega\underline{X}(t)e^{j\omega t} \quad (6.21)$$

With a system prescribed by equation in the form (6.21):

$$\dot{\underline{x}}(t) = F[\underline{x}(t), \underline{g}(t)] \quad (6.22)$$

it is possible to extract the fundamental harmonics of interest and to obtain a system that is transformed into (6.23) that shows the same frequency on the both sides:

$$\dot{\underline{X}}(t)e^{-j\omega t} = F[\underline{X}(t), \underline{S}(t)]e^{-j\omega t} \quad (6.23)$$

The complex amplitude $\underline{X}(t)$ of the phasor $\underline{x}(t)$ is not considered to be constant in modulus and argument. It is a time function of the state variable and may include a harmonic function with different frequencies. Equation (6.23) contains the derivative of the phasor and a steady-state term. The ultimate aim of a control action is to find a switching phasor $\underline{g}(t)$ which would create the required behaviour. This means to find a switching phasor $\underline{g}(t)$ which assures that the derivation of the voltage or current phasor is as required in Fig. 6.8.

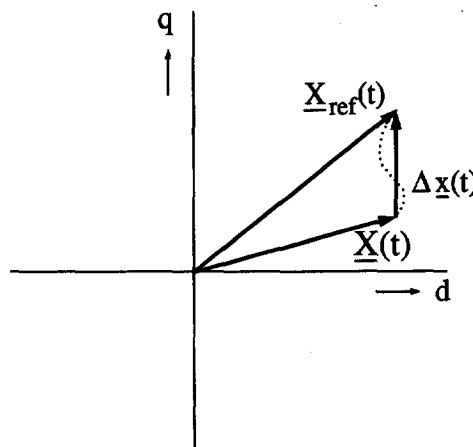


Fig. 6.9 Derivation of the phasor $\underline{X}(t)$ in d, q coordinates

In the ideal stationary case, the derivation of the phasor $\underline{X}(t)$ is zero. Then the phasors $\underline{X}(t)$ and $\underline{X}_{\text{ref}}(t)$ are identical and the phasors are constant in the d, q reference frame.

The described procedure corresponds to the transformation into the d, q rotating reference frame as mentioned in Chapters 2 and 3. The principle of the transformation into a d, q reference frame is based on finding a stationary circuit for a given rotary frame. The procedure is described in Chapter 3 for PWM converters where the transformation of a rotating phasor into steady-state operation is dealt with. Afterwards, a small signal linearization is provided to obtain a dynamic behaviour of the model.

For a polyphase resonant converter, the steady-state operation in the conventional way of understanding does not exist or is difficult to find. Therefore, the described strategy is comparable to the harmonic elimination and the process of generalized averaging [Sanders et al, 1991] or phasor transformation [Rim et al, 1991]. The phasor transformation in the mentioned references is only applicable to the converter operating in the continuous conduction mode. This condition is not supposed here.

The phasor $\underline{X}(t)$ depicted in Fig. 6.8 is time dependent. Next step is linearization which assumes a linear derivation between two operating points and results in a constant phasor $\Delta x(t)$. The trajectory between two phasors for a sinusoidal change is depicted in Fig. 6.8 by a dashed line. To solve equation (6.23), the derivation of the phasor is considered as a difference $\Delta x(t)$ between an actual position $\underline{X}(t)$ and a required reference position $\underline{X}_{\text{ref}}(t)$ over the time interval. The other possibility is to know the shape of the current or the voltage and to take the actual derivation. In the case of a resonant converter, the derivation is given by a sinusoidal shape of the resonant current. The investigated phasors are in general functions of time. For the sake of simplicity, the notation of the time function is omitted.

Let us apply the method suggested here to the set of equations (6.1)...(6.7). The assumed solution for phasor \underline{u}_0 is:

$$\underline{u}_0 = \underline{U}_0 e^{j\omega_0 t} \quad (6.24)$$

where:

- \underline{U}_0 - transformed phasor,
- ω_0 - required frequency of the output voltage.

For an ideal operation, the transformed phasor \underline{U}_0 has a constant value equal to $U_{0\text{ref}}$. The derivation of the phasor \underline{u}_0 is performed according to equation (6.21):

$$\frac{d\underline{u}_o}{dt} = \frac{d\underline{U}_o}{dt} e^{j\omega_b t} + j\omega_b \underline{U}_o e^{j\omega_b t} \quad (6.25)$$

Introduction into equation (6.3) leads to the following expression:

$$C_o \left(\frac{d\underline{U}_o}{dt} e^{j\omega_b t} + j\omega_b \underline{U}_o e^{j\omega_b t} \right) = \underline{s}_{II} i_r^* - \underline{I}_1 e^{j\omega_b t} \quad (6.26)$$

with:

$$\underline{s}_{II} = S_{II} e^{j\psi_2} \quad (6.27)$$

where:

\underline{s}_{II} - required switching phasor of the switching bridge SM2 with amplitude S_{II} and time dependent phase ψ_2 .

By extracting the basic harmonic with frequency ω_o and rotating the equation (6.26) into the d, q reference frame, we obtain:

$$S_{II} e^{j(\psi_2 - \omega_o t)} = \frac{C_o \left(\frac{d\underline{U}_o}{dt} + j\omega_b \underline{U}_o \right) + \underline{I}_1}{i_r^*} \quad (6.28)$$

and into d and q components:

$$S_{II d} = \frac{C_o \left(\frac{dU_{od}}{dt} - \omega_b U_{oq} \right) + I_{1d}}{i_r^*} \quad (6.29)$$

$$S_{II q} = \frac{C_o \left(\frac{dU_{oq}}{dt} + \omega_b U_{od} \right) + I_{1q}}{i_r^*} \quad (6.30)$$

Equations (6.4) and (6.5) prescribe the dynamics of the source filter of the converter. By derivation of equation (6.4) and substitution of \underline{u}_1 from (6.5), we get the following equation:

$$-C_s L_s \frac{d^2 i_s}{dt^2} + C_s \frac{d u_s}{dt} = i_s - \underline{s}_I i_r^* \quad (6.31)$$

Thus, the filter voltage \underline{u}_1 is eliminated. The phasor transformation is also performed with equation (6.31).

The source \underline{u}_s is considered to be an ideal voltage source, that means $\underline{u}_s = U_s e^{j\omega_s t}$. Therefore the derivative contains only the steady-state term:

$$\frac{d\underline{u}_s}{dt} = j\omega_s U_s e^{j\omega_s t} \quad (6.32)$$

Next, we construct the derivative of the current i_s :

$$\frac{di_s}{dt} = \frac{dI_s}{dt} e^{j\omega_s t} + j\omega_s I_s e^{j\omega_s t} \quad (6.33)$$

$$\frac{d^2 i_s}{dt^2} = \frac{d^2 I_s}{dt^2} e^{j\omega_s t} + 2j\omega_s \frac{dI_s}{dt} e^{j\omega_s t} - \omega_s^2 I_s e^{j\omega_s t} \quad (6.34)$$

By using expressions (6.32), (6.33) and (6.34), the equation (6.31) yields:

$$-C_s L_s \left(\frac{d^2 I_s}{dt^2} e^{j\omega_s t} + 2j\omega_s \frac{dI_s}{dt} e^{j\omega_s t} - \omega_s^2 I_s e^{j\omega_s t} \right) + C_s \frac{d\underline{u}_s}{dt} = I_s e^{j\omega_s t} - s_{I1} i_r^* \quad (6.35)$$

where:

s_{I1} - required switching phasor of the switching bridge SM1 with amplitude S_{I1} and phase ψ_{I1} .

The solution of equation (6.35) is:

$$S_{I1} e^{j(\psi_{I1} - \omega_s t)} = \frac{C_s L_s \frac{d^2 I_s}{dt^2} + 2j\omega_s C_s L_s \frac{dI_s}{dt} + I_s (1 - \omega_s^2 C_s L_s) - j\omega_s C_s U_s}{i_r^*} \quad (6.36)$$

By assuming the first derivative of the source current I_s to be constant, the second derivative is zero. Equation (6.36) in d, q coordinates is then equal to:

$$S_{Id} = \frac{I_{sd} (1 - \omega_s^2 C_s L_s) - 2\omega_s C_s L_s \frac{dI_{sq}}{dt}}{i_r^*} \quad (6.37)$$

$$S_{Iq} = \frac{I_{sq} (1 - \omega_s^2 C_s L_s) + 2\omega_s C_s L_s \frac{dI_{sd}}{dt} - \omega_s C_s U_s}{i_r^*} \quad (6.38)$$

Assuming that the phasor \underline{I}_s in the d, q coordinates is equal to the constant reference phasor \underline{I}_{sref} equations (6.37) and (6.38) are reduced to:

$$S_{Id} = \frac{I_{sref_d}(1 - \omega_s^2 C_s L_s)}{i_r^*} \quad (6.39)$$

$$S_{Iq} = \frac{I_{sref_q}(1 - \omega_s^2 C_s L_s) - \omega_s C_s U_s}{i_r^*} \quad (6.40)$$

Expressions (6.39) and (6.40) are the equivalent switching space phasors for the sliding mode. Since a discrete system such as a series-resonant converter is considered to be a quasi-sliding mode system, the actual switching space phasor does not move on a defined sliding surface. The actual switching space phasor is understood as the phasor calculated with the actual current \underline{I}_s based on equations (6.39) and (6.40). With the assumption of an infinite switching frequency and infinite resonant frequency, the actual switching phasor and equivalent switching space phasor are identical.

Expressions (6.39) and (6.40) are equal to expression (3.39) which defines the reference phasor for a PWM modulator. For an infinite PWM switching frequency (Chapter 3), the actual phasor follows the reference phasor exactly. Expressions (6.39), (6.40) and (3.39) create a link between PWM modulation and the quasi-sliding mode studied here. PWM and PFM modulation principles of external waveforms are identical for an infinite switching frequency and an infinite resonant frequency.

The derivation of the resonant link current is starting from equation (6.19), expressed as:

$$L_{eq} \frac{di_r^*}{dt} - \frac{3}{2} \operatorname{Re}\{s_I^* \underline{U}_1\} = -\frac{3}{2} \operatorname{Re}\{s_{II}^* \underline{U}_0\} \quad (6.41)$$

Using equation (6.4), equation (6.41) is written as:

$$L_{eq} \frac{di_r^*}{dt} = \frac{3}{2} \operatorname{Re}\{S_I e^{j(\psi_1 - \omega_s t)} [U_s - L_s (\frac{dI_s}{dt} - j\omega_s I_s)]\} - \frac{3}{2} \operatorname{Re}\{S_{II} e^{j(\psi_2 - \omega_b t)} \underline{U}_0\} \quad (6.42)$$

Obtained equations (6.28), (6.36) and (6.42) have variables s_I and s_{II} rotating with speed ω_s and ω_b , respectively. An adequate strategy has to be applied in order to be able to select the switching space phasor from the set defined in Chapter 2. The three-phase voltages \underline{U} and currents \underline{I} are in steady state stationary phasors in their d, q reference frames. Generally, they are time-varying functions.

6.6 Switching space phasor selection

Equations (6.28), (6.36) and (6.42) yield a solution for a dynamic model defined in Chapter 6.2. The obtained expressions for the phasors \underline{s}_I and \underline{s}_{II} define the ideal phasors (located arbitrarily in the complex plane). The switching phasors \underline{s}_I and \underline{s}_{II} have to be selected from the set of defined phasors for a voltage configuration. A suitable strategy has to be applied to be able to select from Table 2.2 a defined phasor for a voltage configuration or a zero phasor \underline{s}_0 . The switching matrixes SM1 and SM2 switched by the switching phasors \underline{s}_I and \underline{s}_{II} connect a resonant circuit to the terminals of the three-phase source and the three-phase load. A resonant pulse is thus generated by excitation of the resonant circuit. A resonant pulse must contribute to the energy transfer in such a way that the voltages and the currents at the converter terminals track the reference waveforms.

Since it is recognized that pulse modulators for resonant converters are quasi-sliding mode controllers, in the following, a sliding mode theory is introduced. Because of the discrete character of the resonant pulse, a quasi-sliding mode is achieved as noted in Chapter 5. The selection of a switching phasor defined for a voltage configuration (Chapter 2, Table 2.2) results in a discrete resonant pulse and gives the modulator a discrete character. However, the operation has a continuous character after selecting a zero phasor as shown later. This is because the duration of the zero phasor is not constant and does not depend on the resonant frequency. The selected switching phasor has to drive the converter voltages and currents towards its template. This means that the selection of \underline{s}_I has to assure that the current i_s tracks its template, and the selection of \underline{s}_{II} has to assure that the voltage u_o tracks its reference. To select a switching space phasor on the basis of a calculated one for equations (6.28), (6.36) and (6.42) does not appear to be an easy task. These equations define an ideal switching space phasor, but the criterium to select one to track the reference is missing. In the following, this problem is studied.

Selection of a switching space phasor \underline{s}_I

The application of a sliding mode condition (5.4) for a filter capacitor voltage yields:

$$\text{sgn}[u_{ik\text{ref}} - u_{ik}] \left(\frac{du_{ik\text{ref}}}{dt} - \frac{du_{ik}}{dt} \right) \leq 0 \quad (6.43)$$

for $k = d, q$ or α, β

The condition is applied either for d, q or for α, β coordinates separately. The condition is applicable in a d, q plane as well as in an α, β plane, whichever is more convenient for switching space phasor selection. The single terms of equation (6.43) in a complex α, β plane are further analyzed. The voltage $u_{i\text{ref}}$ is the reference voltage of a capacitor input filter C_s and is expressed with the use of (6.4) as:

$$\underline{u}_{i\text{ref}} = \underline{u}_s - L_s \frac{di_{s\text{ref}}}{dt} \quad (6.44)$$

where:

$i_{s\text{ref}}$ - phasor of the required source current; $i_{s\text{ref}} = I_{s\text{ref}} e^{j\omega_s t}$, $I_{s\text{ref}} = \text{const.}$

The phasor \underline{u}_i is a phasor of the measured capacitor voltage. The time derivative of $\underline{u}_{i\text{ref}}$ is expressed as:

$$\frac{d\underline{u}_{i\text{ref}}}{dt} = (j\omega_s U_s + \omega_s^2 L_s I_{s\text{ref}}) e^{j\omega_s t} \quad (6.45)$$

The time derivation of the capacitor voltage expressed by equation (6.5) depends on the selected switching space phasor as:

$$\frac{d\underline{u}_i}{dt} = \frac{1}{C_s} (\underline{i}_s - \underline{i}_i) = \frac{1}{C_s} (I_s - \underline{s}_I i_r^*) e^{j\omega_s t} \quad (6.46)$$

Equations (6.43)...(6.46) yield the condition for the selection of the switching space phasor \underline{s}_I :

$$(\underline{s}_I)_{\alpha,\beta} \leq \left(\frac{I_s - \omega_s^2 L_s C_s I_{s\text{ref}} - j\omega_s C_s U_s}{i_r} e^{j\omega_s t} \right)_{\alpha,\beta} \quad (6.47)$$

$$\text{sgn}[(U_s - L_s \frac{dI_{s\text{ref}}}{dt} - \underline{U}_i) e^{j\omega_s t}]_{\alpha,\beta}$$

The inequality (6.47) is applied for α, β coordinates of \underline{s}_I separately as indicated by the initial condition (6.43). The second part of this inequality influences the condition only by sgn of its expression giving the direction for the required motion. The selection itself appears more convenient in the α, β reference frame because the switching phasors are in this frame in reality. The set of the switching phasors together with the switching phasor yielded by equation (6.47) are shown in Fig. 6.10.

The inequality (6.47) gives one of the quadrants marked I...IV from which the switching space phasor is selected. This way, having the required switching phasor in quadrant I, the switching space phasor \underline{s}_1 is selected. In quadrant II phasor \underline{s}_6 , in quadrant III phasor \underline{s}_0 (zero phasor) and in quadrant IV phasor \underline{s}_2 are selected. The quadrant III offers the possibility to select also a switching space phasor \underline{s}_4 or \underline{s}_5 . These phasors fulfill the condition (6.47) too. However, the zero phasor \underline{s}_0 results in lower ripple of the voltage of the filter capacitor C_s as it yields from (6.46). Consequently, also the ripple of the source current and the excursions of the resonant current i_r and the resonant voltage u_{Cr} are lower. Therefore in this thesis a zero switching space phasor is used in the ambiguous cases like this. This ambiguity is mentioned also in Chapter 2 and gives space for optimization.

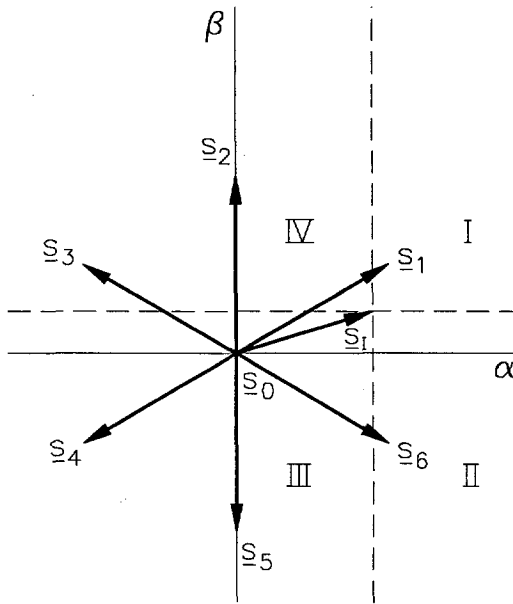


Fig. 6.10 Switching space phasor selection

Similarly for other positions of the calculated switching space phasor \underline{s}_I from (6.47), a switching space phasor from the set defined for a voltage configuration or a zero phasor is selected.

Selection of a switching space phasor \underline{s}_{II}

Using the same principle, the switching space phasor \underline{s}_{II} is calculated:

$$(\underline{s}_{II})_{\alpha,\beta} \geq \left[\frac{I_1 + j\omega_0 C_o \underline{U}_{oref}}{i_r} e^{j\omega_0 t} \operatorname{sgn}[(U_{oref} - U_o) e^{j\omega_0 t}] \right]_{\alpha,\beta} \tag{6.48}$$

The inequality (6.48) gives the selection of a switching space phasor for switching bridge SM2 and is applied for the α, β coordinates of the switching space phasor \underline{s}_{II} separately.

Inequalities (6.47) and (6.48) give position of the required switching space phasor. By selecting a switching space phasor according to these inequalities, the source and load currents follow their template. If $\underline{I}_s = \underline{I}_{sref}$ and $\underline{U}_o = \underline{U}_{oref}$, equations (6.47) and (6.48) are identical to equations which give an equivalent phasor. Equation (6.47) gives the same result as equations (6.39) and (6.40), and equation (6.48) gives the same result as (6.29) and (6.30). This is correct because if currents and voltages follow the reference, there is a zero deviation of the switching space phasor.

6.7 Simulation results

To verify the suggested modulation principle, a converter with the following parameters is simulated:

$$\begin{array}{lll}
 U_s = 311 \text{ V} & L_s = 10 \cdot 10^{-3} \text{ H} & C_s = 5 \cdot 10^{-6} \text{ F} \\
 L_{eq} = 2.5 \cdot 10^{-3} \text{ H} & C_o = 5 \cdot 10^{-6} \text{ F} & L_o = 10 \cdot 10^{-3} \text{ H} \\
 \omega_s = 2\pi 50 \text{ s}^{-1} & \omega_o = 2\pi 100 \text{ s}^{-1} &
 \end{array}$$

The selection of the value of the equivalent inductor L_{eq} depends on the values of the resonant circuit elements. The *quantum transformed* converter acts as an AC-to-AC converter with DC current link. The selection of the value of the link inductor L_{eq} for this type of current link converter would be one order higher because the value of the link inductor is unproportional to the switching frequency.

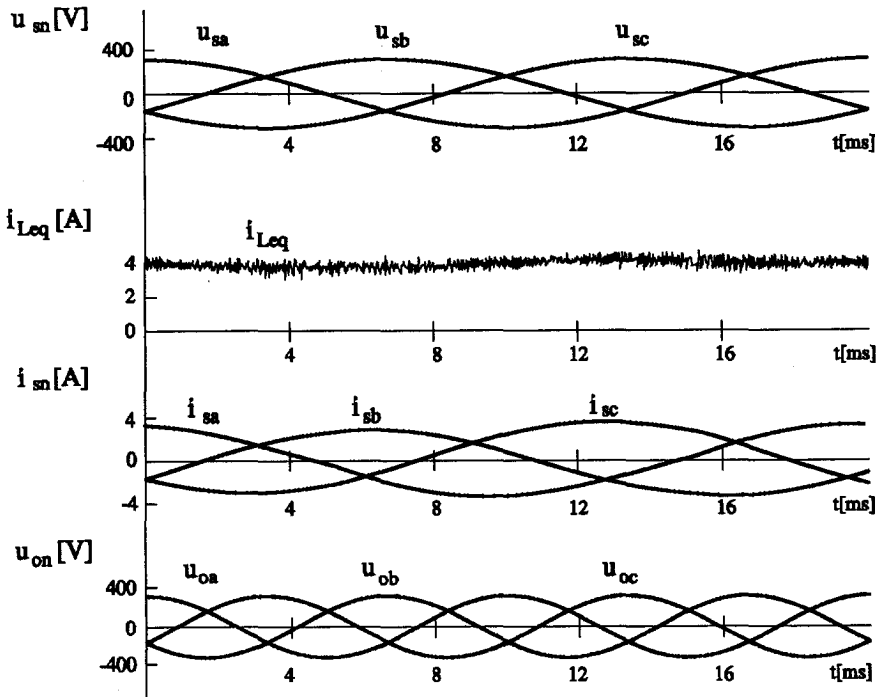


Fig. 6.11 Source and load voltages, source currents and current of the equivalent inductor i_{Leq}

The applied switching frequency of the bridges SM1 and SM2 and the value of the link inductor determine the ripple of the current in the link and the stability of the system. According to the quantum transformation, the value of an equivalent

inductor L_{eq} and the value of the resonant inductor L_r are related. The value of L_r determines the impedance of the resonant circuit and, consequently, the maximum power of the series-resonant link converter. Therefore, the value of an equivalent inductor L_{eq} was chosen as $1.25 \cdot 10^{-3} \text{H}$ and the switching frequency close to the double of the resonant frequency of the resonant link circuit ω_r given by equation (6.11).

The waveforms obtained by simulation of a quantum transformed model are shown in Fig. 6.11. The load voltage u_o with the frequency 100 Hz is presented for all three phases a, b, c . The 50 Hz source current i_s is in phase with the source voltages u_s . The current of the quantum inductor L_{eq} is also depicted. The current of an equivalent inductor L_{eq} is stable as a result of the properly chosen reference source current phasor i_s^* . The amplitude of the current $i_{Leq} = i_r^*(t)$ is given by selecting the reference source current i_s . Therefore, we expect that the resonant current and resonant capacitor voltage are also stable. This will be proved later.

After the modulation is verified on the quantum transformed model, the inductor L_{eq} is replaced by a series resonant circuit with the parameters $L_r = 0.5 \cdot 10^{-3} \text{H}$, $C_r = 31.6 \cdot 10^{-3} \text{F}$. The selection of the switching space phasor \underline{s}_I and \underline{s}_{II} is the same as for the quantum transformed converter. The current i_r has an alternating polarity, but equations of phasor \underline{s}_I (6.47) and \underline{s}_{II} (6.48) consider this fact. The simulation results are shown in Fig. 6.12, Fig. 6.13, Fig. 6.14 and Fig. 6.15.

In Fig. 6.12, the source current i_{sa} and the current i_{ia} of the same phase a are depicted. The source filter creates a smooth source current from current i_i that contains the resonant current pulses.

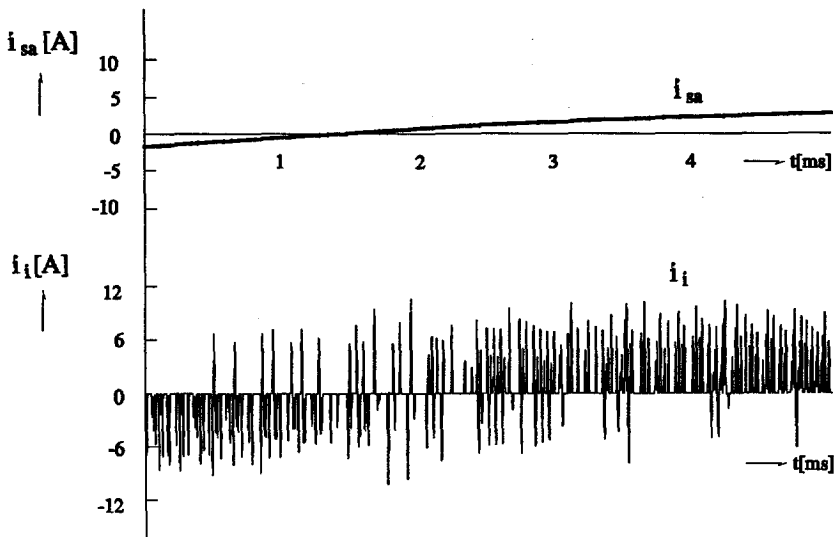


Fig. 6.12 Unfiltered current i_{ia} and source current i_{sa}

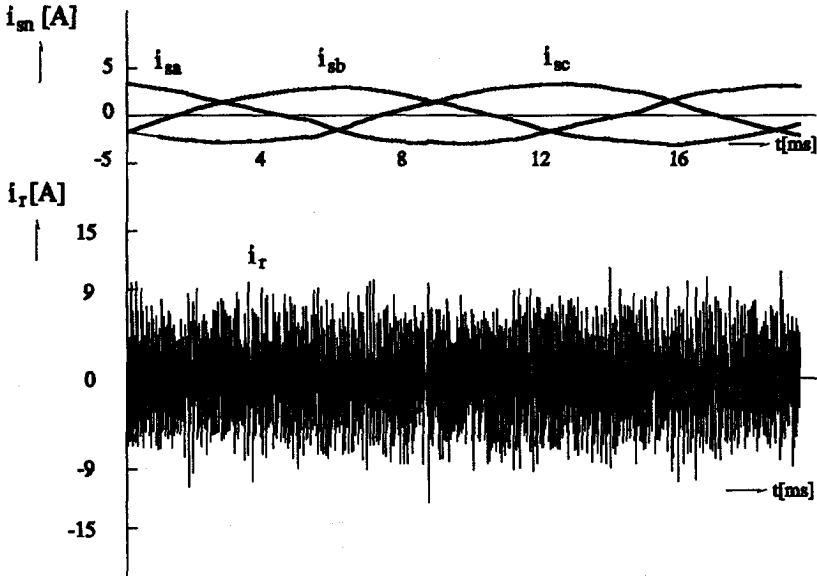


Fig. 6.13 Three-phase source currents and resonant current

The three-phase currents i_B and the resonant current i_r are shown in Fig. 6.13. The amplitude of the resonant current i_r stays stable with a ripple which is comparable to the ripple of the current of the quantum resonant inductor L_{eq} .

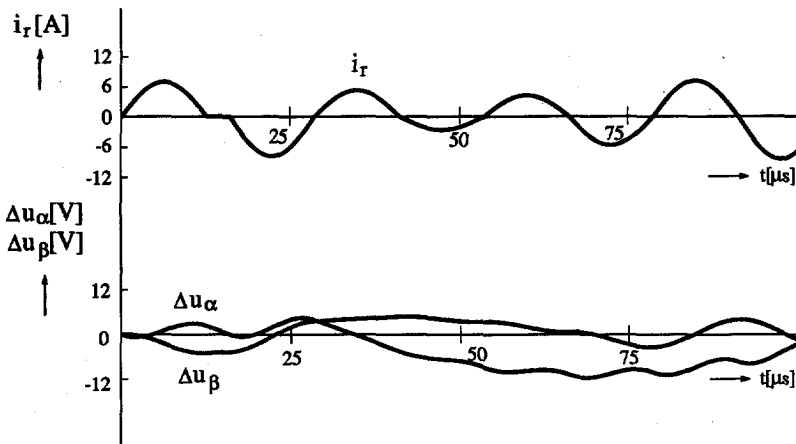


Fig. 6.14 Resonant current i_r and error signals Δu_α and Δu_β

The details of the resonant current i_r , Δu_α and Δu_β which are the differences $u_{ref} - u_i$ in α, β coordinates are shown in Fig. 6.14. It can be seen that the second resonant pulse is not initiated because the errors of the voltage u_i are decreasing

as a result of the dynamic behaviour of the filter $L_s C_s$. The next pulse is initiated after the α coordinate of error signal Δu_α increases.

The amplitude of the resonant capacitor voltage stays within the acceptable limits as shown in Fig. 6.15. According to equation (6.12), the values of the capacitor voltage depend on the applied mirror voltage. Therefore, for high power applications, an independent control of the resonant capacitor voltage is necessary. This can be achieved by placing a switching network across the resonant link elements $L_r C_r$ as shown in [Murray, et.al., 1989].

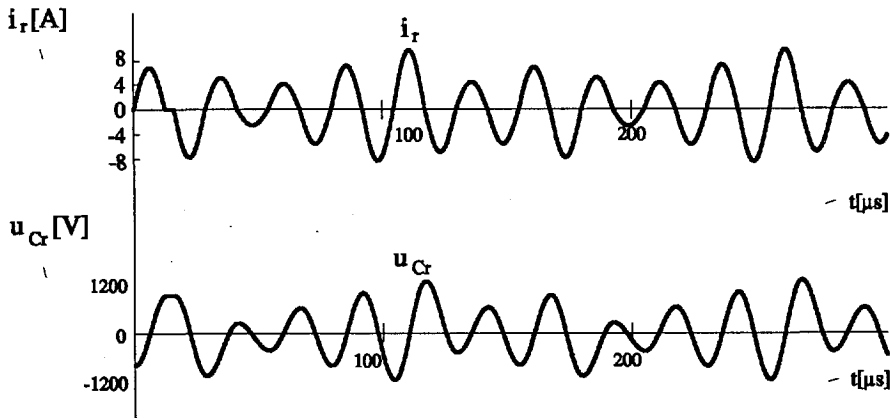


Fig. 6.15 Resonant current i_r and resonant capacitor voltage u_{Cr}

The simulated waveforms verify the good working of the suggested modulation principle.

6.8 Conclusions

A dynamic model of a three-phase-to-three-phase series-resonant converter is given. This model is based on the switching space phasors and the space phasors of the three-phase voltages and currents. The series-resonant link is prescribed by integrodifferential equations.

First, a sampled model is suggested to calculate the resonant capacitor voltage at the end of a resonant pulse and the resonant current is approximated by a half of the sine wave.

As the second approximation, linearization of the resonant current is provided. The transformation called *quantum* transformation allows the replacement of a resonant circuit by an equivalent inductor. This approximation makes the dynamic synthesis simple and readable. The selection of the switching phasors \underline{s}_I and \underline{s}_{II} is first provided for the quantum transformed model. The relation between the

quantum transformed model and the original dynamic model is presented and explained. The calculated switching space phasor under the assumption of an infinite resonant frequency and an infinite switching frequency is identical with the reference switching space phasor of PWM presented in Chapter 3. This fact gives a link between the already defined PWM and the described quasi-sliding pulse modulation. The linearization and rotation into a d,q reference frame (or harmonic elimination) are the steps made to solve the dynamic model. The result of the dynamic synthesis is a modulation process for a three-phase-to-three-phase series-resonant converter. The new modulator creates output voltages and source currents with unity power factor. The resonant link energy is maintained at the required level. It is the first modulation to solve the control of this converter topology.

7

**PARALLEL-RESONANT
CONVERTER**

7.1 Introduction

In Chapter 4, two basic groups of resonant converters are defined: zero-voltage switching and zero-current switching converters. A zero-current switching converter and the dynamic analysis and synthesis of a modulation process are studied in details in Chapter 6. The alternative is a zero-voltage switching that can be realized as a parallel-resonant converter. Because the space phasor model was utilized in Chapter 6 to provide a dynamic synthesis of the modulation of the converter waveforms, here, the switching function model of a switching bridge leg is considered. The dynamic synthesis provided on the basis of this model is explained. The parallel-resonant link is not so well studied in literature as its counterpart, the series-resonant link. A new control principle is investigated.

For parallel-resonant link converters, the total energy is transferred via the resonant circuit in four steps [Kim, Cho, 1990]. In the initial solutions of pulse-density modulated converters [Sood, Lipo, 1988], integral-PWM modulated converters [Divan, 1986] or quantum converters [Joung, et.al., 1990], the load was connected directly in parallel to the resonant link which appears to be a disadvantage because the load strongly affects the resonance phenomena. Reference [Mohan, 1991] gives a solution of a DC-link converter which utilizes a parallel resonant circuit to separate the conventional voltage link from the three-phase PWM inverter during the switching instants.

In Chapter 4, two basic problems of resonant techniques were encountered: the generating of the external waveforms at the input and output of the converter and the stabilization of the critical quantities (the control of energy level in the high-frequency link). The parallel load connected directly parallel to a resonant circuit strongly affects the resonance phenomena and makes the stabilization of critical waveforms difficult. Therefore, to solve the second condition, a new control principle is suggested [Bauer, Klaassens, 1992]. The process of the synthesis of the external waveforms is studied with the help of a switching bridge leg model defined in Chapter 2.

The proposed solution differs from known solutions by the fact that the resonant-link serves mainly to create the zero-voltage switching conditions while the main power is not transferred through the passive components of the resonant link. The operational principle is explained on the example of a three-phase-to-DC step-up converter and a three-phase-to-three-phase converter. The parallel-resonant link converters were classified according to whether they involve a resonant AC voltage in the link or incorporate a pulsating DC voltage, e.g. the link is DC resonant [Divan, 1986]. The suggested control principle can be used for the parallel-resonant AC and the resonant-DC link concept. The new control principle for stabilizing critical waveforms is explained on an example of a AC-to-DC step up power converter.

7.2 AC-to-DC parallel-resonant DC link step-up power converter

Circuit operational principle

Fig. 7.1 shows the schematic of a three-phase AC-to-DC step-up (boost) parallel-resonant DC-link power converter.

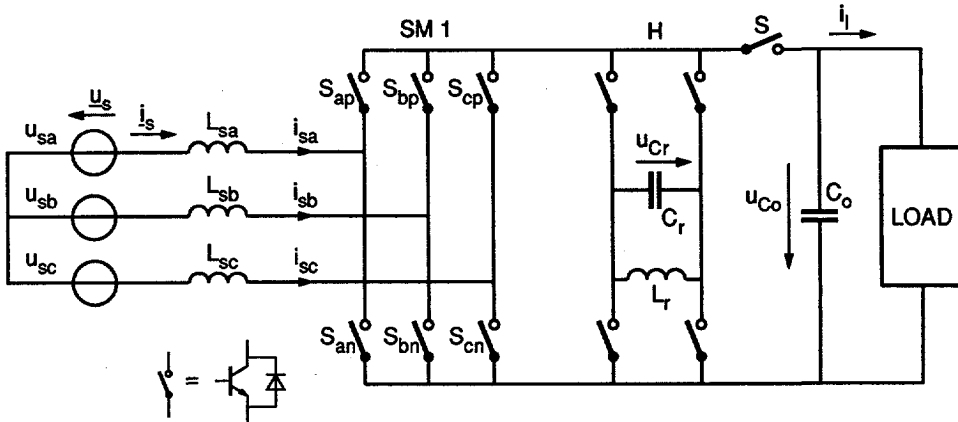


Fig. 7.1 Three-phase-to-DC parallel-resonant DC link converter

A three-phase power source with voltages u_{sn} ($n=a,b,c$) is connected to the switches in a bridge configuration SM1 via inductors L_{sn} ($n=a,b,c$) composing a current source (Fig. 7.1). A high-frequency parallel- $L_r C_r$ link is excited and creates a zero-voltage condition for the switches in the switching bridge SM1 when the proper switches of the H -bridge are closed. The switches of the H -bridge are switching alternatively as there is an unipolar voltage in the resonant DC link. The switching of the bridge SM1 is restricted to the moment of the zero-crossing of the resonant capacitor voltage u_{Cr} . The process of waveshaping of the input currents i_{sn} ($n=a,b,c$) is a discrete process and is explained later. The input currents are required with unity power factor. To simplify the presentation, we replace the input voltage sources including the inductor L_{sn} by a single DC current source with current I_s as shown in Fig. 7.2 This current source performs a resulting current flowing into the link. It is allowed to introduce this current source, because all three input phases are simultaneously connected to the link to control the source currents. The equivalent current source has a DC value since the low-frequency input current remains quasi constant during a period of the high-frequency link. The switches in the H -bridge are switching alternatively to obtain a unipolar voltage in the link and connect or disconnect the resonant circuit from the link. The H -bridge is, therefore, replaced by a single switch S_H which connects or disconnects the parallel resonant circuit. The output filter capacitor C_o is connected to the link via switch S .

To shape the voltage on the output capacitor, we use forward or reverse operation as will be explained.

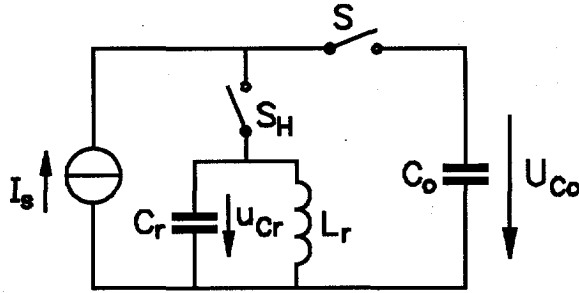


Fig. 7.2 Equivalent circuit

7.2.1 Forward operation

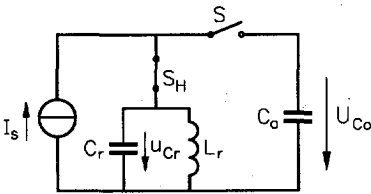


Fig. 7.3 Mode 1 time interval T_1

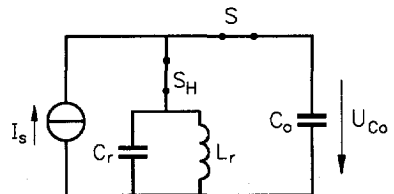


Fig. 7.4 Mode 2 = Mode 4 time interval T_2 and T_4

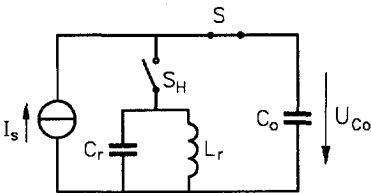


Fig. 7.5 Mode 3 time interval T_3

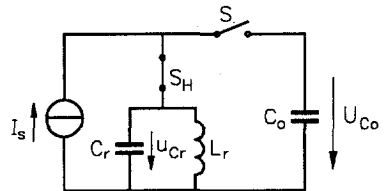


Fig. 7.6 Mode 5 time interval T_5

The forward operation is active, when switching bridge SM1 and switch S connect the input current source I_s to the output capacitor C_o ($C_o \gg C_r$) to increase the loaded output capacitor voltage u_{C_o} . The parallel-resonant circuit is mainly used to create the zero-voltage switching conditions. The principle of operation is described for one switching cycle of the resonant pulse. Each switching cycle is divided into five modes. In Fig. 7.3..Fig. 7.6, the equivalent networks are shown for the four different positions of the switches S_H and S . Fig. 7.7 shows how the duration of certain modes depends on the ratio of the voltages of the capacitors C_o and C_r .

Mode 1:

In *mode 1* (time interval T_1 , Fig. 7.3 and Fig. 7.7), the current source is connected to the link with the selected polarity at the instant, when the resonant capacitor voltage is at a zero-crossing point (creating a zero-voltage condition). The switch S_H is closed and the current source I_s is supplying the parallel-resonant $L_r C_r$ circuit. The switch S is opened and the output capacitor C_o is disconnected from the link. Thus, for *mode 1*, the input power source is powering the resonant $L_r C_r$ tank.

Mode 2:

At the instant t_1 (Fig. 7.4 and Fig. 7.7) when the resonant capacitor voltage u_{C_r} reaches the value of the voltage of the output capacitor C_o , the switch S is closing with zero-voltage conditions. Output capacitor C_o is connected via switch S to the resonant capacitor C_r . Capacitor C_o and C_r have the same polarity. Switch S_H can be disconnected at any time also under zero-voltage conditions. In *mode 2* (Fig. 7.4), the resonant capacitor is clamped by the output capacitor. The energy in the resonant tank will decrease.

Mode 3:

(Time interval T_3 , Fig. 7.5 and Fig. 7.7) *Mode 3* starts when switch S_H disconnects the parallel resonant tank from the link. In *mode 3*, the current source powers the output capacitor C_o via a switching bridge SM1, the link and the switch S . This *mode* continues until the resonant capacitor voltage reaches the same value as the one of the voltage of capacitor C_o . A zero-voltage switching condition for switch S_H is created again.

Mode 4:

In *mode 4* (time interval T_4 , Fig. 7.4), the resonant capacitor C_r is clamped by the output capacitor. Thus, the energy in the resonant tank can be increased. The switch S can be opened any time under zero-voltage conditions.

Mode 5:

At the time instant t_4 , switch S is opened (*mode 5*, Fig. 7.6 and Fig. 7.7). Current source I_s is powering the resonant circuit. As seen in Fig. 7.7, the duration of certain modes depends on the ratio of the voltages u_o and u_{C_r} of the capacitors C_o and C_r . In Fig. 7.7 *mode 2* and *mode 4* have zero time duration.

Analysis and design considerations

The analysis and design for the forward operation presented in this section are based on the following simplifying assumptions:

- all components are ideal,
- the input current I_s remains constant during a resonant pulse,
- the output capacitor voltage U_{C_o} stays constant during a resonant pulse,
- *mode 2* and *mode 4* have zero time duration (time interval $T_2=T_4=0$),
- the resonant capacitor waveform shape is approximated as half of the sinusoid.

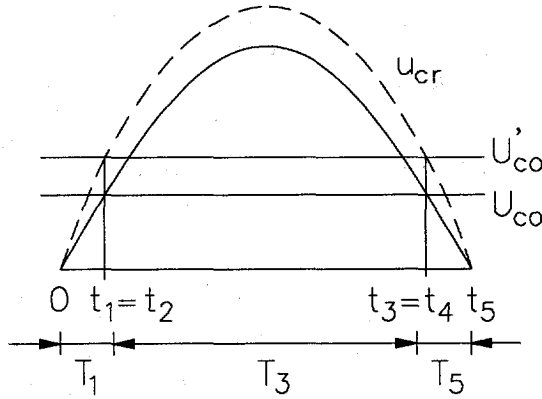


Fig. 7.7 Resonant capacitor voltage u_{Cr} and output capacitor voltage U_{Co}

Fig. 7.7 shows the voltage of the resonant capacitor C_r and the voltage of the output capacitor C_o . During the time interval $0-t_1$ (T_1) and t_4-t_5 (T_5) the resonant capacitor C_r is powered (*mode 1* and *mode 5*) and in the time interval t_2-t_3 (T_3) the output capacitor C_o is powered (*mode 3*). Based on the simplifying assumptions $T_1=T_5$, it is interesting to see how the amount of energy is transferred to the link and to the output. If the amplitude of the resonant capacitor voltage is increased (dashed line), the time intervals T_1 and T_5 are shorter (the intersection point of the voltages yields shorter intervals T_1 and T_5). Hence, the output capacitor is powered for a longer time. If the resonant capacitor voltage is lower, the output is powered for a shorter time. Thus, there is a stable point of operation, an *operating point*, for which the resonant $L_r C_r$ -link seeks. The assumption which we will prove is that the *operating point* which the resonant link will maintain is reached when the time intervals of all the modes stay constant, this means the increment in the both voltages stays proportional.

We assign the increment of the amplitude of the resonant capacitor voltage during a pulse ΔU_{Crmax} and the increment of the output voltage ΔU_{Co} .

$$\Delta U_{Crmax} \sin(T_1) = \Delta U_{Co} \tag{7.1}$$

Charge delivered to the resonant link with constant current $I_s=I$ is:

$$Q_1 = 2IT_1 \tag{7.2}$$

Charge delivered to the unloaded output capacitor with constant current I is:

$$Q_2 = IT_3 \tag{7.3}$$

The increments in voltages over C_r and C_o are:

$$\Delta U_{C_{\text{rmax}}} = \frac{Q_1}{C_r} = \frac{2IT_1}{C_r} \quad (7.4)$$

$$\Delta U_{C_0} = \frac{Q_2}{C_0} = \frac{IT_3}{C_0} \quad (7.5)$$

Equations (7.1), (7.4) and (7.5) yield:

$$\frac{2T_1}{T_3} \sin(T_1) = \frac{C_r}{C_0} \quad (7.6)$$

The result is that the *operating point* for non-load conditions depends on the ratio of the two capacitors. The above-mentioned consideration was based on the assumption that the switching instant t_3 appears in the nearest intersection point of the voltages u_{C_r} and u_{C_0} (at the nearest zero-voltage condition). Since the resonant circuit does not really participate in the energy transfer, *mode 3* can be prolonged and the switching can take place after several resonant pulses. *Mode 3* has then a duration $T_3 + \pi k \sqrt{L_r C_r}$ where k is an integer number. The resonant circuit is employed only when a change in a converter status is required. The resonant circuit serves as a snubber for all switches. In dependence on the modulation of the source currents or on general external waveforms, switching occurs after each pulse or several pulses.

Control of the energy in the resonant link

The load may change significantly and the power added to the load and to the link is dictated by the ratio of the two voltages: amplitude of the resonant capacitor voltage and output voltage.

Generally the resonant link voltage may reach a value which appears to be too high or too low. Therefore, an active control loop for the resonant capacitor voltage is necessary. During the time interval T_2 (*mode 2*), energy can be withdrawn from the resonant circuit. To keep the energy in the resonant tank on a constant level, *mode 2* continues until the resonant inductor current i_{L_r} reaches the value prescribed by the maximum energy in the tank:

$$i_{L_r} = \sqrt{\frac{C_r}{L_r} (U_{C_{\text{rmax}}}^2 - u_{C_r}^2)} \quad (7.7)$$

where:

$U_{C_{\text{rmax}}}$ - amplitude of the link voltage.

The same way, energy can be added to the resonant tank during the time interval T_4 . In Fig. 7.7, the time intervals T_2 and T_4 have zero values.

7.2.2 Reverse operation

Reverse operation is obtained when switching matrix SM1 and switch S connect the input current source I_g and the output capacitor C_o to decrease the output voltage. Energy is withdrawn from the output capacitor. Reverse operation also consists of five *modes*. The configurations of the switches and modes are the same as for forward operation (Fig.7.3...Fig.7.6). The only difference is that the input current source is connected in the opposite way in order to withdraw energy from the output. In *mode 1* and *mode 5* energy is withdrawn from the resonant tank and in *mode 3* from the output capacitor. It is possible to see that *mode 4* is used mainly for the reverse operation (to add energy to the resonant tank) and *mode 2* for the forward operation (to withdraw energy from the resonant tank).

7.3 Modulation of source currents based on a switching function

The control is discrete because the switching instants of the switching bridge SM1 are restricted to the zero-crossing points of the resonant capacitor voltage. Thus, a sliding mode control condition of infinite switching frequency is not possible because of the duration of a resonant pulse. The variable-structure control model for one phase reflecting the time-varying nature of the input voltage is given by equation:

$$L_{sn} \frac{di_{sn}}{dt} = \frac{1}{2} \left(\delta_i(t) - \frac{1}{3} \sum_{i=a,b,c} \delta_i(t) \right) u_{Co} + U_{smax} \sin(\omega t + \varphi_n) \quad (7.8)$$

where:

- $\delta_i(t)$ - switching function representing the positions of the switches of the leg in the bridge SM1 and reaching values in the discrete set $-1, 1$. $\delta_i(t)$ performs a control input of the variable structure control,
- U_{smax} - magnitude of the source phase voltage u_{sn} , $n=a, b, c$,
- i_{sn} - phase current of the phase n , $n=a, b, c$,
- φ_n - phase shift of the voltage in the phase n with respect to the phase a .

Equation (7.8) can be rewritten in the form:

$$L_{sn} \frac{di_{sn}}{dt} = \delta_i(t) k u_{Co} + U_{smax} \sin(\omega t + \varphi_n) \quad (7.9)$$

The coefficient k depends on the switching of the other legs of the input bridge and the value of k is $1/3$ or $2/3$. For the existence of a sliding motion it is necessary that the state trajectories near the switching surface point toward the surface. The switching surface can be represented by the time-varying error signal of the phase currents:

$$s(i_{sn}) = i_{sn} - I_{smax} \sin(\omega t + \varphi_n) \quad (7.10)$$

where:

I_{smax} - magnitude of the reference current i_{sref}

The sufficient conditions for the sliding-mode to exist on $s(i_{sn})$ are expressed mathematically in Chapter 5 by equations (5.2) and (5.3):

$$\lim_{s \uparrow 0} \frac{ds}{dt} > 0 \quad (7.11)$$

$$\lim_{s \downarrow 0} \frac{ds}{dt} < 0 \quad (7.12)$$

and applied to our particular case:

$$\lim_{s \uparrow 0} \frac{ds(i_{sn})}{dt} = \frac{1}{L_{sn}} [-\delta_i(t) k u_{Co} + U_{smax} \sin(\omega t + \varphi_n)] - \omega I_{smax} \cos(\omega t + \varphi_n) > 0 \quad (7.13)$$

$$\lim_{s \downarrow 0} \frac{ds(i_{sn})}{dt} = \frac{1}{L_{sn}} [-\delta_i(t) k u_{Co} + U_{smax} \sin(\omega t + \varphi_n)] - \omega I_{smax} \cos(\omega t + \varphi_n) < 0 \quad (7.14)$$

This condition leads to the selection of $\delta_i(t) = +1$ for $s > 0$ and $\delta_i(t) = -1$ for $s < 0$. Equations (7.13), (7.14) yield the following condition as a sufficient condition for the existence of a sliding motion on $s(i_s)$:

$$-\frac{1}{3} u_{Co} + U_{smax} < -\omega L_{sn} I_{smax} < \omega L_{sn} I_{smax} \cos(\omega t + \varphi_n) < \omega L_{sn} I_{smax} < \frac{1}{3} u_{Co} - U_{smax} \quad (7.15)$$

or briefly:

$$\omega L_{sn} I_{smax} + U_{smax} < \frac{1}{3} u_{Co} \quad (7.16)$$

Equation (7.16) determines the amplitude of the allowable reference current. The importance of equation (7.16) is that it shows a relation between the frequency ω of the modulated current, the value of the inductive filter and maximum current which is possible to modulate by this control principle. The physical limitations of the power of the investigated topology depend on the values of the converter components. An increase of the value of the inductor of the source filter on one side decreases the source current ripple, on the other side limits the maximum

modulated current and this way the power of the converter.

7.4 Simulation of an AC-to-DC converter

To verify the operation principle and the predicted features, the proposed converter from Fig. 7.1 was simulated. The control to keep the maximum voltage on the resonant capacitor constant and sliding mode control of the source currents was applied. The converter was simulated with the following parameters:

$$\begin{aligned} L_{sa} &= L_{sb} = L_{sc} = 10 \cdot 10^{-3} \text{ H} \\ L_r &= 50 \text{ } \mu\text{H}, C_r = 0.5 \cdot 10^{-6} \text{ F} \\ C_o &= 600 \cdot 10^{-6} \text{ F} \\ \text{load: } R_o &= 100 \text{ } \Omega, L_o = 10^{-3} \text{ H} \end{aligned}$$

In Fig. 7.8, one resonant pulse and the active control of the resonant tank energy for forward operation are depicted.

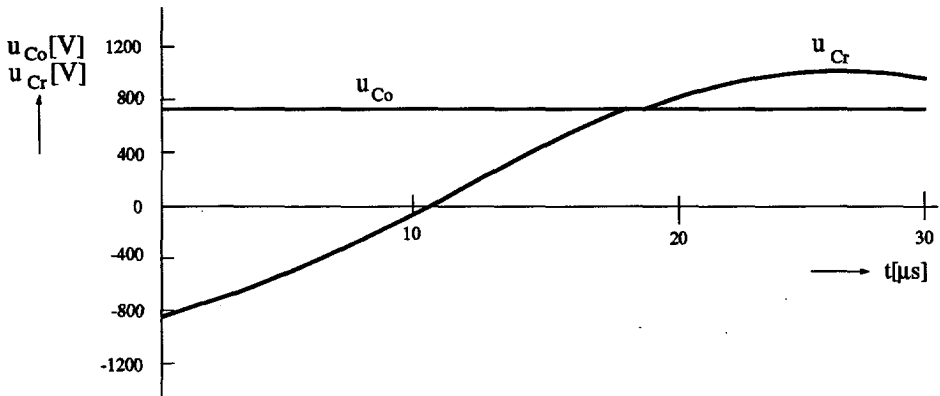


Fig. 7.8 Resonant capacitor voltage u_{Cr} and output capacitor voltage u_{Co} for forward operation

In Fig. 7.9, one resonant pulse and active control of the resonant tank energy for reverse operation is shown.

The time intervals T_2 and T_4 during which the output capacitor voltage is clamped to the resonant capacitor voltage are good visible. During these time intervals switch S is commutating with the switches of the H -bridge.

In Fig. 7.10, the reference current of phase a i_{saref} and the measured current i_{sa} of phase a are shown. In the same figure, the voltage over the switches of switching bridge SM1 and switching function $\delta_1(t)$ are displayed. The switching function is derived from the switching surface equations (7.13) and (7.14).

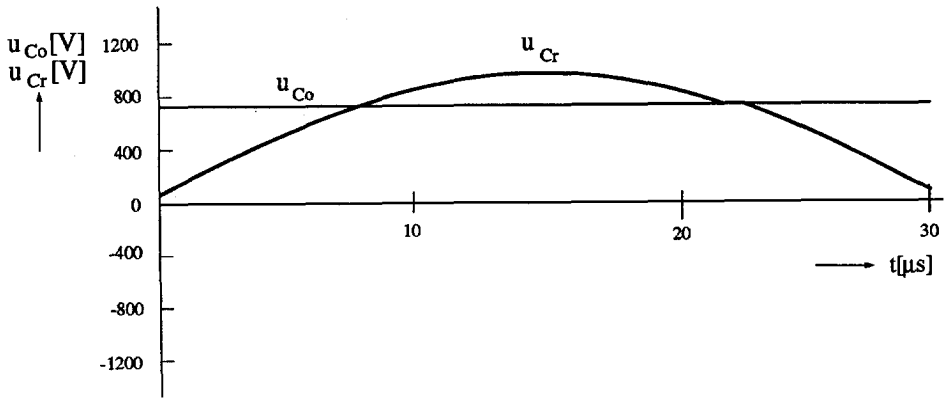


Fig. 7.9 Resonant capacitor voltage u_{Cr} and output capacitor voltage u_{Co} for a reverse operation

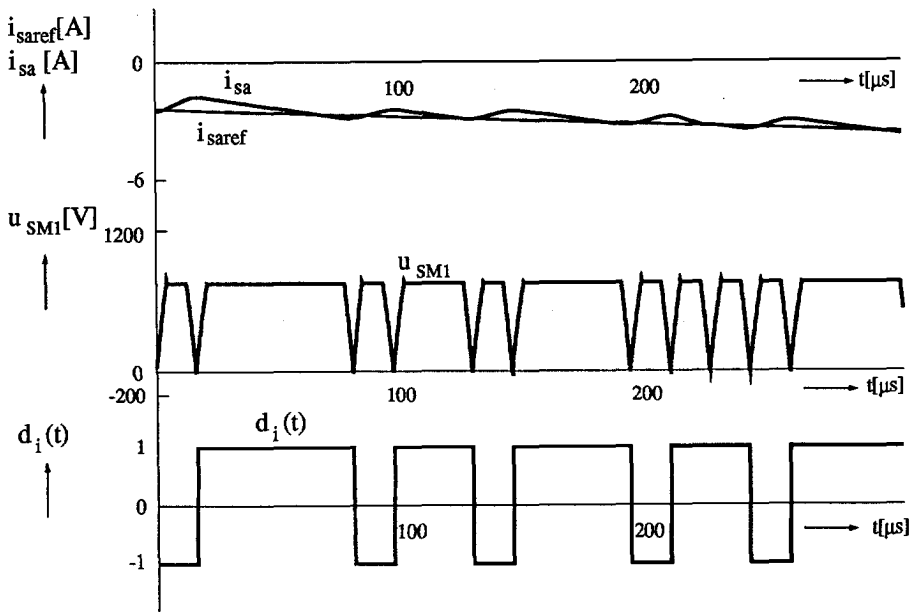


Fig. 7.10 The reference current i_{saref} and current i_{sa} , voltage u_{SM1} and switching function $d_i(t)$

Whenever a switching instant occurs, the parallel-resonant link takes over the voltage in the bus and creates a required zero-voltage condition. As it is possible to see in Fig. 7.10, the voltage u_{SM1} over the semiconductor switches of a switching bridge SM1 has zero value during the switching interval. This voltage

in case of a classical converter would have a constant value equal to the value of the DC bus. The current i_{sa} follows the required reference as shown in Fig. 7.10.

Whenever the current i_{sa} reaches the reference, a change in the configuration of the switches of SM1 occurs. Generally, the change happens with some time delay because the change in a switching configuration can happen only at a zero-crossing of the bus voltage u_{SM1} . The maximum switching frequency of the switching bridge SM1 is thus limited by the resonant frequency of the $L_r C_r$ circuit. Therefore, the "ringing" or "chattering" known by sliding mode controllers cannot occur here. The resonant frequency is in this case chosen as 36 kHz.

In Fig. 7.11, the load current and the low-frequency source currents and the voltages for a powering mode are shown.

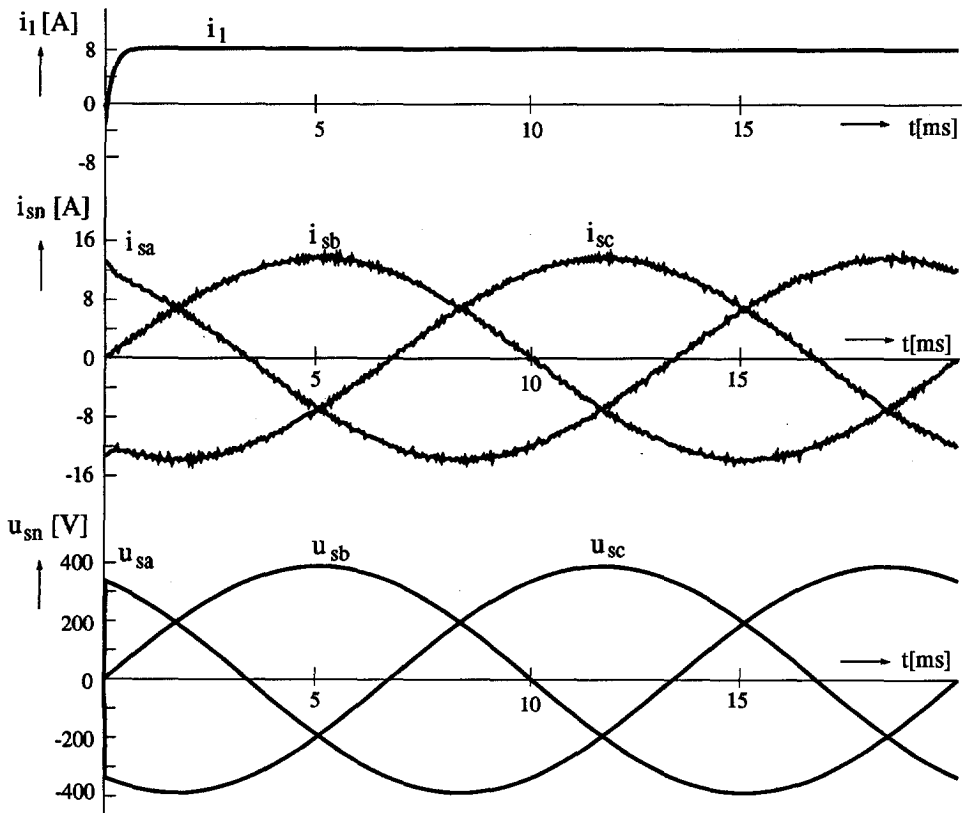


Fig. 7.11 Typical waveforms of an AC-to-DC converter for a powering mode (forward operation)

In Fig. 7.12, the load current and the low-frequency source currents and the

voltages for a regenerating mode are depicted.

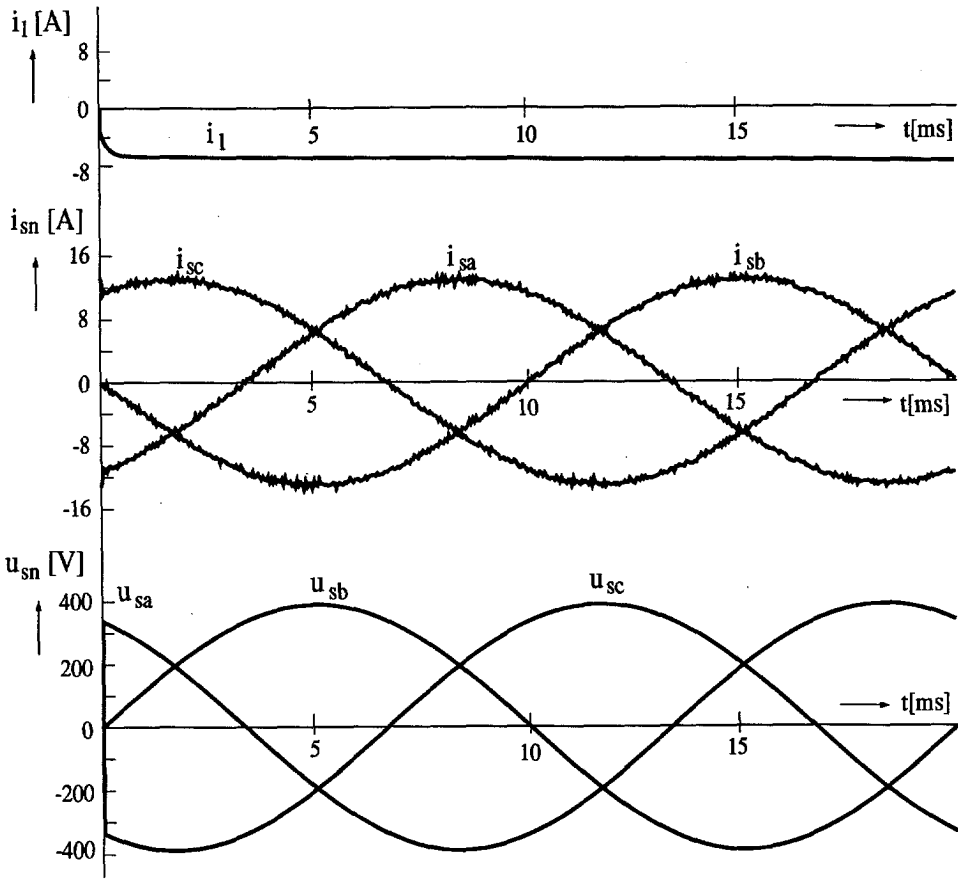


Fig. 7.12 Typical waveforms of an AC-to-DC converter for a generating mode (reverse operation)

The same waveforms (load current and low frequency input currents and voltages) for an abrupt change from a regenerating to a powering mode are shown in Fig. 7.13.

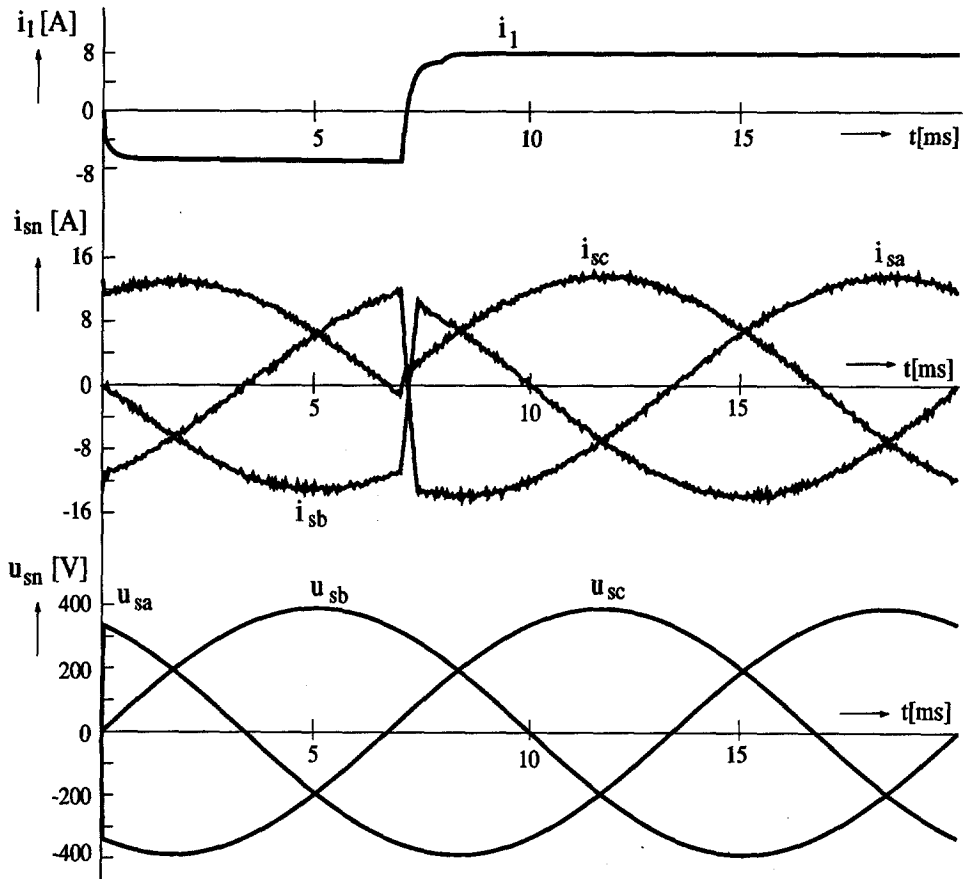


Fig. 7.13 Simulated waveforms for an abrupt change from a regenerating to a powering mode

7.5 A three-phase-to-three-phase parallel-resonant converter

The introduced control principle can be also used for polyphase AC power converters. The schematic of a three-phase-to-three-phase AC-to-AC power converter with resonant AC link is shown in Fig. 7.14 (the parallel-resonant DC link requires additional switches). Because the voltage in the link is AC the input bridge SM1 and the output bridge SM2 must have switches with bidirectional blocking and conducting capability.

By the suggested novel control principle [Bauer, Klaassens, 1992], the source and the load have always complimentary character. That means that one switching bridge uses a voltage configuration as defined in Chapter 2 and the other one uses

a current configuration because the parallel-resonant circuit in the suggested control principle serves as a rotating snubber between current and voltage source. The converter in Fig. 7.14 has source side filters with voltage character and the switching bridge SM1 uses a voltage configuration while the load has current character and SM2 uses a current configuration of the switches. By changing the character of the source and load filters, a step-up AC power converter is again obtained by using the suggested novel control principle.

The switching leg model is not practical for converters which use a voltage configuration as concluded in Chapter 5. Therefore for the design of a modulation of an AC-to-AC parallel-resonant converter, a switching space phasor model is necessary.

For a parallel-resonant converter in Fig. 7.14, the following set of equations can be found:

$$\frac{di_s}{dt} = \frac{1}{L_s} (u_s - u_i) \tag{7.17}$$

$$\frac{di_o}{dt} = -\frac{R_o}{L_o} i_o + \frac{1}{L_o} \frac{1}{2} \underline{S}_{II} \frac{3}{2} \text{Re}\{\underline{S}_I^* \underline{u}_i\} \tag{7.18}$$

$$\frac{du_i}{dt} = \frac{1}{C_s} i_s - \frac{1}{C_s} \underline{S}_I \frac{3}{4} \text{Re}\{\underline{S}_{II}^* i_o\} \tag{7.19}$$

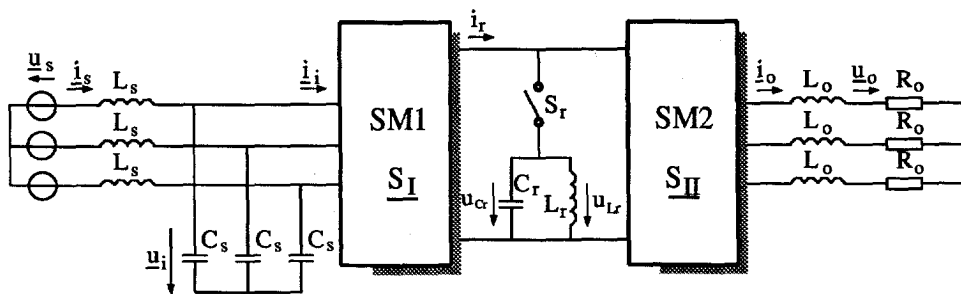


Fig. 7.14 A three-phase-to-three-phase parallel-resonant converter

In the equations (7.17)...(7.19) influence of the current of parallel resonant circuit is neglected since the parallel resonant circuit serves as a snubber. Its energy is refreshed after each change of the configuration and kept on the constant level. The definition of the problem is the same as in Chapter 6: to find such switching phasors S_I and S_{II} that the currents i_s and i_i follow the corresponding reference currents within the required degree of accuracy.

Because the parallel-resonant circuit does not participate on the energy transfer and the energy of the resonant link is independently controlled, the set of equations (7.17)...(7.19) is simpler than the set of equations for a series-resonant converter studied in Chapter 6. However with the use of a quantum transformation which is defined also for parallel resonant circuit [Joung et.al., 1992], it is possible to introduce the quantum transformed circuit influence in the set of equations (7.17)...(7.19).

As a result of the equations (7.17)...(7.19), the switching phasors \underline{S}_I and \underline{S}_{II} are calculated. The ideal switching phasors have to be related to a suitable switching strategy, e.g. the sliding mode control. we will not repeat it here because it is the same procedure as in Chapter 6. The switching phasors \underline{S}_I and \underline{S}_{II} have to be selected from the set of phasors defined for a voltage configuration (phasor \underline{S}_I) and a current configuration (phasor \underline{S}_{II}).

7.6 Conclusions

The usefulness of a parallel-resonant circuit to achieve soft switching is studied. A novel control principle of a parallel-resonant converter is suggested and documented on an example of a three-phase-to-DC step up power converter. The main difference between existing control principles and the suggested principle is that the resonant circuit does not participate on the energy transfer and serves as a rotating snubber.

The usefulness of a switching function model for the design of a modulation of three-phase currents is investigated and introduced on an example of an AC-to-DC step-up power converter. Because a current configuration of semiconductor switches is utilized, the switching function model is eligible. The dynamic analysis based on this model gives a mathematical relation between the filter inductor value and the modulated currents and output voltage.

The concept of the novel control principle of a parallel-resonant converter is extended for three-phase-to-three-phase converters. Complimentary, the character of the switching bridges SM1 and SM2 allows to design a step-down as well as a step-up AC-to-AC power converter. A dynamic model based on the switching space phasor model is given for a three-phase-to-three-phase parallel-resonant link power converter.

CONCLUSIONS

The main objective of the thesis is to report on the study of three-phase AC switching power converters. The work on the analysis of polyphase AC switching power converters includes the desire to develop methods which enable to study the interaction between power semiconductor devices and dynamic elements of the converter, the source and the load.

The investigated topologies of the AC converter are embodied by semiconductor switches in a bridge configuration including passive dynamic components in the link and filters. The switching networks of the specified three-phase AC-to-AC power converter consist of at least twelve semiconductor switches. The switching networks fulfil the required criteria to generate converter waveforms with a prescribed degree of accuracy. Without a special handling, the number of switches operating at a high frequency is causing a cumbersome analysis and synthesis.

The performance and the quality of the power conversion depend on the interaction between the converter elements. This is the main reason to establish a good design of the power converter elements and to use a good dynamic model for the converter control. The purpose of the thesis is to provide a model and method of dynamic analysis and synthesis of three-phase AC power converters.

At the beginning of the study of the dynamics of AC power converters, a survey of topologies and applied methods of modulation is made.

- Two groups of AC converters are defined according to the control system configuration:
1. *open-loop controlled AC converter* (typical for pulse-width modulation (PWM)),
 2. *closed-loop controlled AC converter* (typical for discrete-pulse modulation (PFM)).

The investigation is restricted to converter configurations using a three-phase switching bridge. It is a complicated network that has many different configurations. Not all configurations are allowed and active.

A mathematical model of a converter is suggested in Chapter 2 to perform the dynamic analysis. The *current and voltage configurations* of a three-phase bridge are defined. Two different models of a semiconductor switch in the bridge configuration are suggested and further investigated.

First, the selected switching matrix with switches in a bridge configuration is composed of *switching functions* $\delta(t)$ for each switching leg that contains two switches. A switching leg is the basic element connecting the three-phase side to the one-phase side of a bridge. The operation of both switches is not independent and a switching function $\delta(t)$ is a basic modulation function for one phase. A three-phase switching bridge is consequently represented by three switching functions $\delta_a(t)$, $\delta_b(t)$ and $\delta_c(t)$.

Another model of a three-phase bridge is based on a *space switching phasor representation*. A three-phase switching bridge is represented by a switching space phasor $\underline{s}(t)$. The defined relations between the AC and the DC sides of a switching bridge allow the construction of a dynamic model more or less as a routine work. The defined relations are related to the power flow in a converter.

The relation between both models, the switching functions $\delta_a(t)$, $\delta_b(t)$, $\delta_c(t)$ and the switching space phasor $\underline{s}(t)$ is established. By defining three switching functions $\delta_i(t)$ for $i=a,b,c$ and by applying the α,β transformation, a switching space phasor $\underline{s}(t)$ is constructed. On the other hand, by appointing an arbitrary switching space phasor \underline{s} , there is no unique solution for a switching function $\delta_i(t)$. This ambiguity gives space to optimization. Therefore, dynamic models presented as a switching space phasor are more suitable for the synthesization of a modulation process of a three-phase power converter. The mathematical models are generally valid and suitable for various classes of converters with a three-phase switching bridge.

The dynamic modelling of the selected examples of converters is based on developed mathematical models. As a typical example of an open-loop modulation, the carrier PWM is selected. Transfer functions are matter of interest of a dynamic analysis. As typical examples of a closed-loop modulated converter, soft-switching resonant converters (series resonant link and parallel resonant link converter) are selected. The dynamic synthesis of a modulation process is a matter of our interest.

8.1 Open-loop modulated converters

A typical example of an open-loop modulated converter is the carrier PWM converter with a possible feedforward control. The modulation pattern is predefined. The dynamic analysis of the selected families of converters is provided.

The topologies of three-phase PWM power converters and methods of carrier PWM are reviewed in Chapter 3. These topologies are typical examples of open-loop modulated converters. The selection of a mathematical model depends on a type of the used modulation.

- The switching function model of a bridge leg is suitable in the case where each phase of a three-phase circuit is modulated individually. The *switching functions* $\delta_i(t)$ for $i=a,b,c$ determine the switching action of a bridge leg. An example of such a modulation method is a carrier subs oscillation method.
- The model of a *switching space phasor* is suitable for space phasor modulated three-phase converters. In case of space phasor modulation, the phasors for the voltages resp. currents are modulated at the three-phase side of the converter. The switching space phasor is in fact a normalized

phasor for the modulated currents or voltages. Therefore, the switching space phasor model represents all space phasor modulated PWM converters.

The open-loop modulated converters have a precalculated switching pattern that allows Fourier analysis.

- The Fourier series represents the discontinuous switching behaviour of the converter switches.
- The dynamic model of the system in a rotating reference frame is stationary in the steady-state.
- By linearization of the model, a small-signal transfer function for perturbations around a certain point is developed. The verification by measurements require a phase-gain analyser that is difficult to apply in power circuits. The calculated transfer functions are compared to experimental data obtained from simulation. The calculated transfer functions are accurate in the low-frequency region. For higher switching frequencies, the fidelity of the calculated curve is raising.

The described method is documented for both models of switches in a bridge configuration. Using this method, the transfer functions of AC power converters are calculated. The transfer functions are difficult to obtain from experimental methods.

The defined method performs a general approach to dynamic modelling. Considering only the zero-frequency component of a Fourier series, the state-space averaging method is obtained. State-space averaging is just a special case of the method investigated in this thesis.

8.2 Closed-loop modulated converters

A typical example of a closed-loop modulated converter is the group of soft-switching resonant converters. A survey of topologies and modulation principles is made to clarify the relation between the individual members of the group.

- PWM and PFM modulation methods are investigated. It is concluded that PFM is the natural modulation method for resonant converters.
- Filtering and selection problems are defined. For three-phase resonant converter topologies with a voltage configuration, the modulation is process of selection of the state of the switches in the configuration of the switching bridge. The conventional approach to filtering process is not appropriate because of the fluctuating harmonics of the spectrum of the modulated waveforms.

Two topologies: a zero-current switching series-resonant link converter and a zero-voltage switching parallel-resonant link converter are selected for further study.

There is a relation between resonant pulse-modulation techniques and a sliding mode control. It is proved that an ASDTIC is in fact a quasi-sliding mode modulator. The ASDTIC modulator, originally developed for single phase converters, however, does not solve the selection problem. Therefore, it is suggested to solve the modulation process of a three-phase-to-three-phase power converter with a sliding mode principle.

The discrete nature of the resonant pulse modulator results in a quasi-sliding mode. The disadvantage of a quasi-sliding mode is that the system does not stay on the sliding surface as it does in the case of an ideal sliding motion. The deviation from the ideal sliding surface arises within the sampling period of the sliding modulator. The chattering, which is a disadvantageous property of an ideal sliding motion, does not occur in the case of a quasi-sliding motion. A three-phase-to-three-phase resonant link converter is a multiple-input/multiple-output system. An eventual sliding mode switching scheme is desirable. By transforming this condition (an eventual sliding mode scheme) into a switching philosophy for a three-phase-to-three-phase resonant converter, the sliding mode has to occur at the source and the load sides of the converter simultaneously.

The application of models for the switches in a bridge configuration for the design of a quasi-sliding mode modulator is investigated. The conclusion is that a switching function model of a switching leg is suitable for converters with a current configuration. The switching space phasor model is more general and it is suitable for converters using either a current or a voltage configuration.

The dynamic model for *discrete-pulse modulated converters* is set up with the defined mathematical model of a *switching space phasor*. The switching space phasor model offers the possibility of a dynamic synthesis. The nonlinear resonant circuit is replaced by a linear inductor for the purpose of analysis and synthesis of modulation using the *quantum transformation*. Here, the *quantum transformation* is proved for a series-resonant circuit. A quantum transformed parallel-resonant circuit exists as well.

The modulation process based up to now on intuition is now supported by a dynamic model. The suggested modulation shows the application of the dynamic model.

- To avoid a model with time-varying parameters, a harmonic elimination process is provided. The harmonic component with the utility frequency is extracted. The procedure is essentially identical to the transformation into a rotating reference frame.
- The modulation methods and control are analysed for a model with attention to the filtering and selection problems.

- The space phasor mapping based on the quasi-sliding mode is designed. The criteria of mapping are discussed and analysed generally. The switching process based on the dynamic model is accompanied by simulation results.
- An improved modulation process is designed for a series-resonant link converter. The designed modulation process is only an elementary example. By selecting the modulation criteria, more sophisticated modulations based on the model can be designed.

The dynamic model of a *discrete-pulse modulated converter* is based on an equivalent control equation which presents the averaged behaviour of the switching action. The equivalent switching phasor under the assumption of an infinite resonant frequency and infinite switching frequency is equal to a PWM reference phasor. This fact defines a link between PWM and a quasi-sliding modulation defined in the thesis.

The utilization of a *switching function* model is shown on an example of a parallel-resonant converter. A novel control principle of a parallel-resonant converter is suggested and documented on an example of a three-phase-to-DC step up power converter. The main difference between the existing control principles and the suggested principle is that the resonant circuit does not participate in the energy transfer and serves as a rotating snubber. This opens a way to construct converters with a higher efficiency than is usual for resonant converters. The dynamic analysis based on the switching function model of a switching bridge leg gives a mathematical relation between the filter inductor value and modulated the currents or output voltage.

The dynamic model for both groups (open- and closed-loop modulated converters) results in an approximated model. The harmonic content of the converter waveforms is the basis for the approximation for both groups. These models include only the utility frequency. The switching function or switching space phasor is thus approximated by the low-frequency component.

The methods of dynamic modelling for both groups of converters have a common base: equations in a d, q reference frame that rotate with a utility frequency.

The *switching function* model of a switching leg is suitable for analysis of existing modulations based on this model. The application of this model for dynamic synthesis is limited to a current configuration.

The *switching space phasor* model of switches in a bridge configuration is a suitable tool for dynamic analysis and synthesis of the converters with a three-phase switching bridge topology. The use of this model for dynamic synthesis of new modulation techniques can be recommended.

BIBLIOGRAPHY

- [1] Akagi H., Nabae A.: The p-q theory in three-phase systems under non-sinusoidal conditions; *ETEP*, Vol.3, No.1, Jan.-Feb. 1993, pp. 27-31.
- [2] Akagi H., Kanazava Y., Nabae A.: Instantaneous reactive power compensators comprising switching devices without energy storage components; *IEEE Transactions on Industry applications*, Vol.IA-20, No.3, May-June 1984, pp. 625-630.
- [3] Bauer P., Klaassens J.B.: A Novel Control Principle for Parallel Resonant Voltage Link Converters; *International Conference on Electrical Drives and Power Electronics*, Kosice, Czechoslovakia, Sept. 1992, pp. 457-461.
- [4] Bauer P., Klaassens J.B.: A Method to Dynamical Analysis of AC Power Converters; *International Conference on Electrical Drives and Power Electronics*, Kosice, Czechoslovakia, Sept. 1992, pp. 180-183.
- [5] Bauer P., Klaassens J.B.: A Novel Control Principle for Parallel Resonant Voltage Link Converters; *IEEE 1992 IAS Conference*, Houston, Texas, USA, Oct. 1992, pp. 796-800.
- [6] Bauer P., Klaassens J. B.: Dynamic Modelling of AC Power Converters; *Power Conversion Conference*, Yokohama, Japan, April 1993, pp. 502-507.
- [7] Bauer P., van Duijsen P.J.: Large Signal and Small Signal Modeling Techniques for AC-AC Power Converters; *Power Conversion Conference*, Yokohama, Japan, April 1993, pp. 520-525.
- [8] Bauer P., Klaassens J.B.: Space vector based power control of resonant converters; *EPE Conference*, Brighton, Sept. 1993, No.377, Vol.3, pp. 338-342.
- [9] Bauer P., Klaassens J.B.: Dynamics and analysis of three phase AC power converters; *EPE Conference*, Brighton, Sept. 1993, No.377, Vol.4, pp. 77-81.
- [10] Bauer P.: Space vector based power factor control of pulse modulated soft-switching converters; *PCIM 94*, Nurnberg, Germany, June 1994, pp. 89-102
- [11] Bauer P.: Mathematical model of a three-phase converter; *Int. Conf. Electrical drives and Power Electronics*, Slovakia, Oct. 1994, pp. 147-153.
- [12] Bauer P.: Transfer functions of PWM three-phase converter; *Int. Conf. Electrical drives and Power Electronics*, Slovakia, Oct. 1994, pp. 13-18.
- [13] Bauer P.: Synthesis of the modulation mechanism for AC-to-AC series resonant converter; *Int. Conf. Electr. Drives and Power Electronics*, Slovakia, Oct. 1994, pp. 169-174.

- [14] Bauer P.: Modulation of low frequency waveforms by AC/AC resonant converter; *Intelec 94*, Vancouver, Canada, Oct.-Nov. 1994, pp. 643-648.
- [15] Boudjema F., Abatut J.L.: Sliding mode - a new way to control series resonant converters; *IEEE Annual Meeting*, 1990, pp. 938-943.
- [16] Bose B.K.; Recent Advances in Power Electronics; *IEEE Transactions on Power Electronics*, Vol. PE-7, No.1, Jan. 1992, pp. 2-16.
- [17] Chen C.T.: Linear system theory and design. *Holt, Renhart and Winslon*, N.Y. 1984.
- [18] Cheron Y., Foch H.: Series resonant converters; *EPE Tutorial resonant converters*, Brighton, Great Britain, 1993, pp. 15-32.
- [19] Cho J.G., Cho G.H.: Soft switched matrix converter for high frequency direct AC-to-AC power conversion; *EPE*, 1991, Firenze, pp. 196-201.
- [20] Cuk S., Middlebrook R.D.: A general unified approach to modeling switching dc-dc converters in discontinuous conduction mode; *PESC*, 1977, pp. 36-57.
- [21] Divan D.M.: The Resonant DC Link Converter - A New Concept in Static Power Conversion; *IEEE-IAS Annual Conference Record*, 1986, pp. 648-656.
- [22] Divan D.M., Venkataramanan G.: Comparative evaluation of soft switching inverter topologies; *EPE*, 1991, Firenze, pp. 13-18.
- [23] Venkataramanan G., Divan D.M.: Pulse Width Modulation with Resonant DC Link Converters; *IEEE-IAS Annual Conference Record*, 1990, pp. 1215-1221.
- [24] Elbuluk M.E., Verghese G.C., Kassakian L.G.: Sampled data modeling and digital control of resonant converters; *IEEE Transactions on Power Electronics*, No.3, 1988.
- [25] Ferrero A., Morando A.P., Ottoboni R., Superti-Furga G.: On the meaning of the Park Power Components in three-phase systems under non-sinusoidal conditions; *ETEP*, Vol.3, No.1, Jan.-Feb. 1993, pp. 33-43.
- [26] Gyugyi L., Pelly B.R.: Static power frequency changers - Theory, performance and application; *John Wiley & Sons*, 1976.
- [27] Holtz J.H.: Pulse width Modulation - A survey; *IEEE-IAS Annual Meeting*, Vol.2, March 1992, pp. 11-18.

- [28] He Jin, Mohan N., Wold B.: Zero Voltage Switching PWM Inverter for High Frequency DC-AC Power Conversion; *IEEE-IAS Annual Conference Record*, 1990, pp. 1215-1221.
- [29] Hung J.Y., Gao W., Hung J.C.: Variable structure control: A survey; *IEEE Transactions on Industry Applications*, 1992.
- [30] Joung G.B., Cho J.G., Cho G.H.: A generalized quantum resonant converter using a new quantum resonant module; *IEEE Trans. on Power Electronics*, Oct. 1992, pp. 666-672.
- [31] Karnopp D.C., Margolis D.L., Rosenberg R.C.: System Dynamics, A unified approach; *Wiley*, New York, 1990.
- [31] Kassakian J.G., Schlecht M.F., Verghese G.C.: Principles of Power electronics; *Addison-Wesley Publishing Company*, 1991.
- [33] Kim I.D., Cho G.H.: New bilateral zero voltage switching ac/ac converter using high frequency partial resonant link; *IECON*, 1990, pp. 857-862.
- [34] King R.J., Stuart T.A.: Small-signal model for the series resonant converter; *IEEE Transactions on Aerospace and Electronic Systems*, May 1985, pp. 301-319.
- [35] Kislovski A.S.: Dynamical analysis of switching DC-DC converters; *EWV Engineering*, No.1, Bern, Switzerland, 1985.
- [36] Kislovski A.S.: Current mode control. A unified model for open loop instability; *APEC*, 1991, pp. 459-472.
- [37] Kislovski A.S.: Controlled quantity concept in small signal analysis of switching power cells; *IEEE Transactions on Aerospace and Electronics Systems*, No.3, 1983, pp. 438-446.
- [38] Klaassens J.B., de Beer F.G.: Three-phase AC-to-AC series-resonant power converter with a reduced number of thyristors; *IEEE Transactions on Power Electronics*, Vol. PE-6, No.3, June 1991, pp. 346-355.
- [39] Klaassens J.B., van Wesenbeeck M.P.N., Lauw H.K.: Series resonant single-phase AC-to-DC power supply with active power factor control; *EPE*, Aachen, 1989, pp. 1-6.
- [40] Klaassens J.B.: DC-AC series resonant converter system with high internal frequency generating multiphase AC waveforms for multikilowatt power levels; *IEEE Transaction on Power Electronics*, Vol. PE-2, No.3, 1987, pp. 247-256.

- [41] Klaassens J.B., van Wesenbeeck M.P.N., Bauer P.: Soft Switching : From Idea to Reality; *International Conference on Electrical Drives and Power Electronics*, Kosice, Czechoslovakia, Sept. 14-16, 1992, pp. 187-192.
- [42] Klaassens J.B., van Wesenbeeck M.P.N., Bauer P.: Soft Switching Power Conversion; *EPE Journal*, Sept. 1993, Vol.3, No.3, pp. 155-166.
- [43] Klaassens J.B., van Wesenbeeck M.P.N., Bauer P.: Soft Switching Power Conversion; *EPE Tutorial Resonant Converters*, Brighton, Sept. 1993, pp.1-14.
- [44] Klaassens J.B., van Wesenbeeck M.P.N., Lauw H.K.: AC-AC Converters with Soft-Switching; *Proceeding of the 4th European Conference on Power Electronics and Applications*, Vol.4, Firenze, Sept. 1991, pp. 151-157.
- [45] Kovacs K.P., Racz I.: Transiente vorgange in Wechselstrommaschinen; *Akademia Kiado*, Budapest, Hungary, 1959.
- [46] Lau B.Y., Middlebrook R.D.: Small signal frequency response theory for piecewise constant two switched network dc to dc converter systems; *PESC*, 1986, pp. 186-200.
- [47] Lee F.C., Tabisz W.A, Javanovic M.M.; Recent Developments in High-Frequency Quasi-Resonant and Multi-Resonant Converter Technology; *EPE*, Aachen, Germany, Oct. 1989, pp. 401-410.
- [48] Mertens A.: Performance analysis of three-phase inverters controlled by Synchronuous Delta-Modulation systems; *IEEE-IAS Annual Meeting*, Vol.1, 1992, pp. 779-788 (a).
- [49] Mertens A.: Harmonic distorsion in three-phase inverters controlled by synchronuous Sigma-Delta-Modulation; *ETEP*, Vol.2, 1992, pp. 351-358 (b).
- [50] Middlebrook R.D.: Small signal modeling of pulse-width modulated switched power converters; *Proceedings of IEEE*, No.4, 1988, pp. 343-354.
- [51] Mohan N., Undeland T.M., Robbins W.P.: Power Electronics: Converters, Applicatons, and Design; *John Wiley & Sons*, 1989.
- [52] Murai Y., Mochizuki S., Caldeira P., Lipo T.A: Current Pulse Control of High Frequency Series Resonant DC Link Power Converter; *IEEE-IAS Annual Conference Record*, 1989, pp. 1021-1030.
- [53] Nakahara M., Higashi T., Ninomiya T., Horada K.: Dynamic characteristics and stability analysis of resonant converters; *PESC*, 1989, pp. 752-759.

- [54] Ngo K.D.T.: Low frequency characterization of PWM converters; *IEEE Transactions on Power Electronics*, Oct. 1986, pp. 223-230.
- [55] Oruganti R., Lee F.C.: Implementation of optimal trajectory control of series resonant converter; *PESC*, 1987, pp. 451-459.
- [56] Oruganti R., Lee F.C.: State plane analysis of parallel resonant converter; *PESC*, 1985, pp. 56-73.
- [57] Redl R.: Small signal analysis of the free-running current-mode-controlled converter; *PESC*, 1991, pp. 897-906.
- [58] Rim C.T., Hu D.Y., Cho G.H.: The graphical D-Q transformation of general power switching converters; *IEEE-IAS Annual Meeting*, 1988, pp. 940-945.
- [59] Rim C.T., Hu D.Y., Cho G.H.: General proofs and D-Q transformation based analyses; *IEEE Transactions on Industrial Applications*, July 1990, pp. 777-784.
- [60] Rim C.T., Cho G.H.: Phasor transformation and its application to the dc ac analyses of frequency phase controlled SRC; *IEEE Transactions on Power Electronics*, April 1990, pp. 201-221.
- [61] Sanders S.R., Noworolski J.M., Liu X.Z., Verghese G.C.: Generalized averaging method for power conversion circuits; *IEEE Transactions on Power Electronics*, Feb. 1991, pp. 333-339.
- [62] Schwarz F.C.: Engineering information on an analog signal to discrete time interval converter; *NASA CR-1344544*, 1974, pp. 175.
- [63] Schwarz F.C.: An improved method of resonant current pulse modulation for power converters; *IEEE Transactions on Industrial Electronics and Control Instrumentation*, Vol.IECI-23, No.2, May 1976, pp. 133-141.
- [64] Stefanovic V.R.: Industrial AC Drives Status of Technology; *EPE Journal*, 4 Vol.2, No.1, March 1992, pp. 7-24.
- [65] Utkin V.I.: Variable structure systems with sliding modes; *IEEE Transactions on Automatic Control*, April 1977, pp. 212-219.
- [66] Venkataramanan G., Divan D.M.: Discrete time integral sliding mode control for discrete pulse modulated converters; *PESC*, 1990, pp. 67-73.
- [67] Vergese G.C., Elbuluk M.E., Kassakian J.G.: A general approach to sampled data modeling for power electronic circuits; *IEEE Transactions on Power Electronics*, No.4, 1986, pp. 76-87.

-
- [68] Visser H.R., Van den Bosch P.P.J.: Modelling of periodically switching networks; *PESC*, 1991, pp. 1-8.
- [69] Vorperian V., Cuk S.: Small signal analysis of resonant converters; *PESC*, 1983, pp. 269-282.
- [70] Vorperian V.: Aproximate small signal analysis of the series and parallel resonant converters; *IEEE Transactions on Power Electronics*, Jan. 1989, pp. 15-24.
- [71] Witulski A.F., Ericson R.W.: Small signal AC equivalent circuit modelling of the series resonant converter; *IEEE IAS Annual Meeting*, 1987, pp. 693-704.
- [72] Witulski A.F., Hernandez A.F., Ericson R.W.: Small signal equivalent circuit modeling of resonant converters; *IEEE Transactions on Power Electronics*, No.1, 1991, pp. 11-16.
- [73] Woo B.O., Kim I.D., Cho G.H.: Zero voltage switching AC/DC/AC converter using modified high frequency DC-link; *IEEE-IAS Annual Conference*, 1990, pp. 1243-1250.
- [74] Wu R., Dewan S.B., Slemon G.R.: Analysis of a PWM ac to dc voltage source converter under the predicted current control with a fixed switching frequency; *IEEE Transactions on Industrial Applications*, No.4, 1991, pp.756-764
- [75] Wu R., Dewan S.B., Slemon G.R.: Analysis of a PWM ac to dc voltage source converter using PWM with phase and amplitude control; *IEEE Transactions on Industrial Applications*, No.3, 1991, pp. 355-364.

**LIST OF NOTATIONS
AND SYMBOLS**

\underline{a}	instantaneous phasor of a complex power
A	system matrix
AC	alternating current
ASDTIC	analog-signal-to-discrete-time-interval converter
B	input matrix
C	capacitor
D	diode
DC	direct current
d	duty cycle
f	frequency
$F(x)$	function of variable x
I	steady-state value of the current
i	instantaneous value of the current
\underline{i}	current phasor
H	existence matrix
L	inductor
NS	nondissipative electrical network in series
NP	nondissipative electrical network in parallel
PWM	pulse-width modulation
PFM	pulse-frequency modulation, discrete-pulse modulation
t	time
T	period
T	transformation matrix
Th	thyristor
T_{sw}	switching period of PWM
$\underline{s}, \underline{S}$	switching phasor in $\alpha\beta$ and dq coordinates
S	switch
SB	switching bridge
S_{ij}	switch in phase i ($i = a, b, c$) and ($j = n, p$) p -upper group, n -lower group
SM	switching matrix
SOA	safe operating area
U	steady state value of the voltage
u	instantaneous value of the voltage
\underline{u}	voltage phasor
P	power
p	instantaneous active (real) power
q	instantaneous reactive (imaginary) power
w	instantaneous complex power
δ	switching function
ψ	phase of the switching phasor in $\alpha\beta$ coordinates
ρ	scaling factor
$+\rightarrow$	polarity of the voltage

Indexes

a, b, c	three-phase a,b,c coordinate system
ac	ac side

c	absorbed
cond	conducting
<i>d</i>	<i>d</i> phasor coordinate in <i>d,q</i> coordinate system
dc	dc side
e	injected
eq	equivalent
o	output
off	switching off
OFF	time interval with the switch off
on	switching on
ON	time interval with the switch on
<i>q</i>	<i>q</i> phasor coordinate in <i>d,q</i> coordinate system
r	resonant
ref	reference
s	source
saw	sawtooth waveform
α	α phasor coordinate in α,β coordinate system
β	β phasor coordinate in α,β coordinate system

SUMMARY

Three-phase AC power converters create an important class of power converters. In the recent years, significant advances in three-phase AC converter topologies and applied semiconductor devices have been reported. Increased attention is paid to the dynamics and control of the converters to achieve a high performance. The development of new converter topologies with soft-switching techniques and with pulse-modulation techniques increased the necessity for modelling and analysis.

In the past, for control purposes, the converter has often been represented as a gain, possibly with a time delay. To fully utilize the potential of the converter and to account the uncertainties in the system, it is important to really understand and qualify the dynamic performances of the converter, especially in the presence of parameters of variations and disturbances.

Much valuable work has been done in the field of the analysis of DC-to-DC converters. However, this work cannot immediately be transferred to the analysis of AC converters because the system have a fundamental time-varying frequency component. Thus, alternative methods have to be sought or existing methods have to be extended. The complexity of AC power converters is much higher than the one of DC converters and so is the analysis of their operation and dynamics.

The converter topologies and related control techniques depend on the character of the passive network located between the switching matrixes and the character of the filters. The research work is dealing with pulse-width modulated (PWM) and discrete-pulse modulated techniques (PFM). For the purpose of dynamic analysis and modelling, the AC converter topologies and related control techniques are classified.

The study of the dynamic behaviour of three-phase AC power converters for all modes of operation require the establishment of a set of dynamic equations. The development of a dynamic model applying differential equations is a well described subject. However, three-phase AC power converters include a substantial number of semiconductor switches. Therefore, defining a mathematical model for the operation of the switches is a crucial point. Two methods are investigated. One of them is a switching function model of a switching bridge leg and the other one is the application of a switching space phasor. The mathematical relations between the AC and the DC sides of the switching bridge based on the instantaneous real power are found and proved for both models. Defined models of switches in a bridge configuration allow to derive a dynamic model for any converter that utilizes this topology. The establishment of such a model is a first step to design a control and modulation system of the converter with this topology.

As a typical example of an open-loop modulation, carrier PWM method is selected. For carrier suboscillation PWM modulation and space phasor modulation, a dynamic model with the defined mathematical models has been developed. This model contains a discontinuous time function $\delta(t)$ that represents the action of a switching leg in a three-phase bridge configuration. For space phasor modulation, it is a discontinuous switching phasor \underline{s} that represents the action of the switching

bridge.

To reduce the complex problem of a switching network, a Fourier transformation at the resulting switching pattern is applied. This application is possible to establish because the switching pattern is precalculated. In fact, the averaging methods, where we consider one-cycle average, require a calculation of the DC coefficient in the Fourier series representation.

This fact offers a clear relation between the averaging methods applied to DC-to-DC power converters and the method suggested here. The suggested method is a generalization of an existing averaging method. By using a state-space description and by calculating the zero Fourier component, the state-space averaging method is obtained. This means that the state-space averaging is a special case of the proposed method.

As a typical example of a closed-loop modulation, a modulation process of a soft-switching resonant link converter is selected. A survey of topologies and modulation principles is made to clarify the relation between the individual members. Two examples: a three-phase-to-three-phase converter with series-resonant link and a three-phase-to-three-phase converter with parallel-resonant link are explored in details. The dynamic synthesis for both examples is provided.

The *switching space phasor* model offers the possibility of a dynamic synthesis. The modulation process for a three-phase-to-three-phase series-resonant converter based so far on intuition is now supported by a dynamic model. The mapping of the switching space phasor based on a quasi-sliding mode is designed. The criteria of the mapping are discussed and analyzed in general. The switching process based on a dynamic model is accompanied by results of simulation.

The utilization of a *switching function* model is shown on the example of a parallel-resonant converter.

The designed modulation process is only an elementary example. By selecting the modulation criteria, more sophisticated modulations based on the models can be designed for any converter utilizing the topology with the switches in a bridge configuration.

SAMENVATTING

Dynamische Analyse van Drie-Fasen AC Omzeters

Driefasen AC vermogensomzeters vormen een groep van betekenis binnen de vermogensomzeters. In de afgelopen jaren zijn er belangrijke ontwikkelingen op het gebied van deze driefasen AC omzeters en de daarin toegepaste halfgeleider-elementen gerapporteerd. In toenemende mate wordt er aandacht gegeven aan de regeling en de dynamica van omzeters om een hoge prestatie te kunnen leveren. De ontwikkeling van nieuwe resonante omzeters die pulsmodulatie technieken met een methode voor soft-switching combineren, vergroot de behoefte aan verbeterde technieken voor de modelvorming en de analyse. In het verleden is de omzetter vaak voorgesteld door een versterkingsfactor al of niet in combinatie met een tijdvertraging. Om de potentiële mogelijkheden van de omzetter volledig te kunnen benutten en rekening te kunnen houden met verstoringen in het systeem, is het belangrijk het dynamische bedrag van de omzetter te kunnen bepalen in bijzonder voor veranderende parameters.

Veel waardevol werk is gedaan op het gebied van de analyse van DC omzeters. Dit werk is echter niet geschikt om de analyse aan AC omzeters uit te voeren omdat het basisprobleem het bestaan van een grondharmonische tijdvariabele golfvorm is. Er moet naar alternatieve methoden worden gezocht of bestaande methoden moeten worden uitgebreid. De complexiteit van AC vermogensomzeters is veel groter dan die van DC vermogensomzeters, hetgeen ook geldt voor de analyse van de functies en het dynamische gedrag.

De eigenschappen van converternetwerken en de daarbij behorende regelsystemen hangen af van de eigenschappen van de passieve netwerken welke zijn geplaatst tussen de schakelmatrices en van de eigenschappen van de filters.

Het uitgevoerde onderzoek is gericht op pulsbreedte modulatie (PBM) en discrete pulsmodulatie technieken (zoals PFM). Ten behoeve van de analyse van het dynamische gedrag en de modelvorming, worden de netwerken voor AC omzeters en de bijbehorende regeltechnieken geclassificeerd.

De studie naar het dynamisch gedrag van driefasen AC omzeters voor alle bedrijfsomstandigheden, vereist de ontwikkeling van een stelsel dynamisch vergelijkingen. De ontwikkeling van een dynamisch model door toepassing van differentiaal vergelijkingen is een onderwerp dat goed is bestudeerd en beschreven.

De driefasen AC omzetter omvat echter een substantieel aantal halfgeleiderschakelaars. Daarom is een mathematisch model dat de werking van de schakelaar beschrijft, een cruciaal punt. Er worden twee methoden geïntroduceerd. Eén van deze methoden is het model van de *schakelfunctie* (*switching function*) zoals gedefinieerd voor een *brugschakeling*. Het andere model betreft de toepassing van *schakelende ruimtiefasor* (*switching space phasor*).

De wiskundige relaties tussen de wisselspanningszijde en de gelijkspanningszijde van de brugschakeling baseren zich op het momentane reële vermogen en worden voor beide modellen uitgewerkt. De geïntroduceerde modellen voor de schakelaars in een brugconfiguratie maken het mogelijk om een dynamisch model te

ontwikkelen voor iedere omzetter die gebruik maakt van de aangegeven topologie.

Het introduceren van een dergelijk model is de eerste stap om een regeling en een modulatiemethode te kunnen ontwerpen voor de omzetter. Als een karakteristiek voorbeeld van de open-loop modulatie methode wordt de "Carrier PWM Method" uitgekozen. Voor de "Carrier Suboscillation PWM Modulation" en "Space Phasor Modulation" wordt een dynamisch model ontwikkeld met behulp van de gedefinieerde mathematische modellen. Het model bevat een discontinuë tijdfunctie $d(t)$ welke de actie van een schakelpoot in een brugconfiguratie voorstelt. Voor Space Phasor Modulation bestaat er een discontinuë schakelfasor s , welke de actie van de schakelbrug presenteert. Om de problemen van een schakelend netwerk te reduceren wordt er een Fourier transformatie op het resulterend pulspatroon toegepast. Een dergelijke transformatie kan worden toegepast omdat het pulspatroon is voorberekend. In feite verlangen middelingsmethoden met een middelingsproces over één periode, de berekening van de gelijkspanningscoëfficiënt van een Fourier reeks. Dit levert een duidelijke relatie tussen middelingsmethoden toegepast op DC omzeters en de hier voorgestelde methode. De voorgestelde methode is een veralgemening van een middelingsmethode. Door gebruik te maken van een beschrijving in de toestandsruimte en door het berekenen van de nul-component in de Fourier reeks, wordt een toestandmiddelingsmethode gerealiseerd. Dat betekent dat de middelingsmethode in de toestandsruimte een speciaal geval is van voorgestelde methode.

Als een karakteristiek voorbeeld van een modulatie methode met een gesloten lus, wordt een *soft-switching resonant-link omzetter* uitgekozen. Een overzicht van de netwerken en de modulatiemethoden is nodig om de relatie tussen de individuele onderdelen duidelijk te maken. Twee voorbeelden: een *driefasen omzetter met een serie-resonante link* en een *driefasen omzetter met een parallel-resonantie link* worden uitgebreid beschreven. Een dynamische synthese wordt voor beide voorbeelden uitgewerkt.

Het model van de *switching space phasor* biedt de mogelijkheid van een dynamische synthese. Het modulatieproces voor een *driefasen serie-resonante omzetter* is tot nu toe gebaseerd op intuïtie en word nu gedragen door een dynamisch model. Een mapping methode van de switching space fasor is uitgewerkt op basis van een quasi-sliding mode. De criteria voor het mapping proces worden in het algemeen besproken en geanalyseerd. Het schakelproces gebaseerd op het dynamische model wordt vergezeld van simulatieresultaten. Het gebruik van *schakelfuncties (switching functions)* wordt verder gedemonstreerd aan de hand van het voorbeeld van een *parallel-resonant omzetter*. Het ontworpen modulatie proces is slechts een elementair voorbeeld. Door het selecteren van modulatiecriteria kunnen geavanceerde modulatiemethoden voor iedere omzetter die gebruik maakt van de topologie van een brugschakeling, worden ontwikkeld.

CURRICULUM VITAE

Pavol Bauer was born in Košice, Slovakia on January 9, 1961. After graduating at the secondary grammar school in 1980, he began to study electrical engineering at the Technical University in Košice. He completed his studies with graduation work Four-quadrant voltage frequency changer in 1985. After obtaining University degree, he continued working at the Department of Power Electronics as a research student. At the same time he was teaching power electronics and related subject. Since August 1990 he is with the Delft University of Technology, Department of Power Electronics and Electrical Machines as a PhD student in the field of dynamic analysis of three-phase-to-three-phase power converters and resonant soft-switching power conversion. He published 30 papers in his field and attended several conferences.